Optical Interaction between Plasmonic Metal Nanoparticles and Triplet-Triplet Annihilation-Based Upconversion Systems

プラズモニック金属ナノ粒子と三重項対消滅型アップコンバージョンシステム間の光学的相互作用に関する研究

Dissertation

Materials and Applied Chemistry Major
Graduate School of Science and Technology
Doctoral Course
Nihon University

January, 2021

Shota Jin
Supervised by Prof. Joe Otsuki

Name	Abbreviation
9,10-bis- (phenylethynyl)anthracene	BPEA
9,10-diphenylanthracene	DPA
Atomic force microscopy	AFM
Bis(2-benzo[*b*]thiophen-2-ylpyridine)(acetylacetonate)iridium(III)	$Ir(BT)_2(acac)$
Boundary element method	BEM
Dimethylformamide	DMF
Ethyleneoxide-epichlorohydrin copolymer	EO-EPI
Intersystem crossing	ISC
Localized surface plasmon	LSP
Octadecane thiol	ODT
Photon upconversion	UC
Polyethylene imine	PEI
Polystyrene sulfonate	PSS
Polyvinyl alcohol	PVA
Scanning electron microscopy	SEM
Silver nanoprism	AgPR
Silver nitrate	$AgNO_3$
Sodium borohydride	$NaBH_4$
Sodium hydroxide	NaOH
TTA-based upconversion	TTA-UC
Transmission electron microscopy	TEM
Triplet-triplet annihilation	TTA
Triplet-triplet energy transfer	TTET
Tris(2,2′-bipyridine)ruthenium(II) hexafluorophosphate	$Ru(bpy)_3$
Upconversion nanoparticle	UCNP
local density of optical states	LDOS
palladium(II)-octaethylporphyrin	PdOEP
palladium(II)-tetraphenyltetrabenzoporphyrin	PdTPTBP
platinum(II)-octaethylporphyrin	PtOEP

Contents

Chapter 1

Introduction

1-0. General Introduction

Incident solar radiation is a vast resource whose potential remains largely untapped in a single hour, the amount of solar energy that reaches the Earth's surface is more than the global population consumes in a year.[1] Effective use of solar energy, a sustainable energy source, is a top priority for realizing a recycling-based society. Recently, solar cells have been intensively studied as one of the optoelectronic devices utilizing sunlight. The power generation cost of the silicon-type solar cells currently in practical use is 0.29 $/kWh (2-3 times the thermal power generation), which poses a problem in terms of cost. Therefore, dye-sensitized solar cells and organic thin-film solar cells,[2-6] which can be produced at a lower cost than conventional silicon-type solar cells, are attracting attention. However, in the solar cell described above, since the device is driven mainly by utilizing ultraviolet to visible light, the long wavelength region in the solar light cannot be effectively utilized. In other words, low-energy light (long-wavelength light) that is lower than the energy gap of the material is lost. For this reason, research aimed at broadening the driving wavelength (material modification) has attracted attention.

Further, there is a similar problem in the photocatalyst. Photocatalyst is a material which shows catalytic function by light irradiation, and has attracted much attention as a material capable of decomposing environmentally harmful organic substances and generating hydrogen. TiO_2 used practically at present has a large band gap of about 3eV and is driven only by irradiation of high-energy ultraviolet light. This ultraviolet light accounts for only about 5% of sunlight with regard to the energy content. That means more than 90% of the energy of sun light (Visible light 52%, Infrared light 42%) is not being used. Therefore, the research aiming with lower energy light is actively carried out (There have been proposed methods of doping TiO_2 with transition metal ions or anions to expand the absorption region, and the use of semiconductor photocatalysts with a small band gap, such as Cu_2O (2.0 eV), CdS (2.4 eV), and WO_3 (2.7 eV); however, these methods use only a part of visible light.).[7-11]

1-1. Photon Upconversion Phenomena

1-1-1. Photon Upconversion System in Upconversion Nanoparticles (UCNPs)

Photon upconversion (UC) is the photochemical phenomenon which converts the long wavelength light to the short wavelength light, and it is the technology which can greatly contribute to the broaden drive wavelength of the photoelectronic device. A typical approach to UC is the use of multistage excitation phenomena. Inorganic nanoparticles (upconversion nanoparticles; UCNPs) doped with lanthanoid elements have been studied as a material to induce multistep excitation.[12-14]

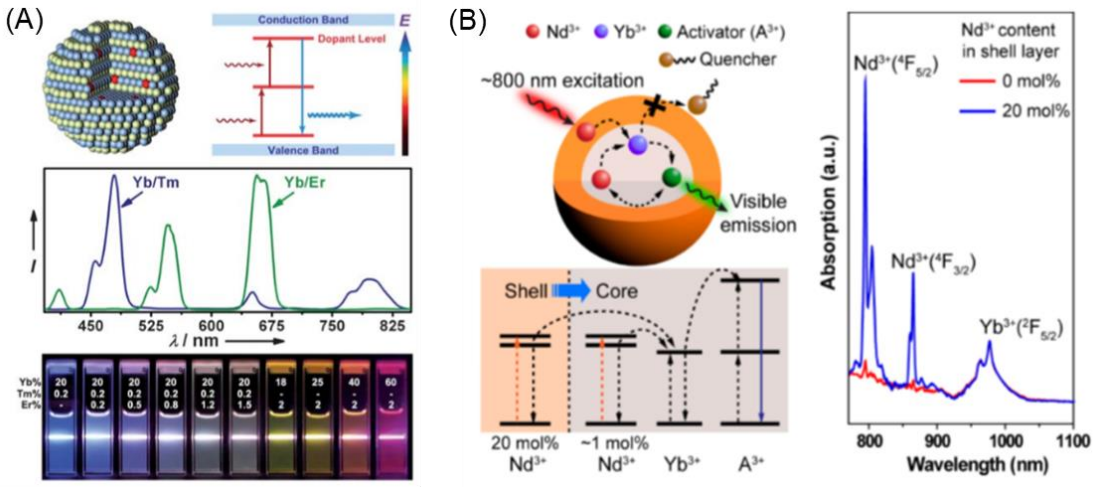

Figure 1-1. (A) The upconverted emission from Er^{3+} and Tm^{3+} in $NaYF_4$:Yb^{3+},Er^{3+} and $NaYF_4$:Yb^{3+},Tm^{3+}. (B) UCNPs with improved excitation efficiency by Nd^{3+} doping by Ref. [15]. Reprinted with permission from *J. Am. Chem. Soc.*, **2013**, *135*, 12608. Copyright (2013) American Chemical Society.

Typical UCNPs use ytterbium (Yb^{3+}) as the photosensitizing center, and this has a light absorption peak around a wavelength of 1000 nm.[12] In addition, since erbium (Er^{3+}) and thulium (Tm^{3+}), which are emission centers, emit light in the visible light region (400 nm to 550 nm), the anti-Stokes shift is very large (Figure 1-1 (A)), and they are easily distinguished from autofluorescence of cells. Therefore, UCNPs are suitable materials for bioimaging and have been extensively studied in recent years. On the other hand, UCNPs have disadvantages in terms of optical functions such as very low emission quantum yield and difficulty in driving unless it is a high-intensity light source (kW to MW/cm^2) with high coherency such as laser light. Therefore, it is considered to be a material unsuitable for solar cells and photocatalysts, which are required to be driven by sunlight (~1 mW/cm^2). Recently, studies aiming at efficiency improvement of quantum yield of UCNPs by using neodymium (Nd^{3+}) as a substitute of Yb^{3+} which is a photosensitization center have been carried out, but UCNPs driven by light intensity of solar light level have

not been found yet (Figure 1-1 (B)).[15,16]

1-1-2. Triplet-Triplet Annihilation-Based Upconversion System in Liquid Phase

Triplet-triplet annihilation-based upconversion (TTA-UC) is a photochemical phenomenon wherein low energy photons are converted to high energy photons via a series of energy transfer processes between photofunctional molecules.[17-21]

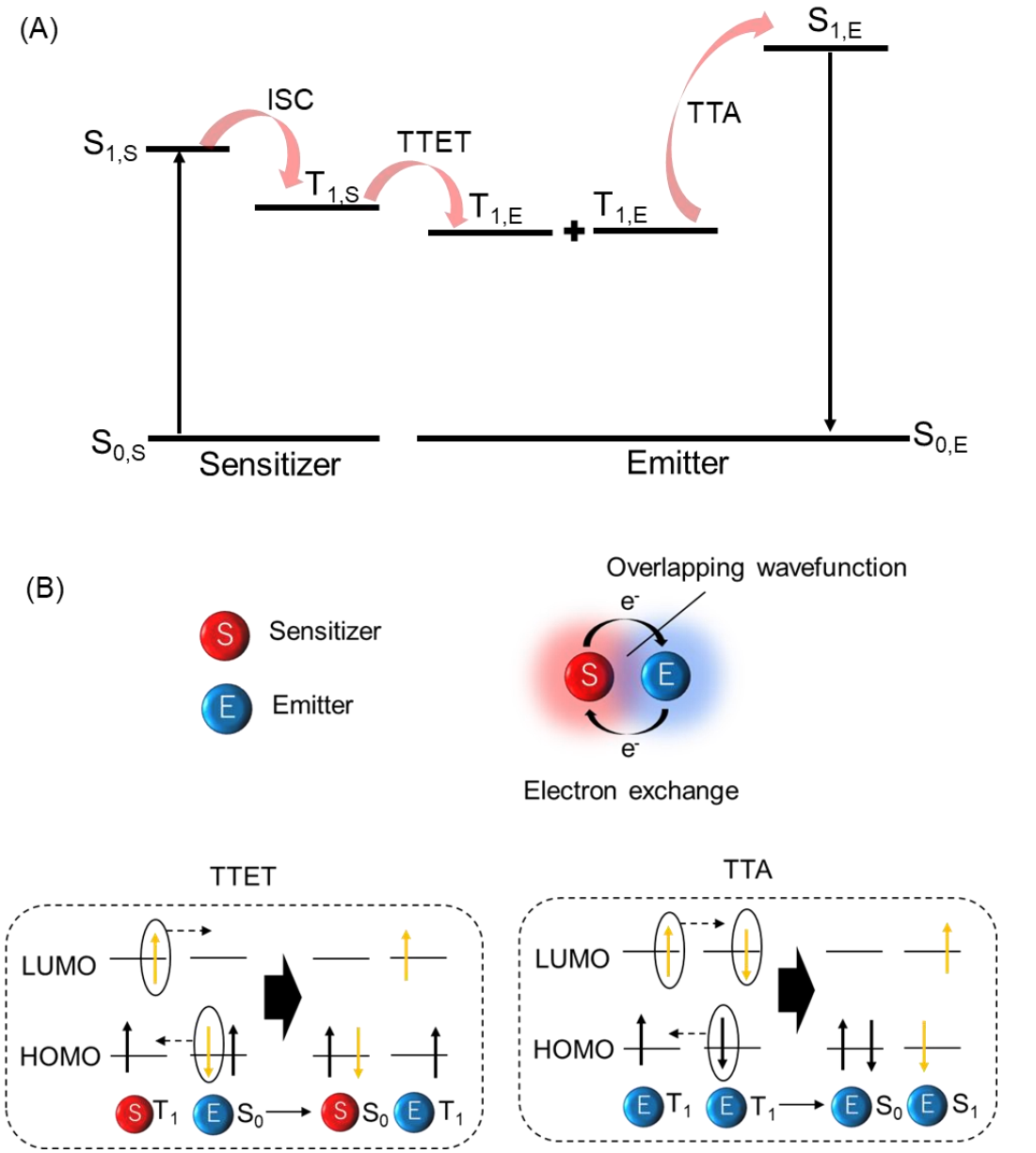

Figure 2-1. (A) Jablonski diagram in the TTA-UC system. (B) Demonstration of Dexter energy transfer via electron exchange between the sensitizer and emitter in TTET process and between emitters by TTA process.

TTA-UC has attracted much attention because it can tune over a wide spectral range and can be driven by low excitation light intensity (1 mW/cm^2) of non-coherent light, corresponding to AM 1.5 solar irradiance intensities and below.[21] The TTA-UC system was first reported by Parker et al. in 1962 at -66 °C or -72 °C;[22] however, the actual development for its practical application started in the early 2000s after the development of heavy metal-organic complexes with long triplet lifetimes at room temperature. In 2003, Baluschev et al. reported for the first time the TTA-UC system at room temperature as a sensitizer/emitter pair of Pd (II) octaethylporphyrin/polyfluorene exhibiting green to blue upconverted emission.[23] In addition, they reported it as a potential solution to increase the efficiency of solar cells beyond Shockley–Queisser limit.[24] After this report, TTA-UC has been extensively studied.

The upconverted emission using TTA can be achieved as follows: (ⅰ) light absorption producing an excited singlet state of the sensitizer, (ⅱ) an intersystem crossing (ISC) from the singlet excited state to the triplet excited state of the sensitizer, (ⅲ) triplet-triplet energy transfer (TTET) from the triplet excited sensitizer to emitter, producing the excited triplet state of the emitter, (ⅳ) a TTA process between two emitters with triplet excited state, producing one excited singlet state of the emitter, and finally, (ⅴ) the radiation of emission of which the energy is larger than the absorbed energy in (i) from the excited singlet state of the emitter (Figure 1-2 (A)). The TTET and TTA efficiencies strongly depend on the collision probability between the triplet excited sensitizer and emitter and two triplet excited emitters, respectively, because these processes are based on Dexter energy transfer (electron change), the photofunctional molecules must be present within the distance of 10 Å with respect to each other (Figure 1-2 (B)).[17-21] The rate of dexter energy transfer (k_{ET}) between the sensitizer and emitter is given by Equation 1,

$$k_{ET} \propto J \exp\left(\frac{-2r}{L}\right) \tag{1}$$

where r is the distance between sensitizer and emitter, L is the sum of van der Waals radius of sensitizer and emitter and J is the spectral overlap integral defined by equation 2,

$$J = \int f_D(\lambda)\, \varepsilon_A(\lambda)\, \lambda^4\, d\lambda \tag{2}$$

λ is wavelength and ε is molar absorption coefficient. The distance between the sensitizer and emitter (r < 10 Å) is the key for an electron exchange to occur. In general, the quantum yields of fluorescence and phosphorescence, which are one-photon process, are constant regardless of the excitation light intensity, while the quantum yield of TTA-UC, which

are two-photon process, depend on the collision efficiency between excited species, and thus depend on the concentration of excited species. That is, when the excitation light intensity is high, the molecular concentration of the triplet excited state increases, and the emission quantum yield increases. Monguzzi et al. proposed a method for estimating threshold excitation intensity (I_{th}) required to optimize the TTA-UC process by solving the rate equation in TTA-UC (equation 3).[25]

$$I_{th} = (8\pi\alpha\phi_{TTET}D_T a_0)^{-1}(\tau_T)^{-2} \quad (3)$$

Where α denotes absorption coefficient at the excitation wavelength, Φ_{TTET} denotes TTET efficiency from sensitizer to emitter, D_T denotes diffusion constant of triplet excited emitters, a_0 denotes the annihilation distance between triplet excited emitters, and τ_T denotes the lifetime of triplet excited emitter. Therefore, high TTET efficiency and high triplet diffusion rate lead to a decrease in I_{th}. Experimentally, it is calculated from the cross section of slopes in quadratic and linear regimes of the double-logarithm plot of upconverted emission intensity against incident laser intensity. On the other hand, the emission quantum yield is defined as the ratio of the number of emitted photons to that of absorbed photons. Therefore, the emission quantum yield of TTA-UC (Φ_{UC}), which is a 2-photon process, is up to 50%. However, most reports have standardized that the obtained upconversion quantum yield is multiplied by 2 to obtain a maximum of 100%. After all, the upconversion quantum yield is defined by the following equation 4,

$$\phi_{UC} = f\,\phi_{ISC}\,\phi_{TTET}\,\phi_{TTA}\,\phi_{Em} \quad (4)$$

where, Φ_{ISC}, Φ_{TTET}, Φ_{TTA} and Φ_{Em} denote quantum yields of sensitizer's intersystem crossing, TTET process from triplet excited sensitizer to triplet excited emitter, annihilation between two triplet excited emitters, and fluorescence from singlet excited emitter. f is the probability that the triplet excited state of the emitter generates a singlet excited state by TTA calculated from the spin statistics. Φ_{ISC} of PtOEP, which is commonly used in the study of TTA-UC, is approximately 1, and the Φ_{Em} of DPA is approximately 1. Further, when the concentrations of molecules are optimized (PtOEP: 100 μM, DPA: 10 mM, laser intensity: 100 mW/cm^2), the TTET efficiency and the TTA efficiency become approximately 1 in the liquid phase TTA-UC system.[26] Therefore, the TTA-UC yield in the liquid phase is determined by the f value. Considering the spin multiplicity, when two emitters of the triplet excited state T_1 collide, the quintet Q, the higher excited triplet state T_2, and the excited singlet state S_1 are generated at 5:3:1,

respectively. This spin statistic gives an f value of 1/9 (About 11%), but the maximum reported Φ_{UC} is much higher at 38%.[27] In the emitter typically used in TTA-UC, the quintet excited state Q is not actually generated because the energy level is too high. If the energy level of T_2 is lower than sum of that of twice T_1 and k_BT ($E(T_2) < E(2T_1) + k_BT$), T_2 and S_1 are generated at a ratio of 3:1, but T_2 is immediately relaxed to T_1 and reused, so that five T_1 produce two S_1 ($f = 2/5$). Here, k_B shows Boltzmann constant and T shows Kelvin temperature. Furthermore, if the energy level of T_2 is higher than sum of that of twice T_1 and k_BT ($E(T_2) > E(2T_1) + k_BT$), then T_2 is not generated and only S_1 is generated ($f = 1$) (Figure 1-3).[28] Regarding the above, an experimental observation of $f = 1$ in perylene as an emitter has been achieved.[28] Although the TTA-UC system in the liquid phase has been described so far, the TTA-UC system in the liquid phase has several serious problems. First, in terms of reducing environmental burden and device weight, it is not practical to incorporate volatile solvents into solar devices, although it is necessary to use low viscosity solvents that are advantageous for molecular diffusion to achieve high efficiency TTA-UC. In addition, the triplet excited state is inactivated by dissolved oxygen in organic solvent, requiring strict deoxidation conditions.

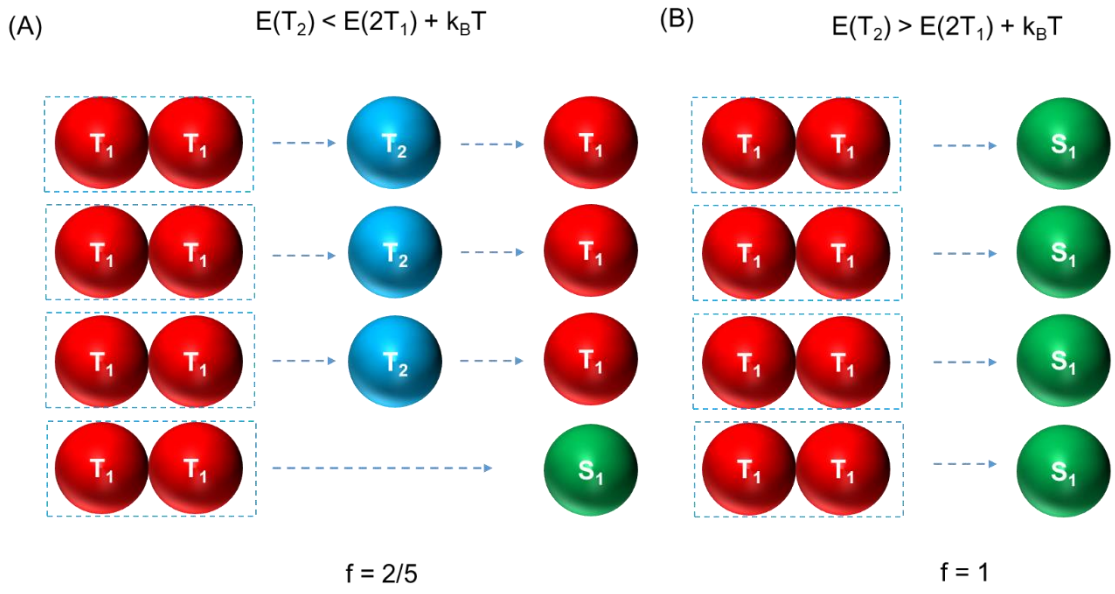

Figure 1-3. Schematic diagram of the TTA process involving four triplet pairs. (A) Probability of generation of singlet excited state when T_2 levels are lower than twice T_1 ($E(T_2) < E(2T_1) + k_BT$). (B) Probability of generation of singlet excited states when T_2 levels are higher than twice T_1 ($E(T_2) > E(2T_1) + k_BT$).

1-1-3. Triplet-Triplet Annihilation-Based Upconversion System in Solid Phase

In order to develop a TTA-UC system that can be driven in a solid phase, a polymer with a glass transition temperature (T_g) lower than room temperature was used as a nonvolatile matrix, and TTA-UC was achieved in the atmosphere without using a volatile solvent by the groups of Castellano and Weder.[29,30] However, the diffusion rate of the molecules is small in the matrix with high viscosity, and it is essentially difficult to take out the high-efficient upconverted emission with low excitation intensity, and it cannot be an ideal system. To solve the above problem, two major solutions have been proposed up to date. The first is the development of condensed photofunctional molecules systems. These systems are achieved by utilizing rapid triplet exciton diffusion in molecular assembly systems instead of conventional molecular diffusion. Thus, even in a solvent-free system, efficient TTA-UC can be achieved when the molecules accumulate at high density.[31-33] In 2015, Kimizuka et al. developed a TTA-UC system in which a sensitizer/emitter is encapsulated in a supramolecular gel matrix, and achieved highly efficient upconverted emission under air saturation conditions. This system can be driven efficiently even at the low excitation intensity such as the solar light, and TTA‐UC is very close to practical applications. (Figure 1-4).

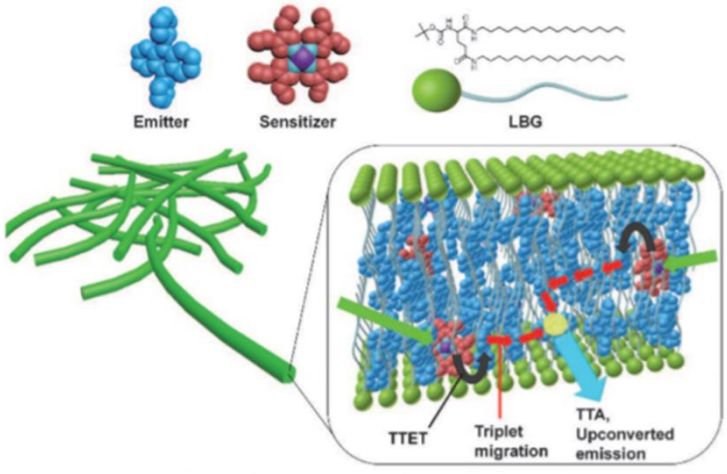

Figure 1-4. Schematic diagram of aggregation-induced TTA-UC. The unit structure of TTA-UC gel system. Sensitizer and emitter are incorporated in the nanofibers as extended domains by Ref. [31]. Reprinted with permission from *J. Am. Chem. Soc.,* **2015**, *137*, 1887. Copyright (2015) American Chemical Society.

The second is the control of the viscoelastic properties of the solid-state matrix. In a polymer matrix with a low T_g, a highly efficient TTA-UC is achieved because of the large diffusion rate of photofunctional molecules.[34-36] In 2016, Mongzzi et al. achieved a high upconversion quantum yield (Φ_{UC} = 21 %) by using polyoctyl acrylate with a low glass transition temperature (211 K) as a matrix of the TTA-UC system. As can be seen from the above research results, many studies were conducted in the 2010s to optimize the energy transfer efficiency between photofunctional molecules for practical application of TTA-UC.

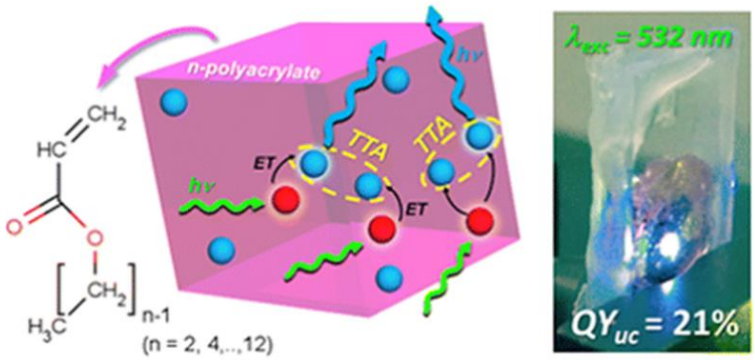

Figure 1-5. Schematic diagram of a sensitizer/emitter doped in a polyacrylate. The pictures show a DPA:PtOEP (10^{-2} M:10^{-4} M) doped poly-octylacrylate sample upon excitation at 532 nm by Ref. [36]. Reprinted with permission from *J. Phys. Chem. C,* **2016**, *120*, 2609. Copyright (2016) American Chemical Society.

1-2. Localized Surface Plasmon Resonance of Metal Nanoparticles

Metal nanoparticles, which produce the vivid colors of stained glass, have attracted much attention as advanced functional materials from a new perspective of nanotechnology. When a plane wave of light is incident on a metal nanoparticle, the electromagnetic field is disturbed due to the difference in the electrical permittivity between the metal and its surroundings. In the inside of metal nanoparticles, free electrons oscillate collectively in harmony with the incident oscillating electric field. When a certain condition is satisfied, the incident oscillating electric field resonates with the oscillation of electrons. This resonance is called localized surface plasmon (LSP) resonance.[37,38] Also, LSP resonance conditions depend on the size and shape of metal nanoparticles.

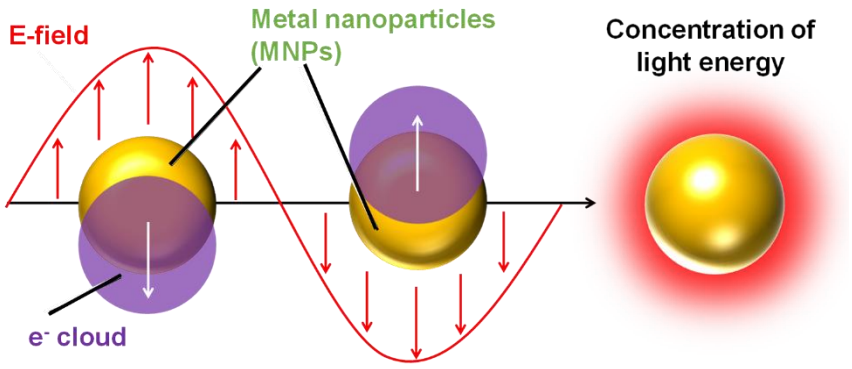

Figure 1-6. Schematic diagram of localized surface plasmon (LSP) resonance phenomenon by metal nanoparticles.

When the metal nanoparticles are spherical and much smaller than the wavelength of incident light, the electric field generated by the oscillating electrons is equivalent to the electric field generated by the dipole located at the center of the particle. Now, using the relative permittivity of the nanoparticles (ε_{np}) and the external medium (ε_{out}), the polarizability (P) of the nanoparticles with a radius (a) can be written as equation (1, 2).[39,40]

$$P = g_d \, a^3 \tag{5}$$

$$g_d = \frac{\varepsilon_{np} - \varepsilon_{out}}{\varepsilon_{np} + 2\varepsilon_{out}} \tag{6}$$

Since the electric field outside the nanoparticle (E_{out}) is approximated as the sum of the

applied electric field (E_0) and the electric field generated by the dipole, when an electric field in the x-direction is applied to the nanoparticle with radius a, E_{out} is given by

$$\boldsymbol{E}_{\text{out}} = E_0\hat{\boldsymbol{x}} - PE_0\left[\frac{\hat{\boldsymbol{x}}}{r^3} - \frac{3x}{r^5}(x\hat{\boldsymbol{x}} + y\hat{\boldsymbol{y}} + z\hat{\boldsymbol{z}})\right] \tag{7}$$

where x, y and z are unit vectors in Cartesian coordinates. This equation indicates that a stronger electric field can be obtained than is applied in the vicinity of the nanoparticles. The electromagnetic field generated by an oscillating electron is defined as a scattering field. The electric field outside the nanoparticle (E_{out}) is the sum of the incident electric field ($E_0\hat{\boldsymbol{x}}$) and the scattering field (second term in Equation 7). However, the power (W_{out}) in the medium is not the sum of the powers of the incident (W_{inc}) and scattering (W_{sca}) fields because these values are linear with respect to the square of the field. The difference between the W_{out} and the sum of the incident power and the scattering power was defined as extinction (W_{ext}).

$$W_{out} = W_{inc} + W_{sca} - W_{ext} \tag{8}$$

The energy conservation requires that the reduced amount of energy which was contained in the incident light must have been absorbed.

$$W_{out} = W_{inc} - W_{abs} \tag{9}$$

Equations 8 and 9 lead to equation 10.

$$W_{ext} = W_{sca} + W_{abs} \tag{10}$$

Taking the lowest order term of a/λ from the solution of the exact Mie theory calculation, the scattering cross section (C_{sca}), the quenching cross section (C_{ext}) and the absorption cross section (C_{abs}) are given by

$$C_{sca} = \frac{8\pi}{3}{k_{out}}^4|g_d|^2 \tag{11}$$

$$C_{ext} = C_{abs} = 4\pi k_{out} Im[g_d] \tag{12}$$

where k_{out} is the wavevector outside of the nanoparticle.[39,40] The formulas for E_{out}, C_{sca}, C_{ext} and C_{abs} contain the factor g_d and hence all of the electric field, scattering, extinction and absorption will be maximized under the condition.

$$\varepsilon_{np} = -2\varepsilon_{out} \tag{13}$$

This is called the Frölich condition and is a necessary condition for LSP resonance to occur.

1-3. Plasmonic Materials

1-3-1. Anisotropic Silver Nanoprisms

The strong electric field intensity generated by LSP resonance changes greatly depending on the metal species (Au, Ag, Cu), size, and shape (spherical, rod, cube, prism) of the nanoparticles.[41] Among various plasmonic nanomaterials, anisotropic silver nanoprisms (AgPRs) are known to exhibit particularly strong electric field intensity at the corner.[42] In addition, the LSP resonance wavelength attributed to in-plane dipole mode of AgPRs is linearly dependent on the edge length (L) and the inverse of the thickness (T).[42] The extinction spectrum for the aspect ratio obtained by the boundary element method (BEM) is shown in Figure 1-7 (refractive index of surrounding medium; 1.33), and the relation is given by $\Delta\lambda_{\mathrm{LSPR}}/\mathrm{nm} = 52.0 \times (L/T)$.[43] The facts are derived from the very small imaginary part (ε_{out}) of silver in the wavelength regions.[44]

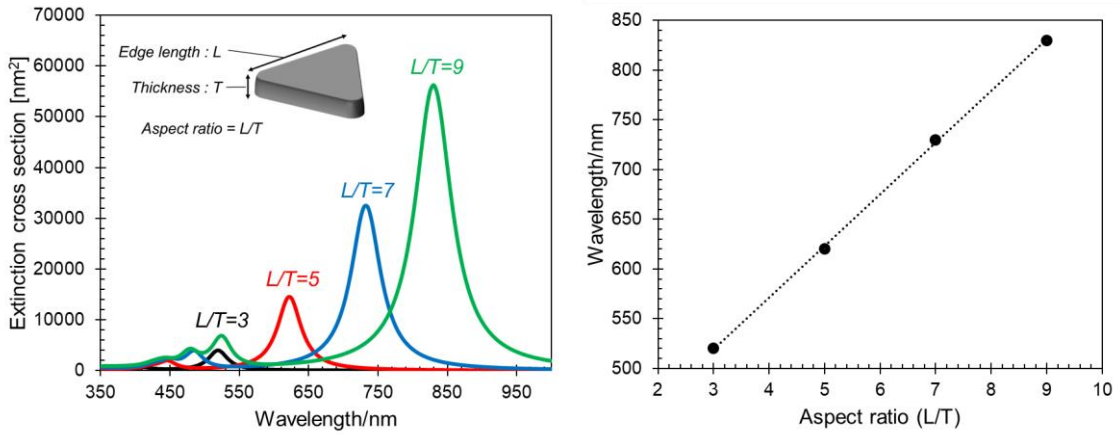

Figure 1-7. Calculated extinction spectra with varying aspect ratios (L/T) for the AgPRs by the BEM framework.

1-3-2. Chemical Synthesis

The LSP resonance wavelength of AgPRs can be controlled broadly from the visible to near infrared region by changing the aspect ratio. In general, chemical synthesis is fast and takes only a few minutes to complete. A chemical protocol to give AgPRs with a unimodal size distribution was reported by Mirkin Group in 2005.[45] The synthetic procedure was simple: $AgNO_3$ was reduced by $NaBH_4$ in the presence of trisodium citrate, poly-vinylpyrrolidone and H_2O_2. Also, it was shown that the concentration of $NaBH_4$ significantly affected the size of the formed AgPRs. Aherne, Kelly and co-workers demonstrated a highly reproducible and fast preparation method of AgPRs.[46] First, seed silver nanoparticles were synthesized by the reduction of $AgNO_3$ by $NaBH_4$ in the presence of trisodium citrate and poly(sodium styrenesulphonate) (as a stabilizer). Next, various quantities of seed solution containing ascorbic acid are added to an aqueous solution of $AgNO_3$, leading to the formation of various AgPRs with different aspect ratios.

1-3-3. Photochemical Synthesis

In 2001, Mirkin, Schatz and co-workers reported a photoinduced method for synthesizing large quantities of silver nanoparticles in high yield for the first time.[47] They discovered that the spherical shape turned to the triangular one by the photoinduced growth, when citrate-protected silver nanoparticles below 10 nm diameter were irradiated with any wavelength light. Reaction mechanism of photoinduced growth of the AgPRs has been proposed as follows.[48-50] First, light irradiation on an aqueous colloidal solution of citrate-stabilized silver nanospheres causes excitation of LSP resonance of silver nanoparticles. Next, after the deactivation of LSP, hot holes and hot electrons are generated on the AgPRs surface. Hot holes oxidize citric acid protecting silver nanoparticles, resulting in electron-rich silver nanoparticles. At the same time, some silver nanoparticles are photo-oxidized by dissolved oxygen, resulting in Ag^+ ($Ag + 1/2\ O_2 + H_2O \rightarrow Ag^+ + 2OH^-$). Finally, Ag^+ reacts with electron-rich sites of silver nanoparticles to form Ag^0, resulting in the formation of AgPRs. The familiar triangular shape of nanoprisms results from highly selective lateral growth from the edges. Silver has a face-centred cubic lattice (fcc), and the fcc crystal has sixfold symmetry around the [111] axis so a hexagonal platelet could have alternating faces ([100], [111], [100]...). [100] is less stable than [111], so the reaction proceeds more rapidly at [100] resulting in triangular silver nanoprisms.

Xue, Mirkin and co-authors succeeded in the size control of AgPRs by the change of pH of silver nanoparticle colloidal aqueous solution and the wavelength change of irradiation light. By adding NaOH to the colloidal aqueous solution under acidic conditions, the repulsion between citric acid-protected silver nanoparticles was strong, and the synthesis of AgPRs with small size was achieved. Furthermore, they found that there was a relationship between the irradiation light wavelength and the size of synthesized AgPRs. Using this approach, they succeeded in generating LSP band in a wide wavelength region from 500 nm to 1200 nm.

1-4. Effects of LSP on Optical Properties of Photofunctional Molecules

1-4-1. The emission enhancement by light-harvesting nanoantenna effect

As mentioned above, LSP resonance excitation generates a strong local electromagnetic field condensed around the metal nanoparticles. In other words, LSPR-responsive metal nanoparticles can behave as light-harvesting nanoantenna. The excitation efficiency of photofunctional molecules present in these locally enhanced electromagnetic fields is significantly enhanced. where the emission power ($P_{emission}$) is given by

$$P_{\text{emission}} = C_{Abs}\, N\, \Phi_{emssion} \tag{14}$$

$$N \propto |E|^2 \tag{15}$$

where C_{Abs}, N, $\Phi_{emission}$, and E represent the absorption cross section of the photofunctional molecules, photon flux at the wavelength of the photoexcitation, fluorescence quantum yield, and electromagnetic field strength, respectively.[51] Therefore, the emission power depends on the square of the electric field strength. In order to enhance the excitation efficiency of photofunctional molecules by the light-harvesting nanoantenna effect, it is necessary to overlap the LSP resonance wavelength of metal nanoparticles with that of molecules (Figure 1-8).

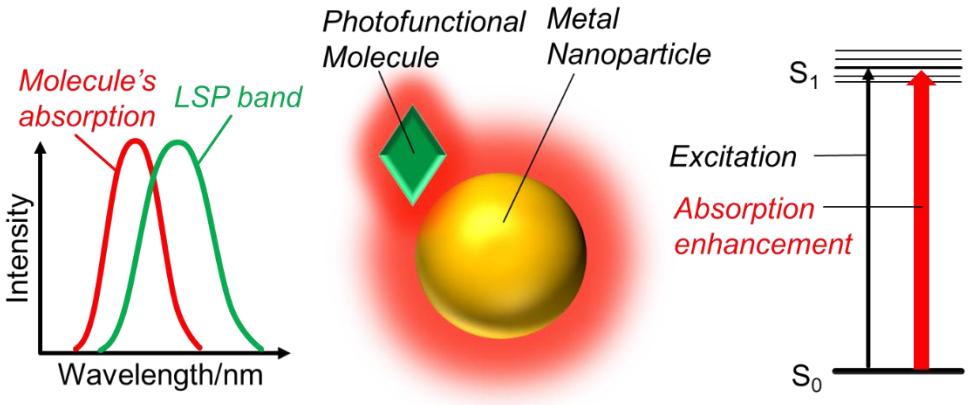

Figure 1-8. Mechanism of the excitation enhancement of photofunctional molecules by light-harvesting nanoantenna effect of metal nanoparticles.

1-4-2. The emission enhancement by acceleration of radiative decay process

In photofunctional molecules, the radiative decay rate from the excited state can be described by Fermi's golden rule as follows;

$$k_{\mathrm{rad,LSP}} = \frac{2\pi}{\hbar^2} \left|M_{if}\right|^2 \rho(\omega) \tag{16}$$

where M_{if} and $\rho(\omega)$ are the transition matrix element between the initial and the final states and the local density of optical states (LDOS), respectively. The LDOS can be modified by changes in the surrounding environment, resulting in a change of the radiative decay rate. Next, we would like to consider the radiative decay rate when a photofunctional molecules are present near a metal nanoparticle that exhibits LSP resonance. The LDOS can be significantly changed by the strong electric field generated by plasmons. When the LSP band overlaps with the fluorescence wavelength of the photofunctional molecule, the LDOS depends on the excitation probability of the LSPR (Figure 1-9)., so the following equation is obtained

$$\frac{k_{rad,LSP}}{k_{rad}} = \frac{3}{4\pi^2} \left(\frac{\lambda_{rad} Q}{n^3 V}\right) \tag{17}$$

where k_{rad}, Q, V, and n are the radiative decay rate in the absence of the metal nanoparticles, quality factor, mode volume of the LSPR, and refractive index of the surrounding medium, respectively. This formula indicates that a higher Q value and a lower V value provide a large enhancement factor of radiative decay rate in photofunctional molecules.

The emission quantum yield of the photofunctional molecules in the absence of the metal nanoparticles given by,

$$\phi_{emission} = \frac{k_{rad}}{k_{rad} + k_{nonrad}} \tag{18}$$

Where k_{nonrad} is the non-radiative decay rate of the photofunctional molecules. The quantum yield modified by changing in the presence of LSP resonance-responsive metal nanoparticles is described follows

$$\phi_{emission,LSP} = \frac{k_{rad} + k_{rad,LSP}}{k_{rad} + k_{rad,LSP} + k_{nonrad} + k_{nonrad,LSP}} \quad (19)$$

where $k_{rad,LSP}$ and $k_{nonrad,LSP}$ are increase in the radiative decay rate by the presence of metal nanoparticles and the nonradiative decay rate through the nonradiative energy transfer.[52]

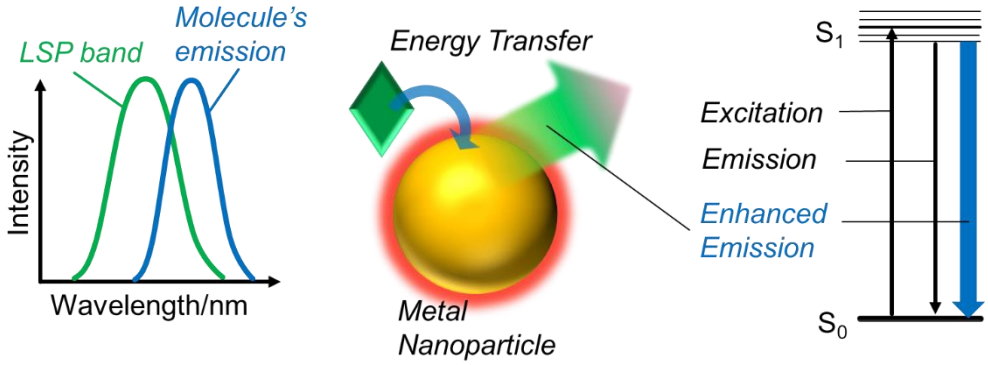

Figure 1-9. Mechanism of the emission enhancement of photofunctional molecules by plasmon-exciton coupling effect of metal nanoparticles.

1-5. Plasmon-enhanced TTA-UC emission

Recently, the TTA-UC emission was successfully enhanced by the effect of the LSP resonance of metal nanoparticles. In 2014, Timothy L. Kelly and co-workers report a plasmon-based enhancement of the TTA-UC process with silver nanoplates embedded in poly(methyl methacrylate) thin films containing the upconverting materials palladium(II) octaethylporphyrin as a sensitizer and 9,10-diphenylanthracene as an emitter (Figure 1-10 (A)).[53] In 2016, Jae-Hong. Kim and co-workers report a plasmon-enhanced sub-bandgap photocatalyst device with a TTA-UC system by using silica (SiO_2) spheres coated with closely assembled silver nanoparticles (AgNPs) as a plasmonic materials (Figure 1-10 (B)).[54] As described above, enhancement of TTA-UC emission has been achieved by using silver nanoplates and silver nanoparticles as plasmonic materials; however, the mechanism of enhancement of the TTA-UC system is unclear. The effect of LSP resonance on TTA-UC is quite complex because TTA-UC includes complicated multiple photoinduced processes.

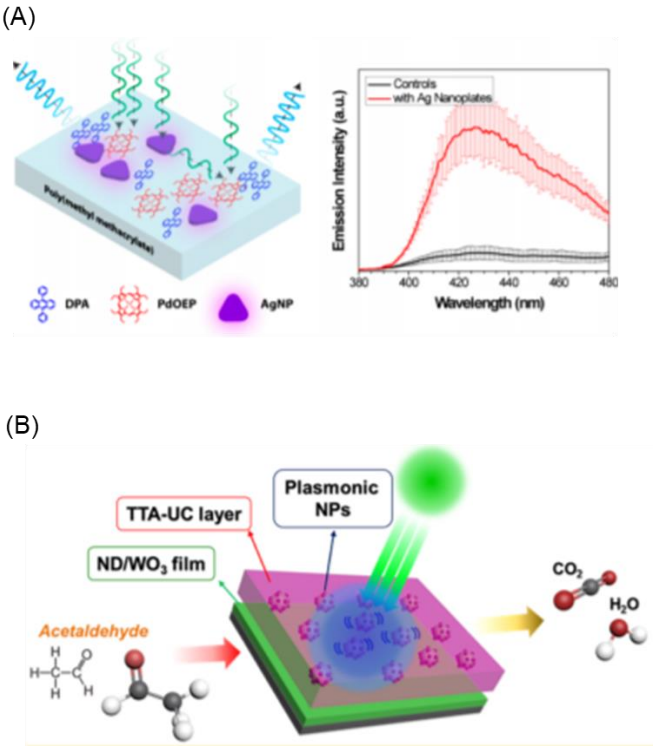

Figure 1-10. Plasmon-enhanced TTA-UC systems using (A) silver nanoplates and (B) silica nanoparticles doped with silver nanoparticles as a plasmonic materials by Ref. [53, 54]. Reprinted with permission from *J. Phys. Chem. C*, **2014**, *118*, 6398. and *Environ. Sci. Technol.* **2016**, *50*, 11184. Copyright (2014 and 2016) American Chemical Society.

1-6. Photon Upconversion-Based Photothermal Conversion in Metal Nanoparticles

Dephasing of LSP resonance of metal nanoparticles leads to absorption of photons.[55] This accumulates energy in the electron distribution, creating excited electrons that spread to different levels in the conduction band.[56] Energy can be deposited on the electron distribution by excitation by inter-band or intra-band metal transitions.[57] The excited electrons are rapidly equilibrated by electron scattering on a time scale of several 100 fs to form a hot electron distribution.[58] The hot electron distribution relaxes phonons on a time scale of several picoseconds, resulting in the generation of thermal energy near nanoparticles.

Gold nanospheres with diameters of several tens of nanometers are activated by light from the ultraviolet region to the approximately 600 nm region due to strong inter-band transitions below ~500 nm and strongly excited LSP resonance from 500 to 600 nm.[59] However, irradiation with longer wavelengths of light (> 600 nm) does not produce efficient heat generation because of its lower light-harvesting ability (Figure 1-11). Photothermal conversion materials driven by sunlight are required to efficiently convert sunlight in a wide wavelength range into thermal energy. In nanotherapy, photothermal conversion should be efficiently induced in the 600~1300 nm wavelength region corresponding to the biological transparency window. To solve this problem, photon upconversion phenomena have recently attracted attention. That is, it becomes possible to broaden the drivable wavelength of the photothermal conversion material by converting the long wavelength light in which the gold nanoparticle cannot absorb into the usable short wavelength light. Inorganic nanoparticles composed of rare earth ions such as Yb^{3+}, Er^{3+} and Nd^{3+} are often utilized as upconversion nanoparticles (UCNP). Efficient near-infrared light-driven photothermal conversion has recently been achieved using a hybrid system of gold nanospheres and UCNP.[60] However, the use of UCNP has several significant problems, including the need for rare earth elements with limited supply, difficulty in tuning the absorption/emission wavelength, and the narrowness of the emission/absorption band.[61-63] Therefore, the development of an alternative upconversion system for photothermal conversion is an important issue.

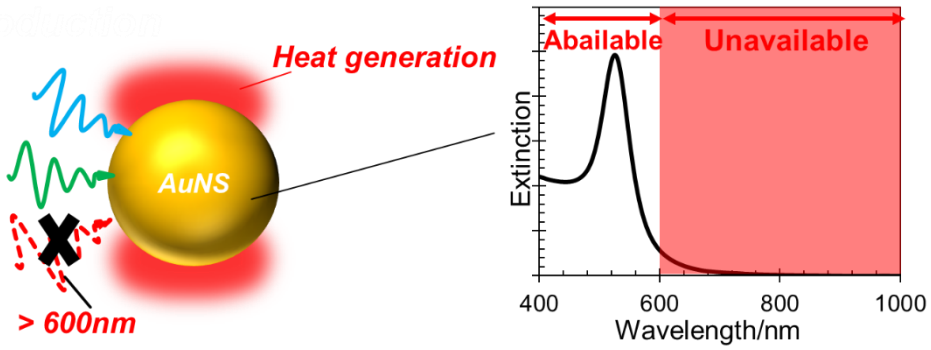

Figure 1-11. Driving wavelength range of gold nanoparticles for photothermal conversion.

1-7. Object and Outline of This Dissertation

The problems mentioned above are summarized below. TTA-UC has attracted much attention because it can tune over a wide spectral range and can be driven by low-intensity non-coherent light, corresponding to AM 1.5 solar irradiance intensities and below. Since the photoreaction process of TTA-UC proceeds by a dexter mechanism, that is, diffusional collision of molecules, a high quantum yield is expected in a liquid phase. Considering the application of TTA-UC to photovoltaic devices, a solid phase system is required from the viewpoint of reducing environmental load and weight. However, in the solid phase, the diffusion of molecules is suppressed, and the lowering of the quantum yield is worried. Recently, the enhancement of TTA-UC emission has been achieved by using plasmonic materials; however, the mechanism of enhancement of the TTA-UC system is unclear. The effect of LSP resonance on TTA-UC is quite complex because TTA-UC includes complicated multiple photoinduced processes.

Also, gold nanospheres with diameters of several tens of nanometers were activated by light from the ultraviolet region to the approximately 600 nm region due to strong inter-band transitions below ~500 nm and strongly excited LSP resonance from 500 to 600 nm. That is, irradiation with longer wavelengths of light (> 600 nm) does not produce efficient heat generation because of its lower light-harvesting ability.

We tried to solve the above problems by investigating the optical interaction between plasmonic metal nanoparticles and a TTA-UC system. Specifically, we focused our research on the following four phenomena.

The first is the enhancement of the excitation efficiency of sensitizer by the light-harvesting nanoantenna effect of LSP resonance. By making the absorption wavelength of the sensitizer and LSP resonance wavelength overlapped, the light absorption ability is significantly enhanced.

The second is to accelerate the fluorescence decay rate of emitter by the plasmon-exciton coupling effect of LSP resonance. By making the fluorescence of the emitter and LSP resonance wavelengths overlapped, the radiative process of the emitter is significantly accelerated, leading to enhancement of the fluorescence quantum yield.

Third, we focused on how to prevent the acceleration of the phosphorescence decay rate of sensitizers by plasmon-exciton coupling effect of LSP resonance. We revealed the phosphorescence decay process of the sensitizer is accelerated, leading to the obstruction of energy transfer (TTET) to the emitter by overlapping the phosphorescence wavelength of the sensitizer and the LSP resonance wavelength. The effect of phosphorescence enhancement on the whole TTA-UC system have not been considered in the studies aiming at the efficiency improvement of TTA-UC by plasmons reported so far. This

discovery will be an important guideline for improving the efficiency of TTA-UC by plasmon. These are discussed in detail in chapter 2. In chapter 3, we found a way to prevent phosphorescence enhancement of the sensitizer, which has a negative effect on TTA-UC. In particular, the larger the spin-orbit coupling constant of the sensitizer, the sensitizer is less susceptible to phosphorescence enhancement by plasmon-exciton coupling, resulting in suppression of upconversion quenching.

The fourth is not an improvement of the TTA-UC system by plasmons of metal nanoparticles, but a modification of the photothermal conversion characteristics of plasmon-responsive gold nanoparticles by the TTA-UC system. We succeeded in broadening the driving wavelength for photothermal conversion of gold nanoparticles by TTA-UC system. These are discussed in detail in Chapter 4.

In Chapter 5, this thesis is summarized. We found guidelines to optimize plasmon-enhancement of TTA-UC by investigating in detail how plasmons interact with TTA-UC systems with complicated photoreactive processes such as TTET and TTA. We also succeeded in broadening the driving wavelength for photothermal conversion of gold nanoparticles by introducing the TTA-UC system. Thus, we clarified that the enhancement and quenching effects coexist in the interaction between TTA-UC and plasmons. We also showed the possibility of the application of TTA-UC.

1-8. References

(1). Lewis, N. S.; Nocera, D. G. Powering the planet: Chemical challenges in solar energy utilization. *Proc. Natl. Acad. Sci.,* **2006**,*103*, 15729-15735.

(2). Jin, H., H.; Sang, H., I.; Jun, H., N.; Tarak, N., M.; Choong-Sun, L.; Jeong, A., C.; Yong, H., L.; Hi-jung, K.; Arpita, S.; Nazeeruddin, M. K.; Michael, G.; Sang, I. S. Efficient inorganic–organic hybrid heterojunction solar cells containing perovskite compound and polymeric hole conductors. *Nat. Photonics*, **2013**, *7*, 486-491.

(3). Bing, C.; Yedi, X.; Zhou, Y.; Wen-Hua, Z.; Jieshan, Q. High performance hybrid solar cells sensitized by organolead halide perovskites. *Energy Environ. Sci*. **2013**, *6*, 1480-1485.

(4). Jun, H., N.; Sang, H. I.; Jin, H., H.; Tarak, N., M.; Sang, I., S. Chemical Management for Colorful, Efficient, and Stable Inorganic–Organic Hybrid Nanostructured Solar Cells. *Nano Lett*. **2013**, *1*, 1764-1769.

(5). James, M., B.; Michael, M., L.; Andrew, H.; Henry, J., S. Low-temperature processed meso-superstructured to thin-film perovskite solar cells. *Energy Environ. Sci*. **2013**, *6*, 1739-1743.

(6). Snaith, H. J. Perovskites: The Emergence of a New Era for Low-Cost, High-Efficiency Solar Cells. *J. Phys. Chem. Lett*., **2013**, *4*, 3623-3630.

(7). Wonyong, C.; Andreas, T.; Michael, R., H. The Role of Metal Ion Dopants in Quantum-Sized TiO_2: Correlation between Photoreactivity and Charge Carrier Recombination Dynamics. *J. Phys. Chem*., **1994,** *67*, 13669-13679.

(8). Sato, S. Photocatalytic activity of NO_x-doped TiO_2 in the visible light region. *Chem. Phys. Lett.* **1986***, 123*, 126-128.

(9). Takeo, A.; Masatoshi, Y.; Yoshinari, K.; Yasukazu, I.; Hideki, S.; Kazuhiro, S. Efficient Complete Oxidation of Acetaldehyde into CO_2 over $CuBi_2O_4/WO_3$ Composite Photocatalyst under Visible and UV Light Irradiation. *J. Phys. Chem. C* **2007**, *111*, 7574-7577.

(10). David, H.; Franz, G. Kinetics of hydrogen production from illuminated $CdS/Pt/Na_2SO_3$ and $ZnS/Pt/Na_2S$ dispersions. *J. Chem. Soc. Faraday Trans*. **1990**, *86,* 3637-3640.

(11). Luo, Y.; Guojian, L.; Xiaoshu, Z.; Xin B.; Guodong, S.; Yong, L.; Po, K., W.; Jimmy, C., Y.; Ying, Y. Enhanced Activity and Stability of Carbon-Decorated Cuprous Oxide Mesoporous Nanorods for CO_2 Reduction in Artificial Photosynthesis. *ACS Catal.* **2016**, *6*, 6444-6454.

(12). Feng, W.; Debapriya, B.; Yongsheng, L.; Xueyuan, C.; Xiaogang, L. Upconversion nanoparticles in biological labeling, imaging, and therapy. *Analyst*, **2010**, *135*, 1839-1854.

(13). Guanying, C.; Hailong, Q.; Paras, N., P.; Xiaoyuan, C. Upconversion Nanoparticles: Design, Nanochemistry, and Applications in Theranostics. *Chem. Rev*., **2014**, *114*, 5161-5214.

(14). Meng, W.; Cong-Cong, M.; Wen-Xing, W.; Cui-Hong, L.; Ying-Fan, W.; Zhang-Run, X.; ChuanBin, M.; Shu-Kun, X. Immunolabeling and NIR-Excited Fluorescent Imaging of HeLa Cells by Using $NaYF_4$:Yb,Er Upconversion Nanoparticles. *ACS Nano,* **2009**, *3*, 1580-1586.

(15). Xiaoji, X.; Nengyue, G.; Renren, D.; Qiang, S.; Qing-Hua, X.; Xiaogang, L. Mechanistic Investigation of Photon Upconversion in Nd^{3+}-Sensitized Core−Shell Nanoparticles. *J. Am. Chem. Soc.,* **2013**, *135*, 12608-12611.

(16). Daqin, C.; Lu, L.; Ping, H.; Mingye, D.; Jiasong, Z.; Zhenguo, J. Nd^{3+}-Sensitized Ho^{3+} Single-Band Red Upconversion Luminescence in Core-Shell Nanoarchitecture. *J. Phys. Chem. Lett*., **2015**, *6*, 2833-2840.

(17). Monguzzi, A.; Tubino, R.; Hoseinkhani, S.; Campione, M.; Meinardi, F. Low power, non-coherent sensitized photon up-conversion: modelling and perspectives. *Phys. Chem. Chem. Phys*. **2012**, *14*, 4322-4332.

(18). Gray, V.; Dzebo, D.; Abrahamsson, M.; Albinsson, B.; MothPoulsen, K. Triplet–triplet annihilation photon-upconversion: towards solar energy applications. *Phys. Chem. Chem. Phys.* **2014**, *16*, 10345-10352.

(19). Baluschev, S.; Miteva, T.; Yakutkin, V.; Nelles, G.; Yasuda, A.; Wegner, G. Up-Conversion Fluorescence: Noncoherent Excitation by Sunlight. *Phys. Rev. Lett.* **2006**, *97*, 143903/1-143903/3.

(20). Duan, P.; Yanai, N.; Kimizuka, N. Photon Upconverting Liquids: Matrix-Free Molecular Upconversion Systems Functioning in Air. *J. Am. Chem. Soc*. **2013**, *135*, 19056-19059.

(21). Cao, X.; Hu, B.; Zhang, P. High Upconversion Efficiency from Hetero Triplet−Triplet Annihilation in Multiacceptor Systems. *J. Phys. Chem. Lett.* **2013**, *4*, 2334-2338.

(22). Parker, C. A.; Hatchard, C. G. *Proc. R. Soc. London, Ser. A* **1962**, 386-387.

(23). Keivanidis, P. E.; Baluschev, S.; Miteva, T.; Nelles, G.; Scherf, U.; Yasuda, A.; Wegner, G. Up‐Conversion Photoluminescence in Polyfluorene Doped with Metal(II)–Octaethyl Porphyrins. *Adv. Mater.* **2003**, *15*, 2095-2098.

(24). Baluschev, S.; Miteva, T.; Yakutkin, V.; Nelles, G.; Yasuda A.; Wegner, G. Up-Conversion Fluorescence: Noncoherent Excitation by Sunlight. *Phys. Rev. Lett.* **2006**, *97, 143903*/1–*143903*/3.

(25). Monguzzi, A.; Mezyk, J.; Scotognella, F.; Tubino, R.; Meinardi, F. Upconversion-induced fluorescence in multicomponent systems: Steady-state excitation power threshold. *Physical Review B* **2008**, *78*, 195112/1-195112/5.

(26). Monguzzi, A.; Tubino, R.; Hoseinkhani, S.; Campione, M.; Meinardi, F. Low power, non-coherent sensitized photon up-conversion: modelling and perspectives. *Phys. Chem. Chem. Phys*. **2012**, *14*, 4322-4332.

(27). Hoseinkhani, S.; Tubino, R.; Meinardi, F.; Monguzzi, A. Achieving the Photon Up-conversion Thermodynamic Yield Upper Limit by Sensitized Triplet-triplet Annihilation. *Phys. Chem. Chem. Phys*. **2015** *17*, 4020-4024.

(28). Schmidt , T., W.; Castellano, F., N. Photochemical Upconversion: The Primacy of Kinetics. *J. Phys. Chem. Lett.* **2014**, *5*, 4062-4072.

(29). Islangulov, R., R.; Lott, J.; Weder, C.; Castellano F. N. Noncoherent Low-Power

Upconversion in Solid Polymer Films. *J. Am. Chem. Soc.* **2007**, *129*, 12652-12653.
(30). Singh-Rachford, T., N.; Lott, J.; Weder, C.; Castellano, F., N. Influence of Temperature on Low-Power Upconversion in Rubbery Polymer Blends. *J. Am. Chem. Soc.* **2009**, *131*, 12007-12014.
(31). Duan, P.; Yanai, N.; Nagatomi, H.; Kimizuka, N. Photon Upconversion in Supramolecular Gel Matrices: Spontaneous Accumulation of Light-Harvesting DonorAcceptor Arrays in Nanofibers and Acquired Air Stability. *J. Am. Chem. Soc.* **2015**, *137*, 1887-1894.
(32). Vadrucci, R.; Weder, C.; Simon, Y., C. Low-power photon upconversion in organic glasses. *J. Mater. Chem. C* **2014**, *2*, 2837-2841.
(33). Duan, P.; Yanai, N.; Kurashige, Y.; Kimizuka, N. *Angew. Chem. Int. Ed.* **2015**, *54*, 7544.
(34). Kim, J.-H.; Deng, F.; Castellano, F., N.; Kim, J.-H. High Efficiency Low-Power Upconverting Soft Materials. *Chem. Mater.* **2012**, *24*, 2250-2252.
(35). Monguzzi, A.; Bianchi, F.; Bianchi, A.; Mauri, M.; Simonutti, R.; Ruffo, R.; Tubino, R.; Meinardi, F. High Effi ciency Up-Converting Single Phase Elastomers for Photon Managing Applications. *Adv. Energy Mater.* **2013**, *3*, 680-686.
(36). Monguzzi, A.; Mauri, M.; Bianchi, A.; Dibbanti, M., K.; Simonutti, R.; Meinardi, F. Solid-State Sensitized Up-Conversion in Polyacrylate Elastomers. *J. Phys. Chem. C* **2016**, *120*, 2609-2614.
(37). Maier, S. A.; and Atwater, H. A. Plasmonics: Localization and guiding of electromagnetic energy in metal/dielectric structures. *J. Appl. Phys.* **2005**, *98*, 011101/1-011101/10.
(38). Coronado, E. A.; Encina, E. R.; Stefani, F. D. Optical properties of metallic nanoparticles: manipulating light, heat and forces at the nanoscale. *Nanoscale* **2011**, *3*, 4042-4059.
(39). Kelly, K., L.; Coronado, E.; Zhao, L., L.; Schatz, G., C. The Optical Properties of Metal Nanoparticles: The Influence of Size, Shape, and Dielectric Environment. *J. Phys. Chem. B* **2003**, *107*, 668-677.
(40). Willets, K., A.; Van, D., R., P. Localized Surface Plasmon Resonance Spectroscopy and Sensing. *Annu. Rev. Phys. Chem.* **2007**, *58*, 267-297.
(41). Hao, E.; Schatz, G. C. Electromagnetic fields around silver nanoparticles and dimers. *J. Chem. Phys.* **2004**, *120*, 357-366.
(42). Knauer, A.; Koehler, J., M. Explanation of the size dependent in-plane optical resonance of triangular silver nanoprisms. *Phys. Chem. Chem. Phys.* **2016**, *18*, 15943-15949.
(43). Waxenegger, J.; Trügler, A.; Hohenester, U. Plasmonics simulations with the MNPBEM toolbox: Consideration of substrates and layer structures. *Comput. Phys. Commun.* **2015**, *193*, 138-150.
(44). Johnson, R., B.; Christy, R., W. Optical Constants of the Noble Metals. *Phys. Rev. B* **1972**, *6*, 4370-4379.

(45). Métraux G. S.; Mirkin, C. A. Rapid Thermal Synthesis of Silver Nanoprisms with Chemically Tailorable Thickness. *Adv. Mater.* **2005**, *17*, 412–415.
(46). Aherne, D.; Ledwith, D., M.; Gara, M.; Kelly, J., M. Optical Properties and Growth Aspects of Silver Nanoprisms Produced by a Highly Reproducible and Rapid Synthesis at Room Temperature. *Adv. Funct. Mater.* **2008**, *18*, 2005-2016.
(47). Jin, R.; Cao, Y.; Mirkin, C. A.; Kelly, K. L.; Schatz G. C.; Zheng, J. G. Photoinduced Conversion of Silver Nanospheres to Nanoprisms. *Science* **2001**, *294*, 1901-1903.
(48). Jin, R.; Cao, Y., C.; Hao, E.; Metraux, G., S.; Schatz, G., C.; Mirkin, C., A. Controlling anisotropic nanoparticle growth through plasmon excitation. *Nature* **2003**, *425*, 487-490.
(49). Wu, X.; Redmond, P., L.; Liu, H.; Chen, Y.; Steigerwald, M.; Brus, L. Photovoltage Mechanism for Room Light Conversion of Citrate Stabilized Silver Nanocrystal Seeds to Large Nanoprisms. *J. Am. Chem. Soc.* **2008**, *130*, 9500-9506.
(50). Langile, M., R.; Personick, M., L.; Mirkin, C., A. Plasmon-Mediated Syntheses of Metallic Nanostructures. *Angew. Chem. Int. Ed.* **2013**, *52*, 13910-13940.
(51). Deng, W.; Xie, F.; Baltar, H. T. M. C. M.; Goldys, E. M. Metal-enhanced fluorescence in the life sciences: here, now and beyond. *Phys. Chem. Chem. Phys.* **2013**, *15*, 15695-15708.
(52). Giannini, V.; Fernández-Domínguez, A.I.; Sonnefraud, Y.; Roschuk, T.; Fernández-García, R.; Maier, S.A. Controlling Light Localization and Light–Matter Interactions with Nanoplasmonics. *Small* **2010**, *6*, 2498-2507.
(53). Poorkazem, K.; Hesketh, A., V.; Kelly, T., L. Plasmon-Enhanced Triplet−Triplet Annihilation Using Silver Nanoplates. *J. Phys. Chem. C* **2014**, *118*, 6398-6404.
(54). Hyoung-Il, K.; Weon, S.; Kang, H.; Hagstrom, A., L.; Kwon, O., S.; Lee, Y.-S.; Choi, W.; Kim, J.-H. Plasmon-Enhanced Sub-Bandgap Photocatalysis via Triplet−Triplet Annihilation Upconversion for Volatile Organic Compound Degradation. *Environ. Sci. Technol.* **2016**, *50*, 11184-11192.
(55). Kreibig, U.; Vollmer, M. *Springer-Verlag: Berlin*, **1995**.
(56). Voisin, C.; Del, F., N.; Christofilos, D.; Vallee, F. Ultrafast Electron Dynamics and Optical Nonlinearities in Metal Nanoparticles. *J. Phys. Chem. B* **2001**, *105*, 2264-2280.
(57). Del, F., N.; Voisin, C.; Achermann, M.; Tzortzakis, S.; Christofilos, D.; Vallee, F. Nonequilibrium electron dynamics in noble metals. *Phys. Rev. B* **2000**, *61*, 16956-16966.
(58). Fann, W., S.; Storz, R.; Tom, H., W., K.; Bokor, J. Direct Measurement of Nonequilibrium Electron-Energy Distributions in Subpicosecond Laser-Heated Gold Films. *Phys. Rev. Lett.* **1992**, *68*, 2834-2837.
(59). Jiang, K.; Smith, D. A.; Pinchuk, A. Size-Dependent Photothermal Conversion Efficiencies of Plasmonically Heated Gold Nanoparticles. *J. Phys. Chem. C* **2013**, *117,* 27073-27080.
(60). Cai, H.; Shen, T.; Kirillov, A. M.; Zhang, Y.; Shan, C.; Li, X.; Liu, W.; Tang, Y. Self-

Assembled Upconversion Nanoparticle Clusters for NIRcontrolled Drug Release and Synergistic Therapy after Conjugation with Gold Nanoparticles. *Inorg. Chem.* **2017**, *56*, 5295-5304.
(61). Wu, X.; Zhang, Y.; Takle, K.; Bilsel, O.; Li, Z.; Lee, H.; Zhang, Z.; Li, D.; Fan, W.; Duan, C.; Chan, E. M.; Lois, C.; Xiang, Y.; Han, G. Dye Sensitized Core/ Active Shell Upconversion Nanoparticles for Optogenetics and Bioimaging Applications. *ACS Nano* **2016**, *10*, 1060-1066.
(62). Chen, G.; Damasco, J.; Qiu, H.; Shao, W.; Ohulchanskyy, T. Y.; Valiev, R. R.; Wu, X.; Han, G.; Wang, Y.; Yang, C.; Ågren, H.; Prasad, P. N. Energy Cascaded Upconversion in an Organic Dye-Sensitized Core/Shell Fluoride Nanocrystal. *Nano Lett.* **2015**, *15*, 7400-7407.
(63). Carnall, W. T.; Goodman, G. L.; Rajnak, K.; Rana, R. S. A systematic analysis of the spectra of the lanthanides doped into single crystal LaF_3. *J. Chem. Phys.* **1989**, *90*, 3443-3457.

Chapter 2

Improvement of Upconverted Emission Efficiency by Precisely-Tuning Plasmon Wavelength

2-0. Abstract

In this study, we demonstrate that the localized surface plasmon (LSP) resonance of metal nanoparticles, depending strictly on the generating wavelength of LSP resonance, can have both beneficial enhancement and harmful quenching effects on a triplet−triplet annihilation-based upconversion (TTA-UC) emission. When the LSP resonance band of anisotropic silver nanoprisms spectrally overlapped with the photoexcitation wavelength of a sensitizer and the fluorescence of an emitter, an increase in the photoexcitation efficiency and an acceleration of the radiative decay rate were respectively induced, resulting in an effective enhancement in the TTA-UC emission. Furthermore, the overlapping with the photoexcitation wavelength led to a significant decrease (93%) in the threshold light excitation intensity, which greatly enhances the figure-of-merit in TTA-UC systems. However, when the LSP resonance band overlapped with the phosphorescence band of the sensitizer, the TTA-UC emission was extremely quenched, accompanied by the enhanced phosphorescence and the decreased phosphorescence lifetime. These results suggest that the decrease in the TTA-UC emission is a result of the competition between the triplet−triplet energy transfer to the emitter and the LSP-induced nonradiative energy transfer to the silver nanoprisms from the triplet-excited sensitizer. This discovery of the conflicting effects of LSP resonance provides an important guideline: a precise adjustment of LSP resonance wavelengths is needed for the efficient enhancement of TTA-UC emission. This requirement is different from those of other fluorescence systems such as single downconverted fluorophores and lanthanide-based upconversion nanoparticles.

2-1. Introduction

The development of solar-energy-driven photoelectronic devices, including semiconductor photocatalysts and solar cells, is one of the most promising strategies for the renewable low carbon society. Active wavelengths of these devices are inherently limited by the bandgap energy (E_g) of the photofunctional materials.[1,2] Recently, photon upconversion techniques have been proposed as a useful way of overcoming the "bandgap limit." In the case where the two photons with low energies are efficiently converted into a single photon with a high energy, the wide bandgap materials can be utilized.[3−7] Currently, upconversion systems consisting of two photofunctional molecules of a sensitizer and an emitter based on a triplet−triplet annihilation (TTA) phenomenon have attracted much attention because the upconverted emission can be generated even by the irradiation of low-intensity noncoherent light such as sunlight.[8−10] The TTA occurs in the following sequence: (i) the singlet excited sensitizer, which is generated by irradiating long-wavelength light, is rapidly converted to a triplet excited sensitizer through the intersystem crossing, (ii) the triplet excitation energy of the sensitizer transfers to an emitter through the Dexter-type triplet−triplet energy transfer (TTET) mechanism, resulting in the formation of a triplet excited emitter, (iii) the TTA between the two resultant triplet-excited state emitters leads to a single excited state of one emitter, and finally, (iv) the emission occurs from the singlet excited state. The emitter molecules should rapidly diffuse and come into collision during their excited state lifetime for efficient TTET and TTA to occur. In several recent researches, the triplet−triplet annihilation-based upconversion (TTA-UC) systems in a liquid phase have shown quantum yields around 30%.[11−13] On the other hand, considering the practical applications to the above-mentioned optoelectronic devices, the achievement of a high quantum yield in solventfree TTA-UC systems is essential. However, the quantum yield of TTA-UC systems in solid matrices suffers from a significant decrease by restricted diffusion of the emitter molecules. To solve this critical issue, two efficient solutions have been suggested recently. The first is the development of condensed chromophore systems. In these systems, the utilization of the high mobility of exciton instead of molecular diffusion leads to an efficient TTA-UC in solid-state matrices.[11,14−16] The second solution is the control of the macroscopic viscoelastic properties of the solid-state matrix. A matrix having a low glass transition temperature (T_g) was employed to obtain a large translational diffusivity of molecules, thereby resulting in an efficient TTA-UC.[17−21] While the TTA-UC efficiency was improved by the above strategies, the efficiency improvement by strengthening the interplay between the photofunctional molecules and light should also be attempted as a useful complementary approach. The optical interplay between the

strong local electromagnetic fields generated by the excitation of localized surface plasmon (LSP) resonance of noble metal nanoparticles[22−24] and photofunctional molecules has led to a considerable enhance ment of the photocurrent through a photoinduced intermolecular electron transfer reaction[25−32] and downconverted fluorescence generated by the relaxation from the singlet excited state.[33−41] The photocurrent enhancement originates from the enhancement of the photoexcitation efficiency of a dye molecule by the light-harvesting nanoantenna effect of plasmonic metal nanoparticles. The fluorescence enhancement can be explained mainly by the acceleration of the radiative decay rate from the excited state by plasmon−exciton coupling as well as the photoexcitation enhancement. Recently, the emission generated via the TTA-UC phenomenon was successfully enhanced by the effect of the LSP resonance of noble metal nanoparticles.[42−46] Although the enhancement of the photoexcitation efficiency of sensitizer is expected to enhance the emission,[47] the mechanism for the enhancement in the case of the TTA-UC systems is still unclear. The effect of LSP resonance on TTA-UC can be quite complex because TTA-UC includes complicated multiple photoinduced processes. In this study, we found that the LSP resonance has a beneficial enhancement and a harmful quenching effects strongly depending on the generating wavelength in solidstate TTA-UC systems. It was experimentally evaluated that while the photoexcitation enhancement of the sensitizer as well as the acceleration in the radiative decay process of the emitter leads to a beneficial enhancement of the TTA-UC emission, a significant decrease in the emission is induced by suppressing the TTET process as a result of the competition with the LSPinduced energy transfer to the plasmonic metal nanoparticles. We suggest that the results obtained in this study provide important guidelines for the tuning of the optical interplay between LSP resonance and photofunctional molecules toward the design of highly efficient plasmonic TTA-UC systems. Furthermore, we succeeded in significantly decreasing the threshold excitation intensity (I_{th}; the useful figure of merit of TTA-UC emission) by 93% with the light-harvesting nanoantenna effect of LSP resonance, indicating that the LSP resonance is capable of achieving a highly efficient TTA-UC in a solid-state matrix by the irradiation of weaker noncoherent excitation light.

2-2. Experimental Section

Materials.

Milli-Q-grade water was used to prepare all aqueous solutions. Sodium tetrahydroborate ($NaBH_4$, Wako Pure Chemical Industries), trisodium citrate dihydrate (Kanto Chemical Co.), silver nitrate ($AgNO_3$, Wako Pure Chemical Industries), sodium hydroxide (NaOH, Kanto Chemical Co), PEI (MW = 50000−100000), Sigma-Aldrich), ammonium solution (NH_3, 28%, Kanto Chemical Co.), hydrogen peroxide solution (H_2O_2, 30%, Kanto Chemical Co.), Pd-TPTBP (Funakoshi Co.), BPEA (Tokyo Chemical Industry), N,Ndimethylformamide (DMF, 99.5%, Wako Pure Chemical Industries), ethanol (99.5%, Kishida Chemical Co.), ODT (Wako), and poly(vinyl alcohol) (PVA, MW: 31000−50000, Sigma-Aldrich) were used as received.

Synthesis of AgPRs with Different Aspect Ratios.

The AgPRs with 2.7, 4.4, and 6.7 of aspect ratios were synthesized by modified photochemical growth methods (the 10 nm thick AgPRs were measured by our previous report).[30,50−54] First, a colloidal aqueous solution of seeds of Ag nanospheres with a mean diameter of 11 nm was prepared by our reported procedure.[30] Typically, an aqueous solution of $AgNO_3$ (1 mM, 100 mL) was added to an aqueous solution (100 mL) containing 0.2 mM of NaBH4 and 5 mM of trisodium citrate under cooling in an ice bath and then stirring for 1 h. Next, the pH of the obtained colloidal silver solution was adjusted to 11.2 by the addition of an aqueous solution of 0.2 M NaOH. This was followed by irradiation of the colloidal solution for about 16 h by light-emitting diodes with center wavelengths of 470 and 550 nm, which resulted in the formation of SAgPRs (edge length: 27 ± 5 nm) and MAgPRs (edge length: 44 ± 5 nm), respectively. The LAgPRs (edge length: 67 ± 10 nm) were synthesized by the sequential irradiation of light-emitting diode to the pH-adjusted silver colloidal solution with 470, 550, and 600 nm for 1.5, 0.5, and 15 h, respectively.

Fabrication of Hybrids of AgPRs and TTA-UC Films.

The fabrication scheme of the hybrids consisting of the AgPRs and the thin films of the TTA-UC systems is shown in Scheme 1. Typically, a glass plate (20 mm × 15 mm) was treated in a mixture of NH_3 aq. (28%)/H_2O_2 aq. (30%; 1/1 v/v) at 100 °C, followed by washing with water. The plate was immersed in an aqueous solution of PEI (4.0 mg mL^{-1}) for 10 min and washed with water to positively charge the surface. Next, the plate was immersed in a colloidal solution of negatively charged AgPRs protected with citric acid for an arbitrary time, followed by washing with water to immobilize the AgPRs on the surface of the glass plate through the electrostatic interaction. Next, the AgPRs-

immobilized plate was immersed in an ethanol solution of ODT (1 mM) for 12 h, producing the SAMs of the ODT on the AgPRs. The hybrids of the AgPRs and the TTA-UC systems were prepared by spin-coating (3000 rpm for 20 s) a DMF solution containing EO-EPI (21 mg), Pd-TBTBP (10 μM), and BPEA (200 μM). Finally, an aqueous solution of PVA (5%, 50 μL) was cast onto the surface of the hybrid thin films and then dried under vacuum. The hybrids were covered with PVA thin films having a low oxygen permeability to suppress the quenching effect of the oxygen because the triplet excited state of the sensitizer can be quenched by the presence of oxygen.

Measurements.

Extinction and absorption spectra were measured by a JASCO V-630 spectrophotometer. Fluorescence and phosphorescence spectra were measured by a JASCO FP6500 and FP-8600, respectively. The SEM observations were performed using a HITACHI S4500 and SU8200 microscopes. The TEM observations were performed using a Hitachi HF2000 system at an acceleration voltage of 200 kV. The AFM (tapping mode) measurements were conducted using SPA-400 (Hitachi High-Tech Science). The fluorescence lifetime was measured using a C11367 Quantaurus-Tau (Hamamatsu). Fluorescence quantum yield measurements were carried out with an Absolute PL Quantum Yield Spectrometer (Hamamatsu, C11347−02 Quantaurus-QY). For phosphorescence lifetime measurements, a He−Ne laser (632.8 nm) equipped with an optical chopper was used as a light source and phosphorescence was detected with a photomultiplier after being dispersed with a monochromator. Signals were processed with an oscilloscope and accumulated with a computer. Electromagnetic field enhancement contours of SAgPRs, MAgPRs, and LAgPRs were calculated by boundary element method within the QS approximation (QS-BEM) framework with the MNPBEM17 program on MATLAB.[76] The dielectric function of silver used was obtained from the previous report by Rakic et al.[77] The fabrication and the optical measurements of all of the hybrids were performed within a day after the synthesis of AgPRs.

2-3. Results and Discussion

2-3-1. Design of materials

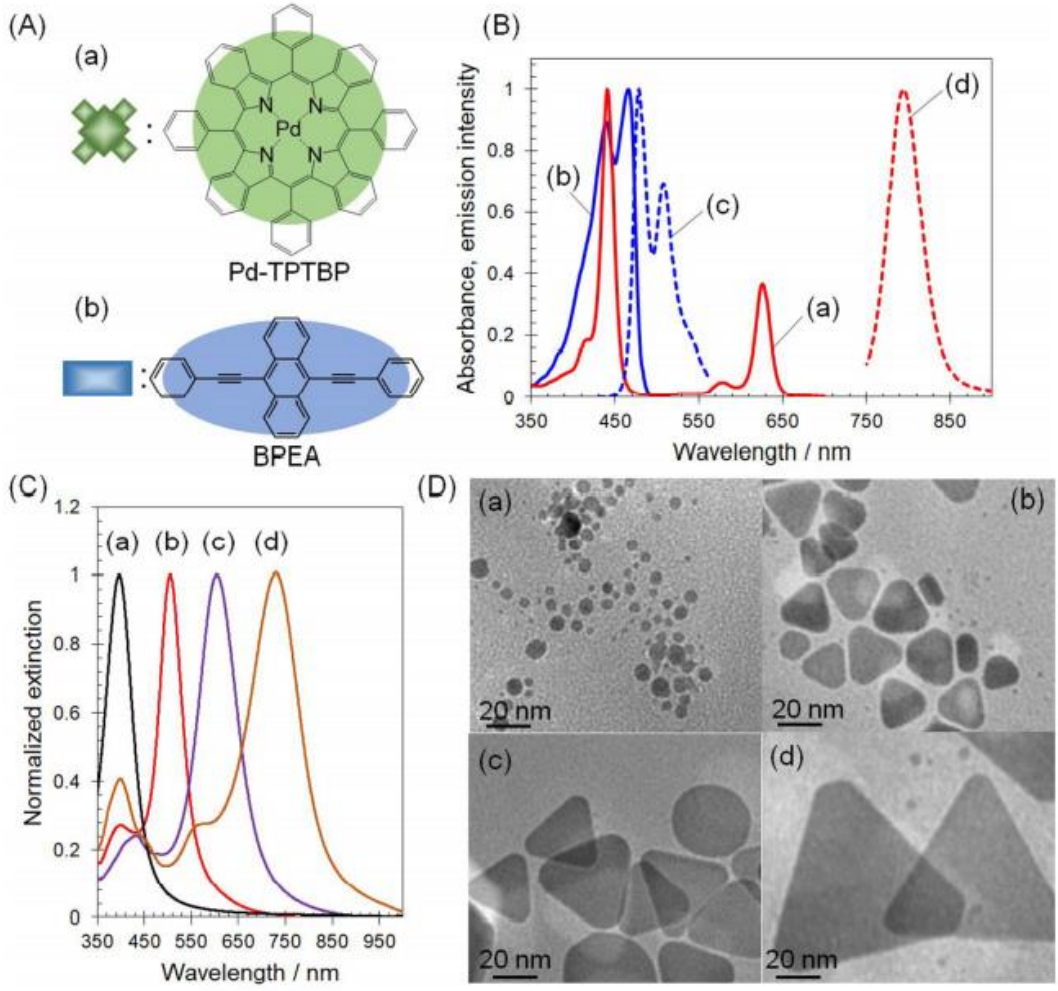

Figure 2-1. Introduction of materials used in this study. (A) Molecular structures of (a) Pd-TPTBP and (b) BPEA. (B) Absorption spectra of DMF solutions of (a) Pd-TPTBP and (b) BPEA, (c) fluorescence spectrum (λ_{ex} = 400 nm) of the BPEA solution, and (d) phosphorescence spectrum (λ_{ex} = 627 nm) of Pd-TPTBP. (C) Extinction spectra of colloidal aqueous solutions of (a) Ag nanospheres, (b) SAgPRs, (c) MAgPRs, and (d) LAgPRs. (D) TEM images of (a) Ag nanospheres, (b) SAgPRs, (c) MAgPRs, and (d) LAgPRs.

In this study, palladium(II) tetraphenyltetrabenzoporphyrin (Pd-TPTBP) and 9,10-bis-(phenylethynyl)anthracene (BPEA), which have frequently been utilized in well-established TTA-UC systems,[48,49] were employed as a photosensitizer and an emitter, respectively; their molecular structures and the absorption and emission spectra are shown in Figure 2-1A and B, respectively. To investigate in detail the effect of LSP resonance on each photoinduced process in TTA-UC, we synthesized three types of anisotropic triangular Ag nanoprisms (AgPRs) by a photoinduced growth method whose

LSP resonance bands overlap well with the photoexcitation and phosphorescence wavelengths of the sensitizer and the fluorescence wavelength of the emitter, respectively.[50−54] While a colloidal aqueous solution of Ag nanospheres, which were used as a seed for the synthesis of these AgPRs, exhibited an LSP resonance peak originating from the dipole mode at 398 nm, each AgPR showed a defined LSP resonance peak of in-plane dipole mode at 505, 605, and 735 nm (Figure 2-1C). The edge lengths of the AgPRs were estimated from transmission electron microscopy (TEM) images to be 27 ± 5 (small-size AgPRs (SAgPRs)), 44 ± 5 (middle-size AgPRs (MAgPRs)), and 67 ± 10 nm (largesize AgPRs (LAgPRs)), as shown in Figure 2-1D.

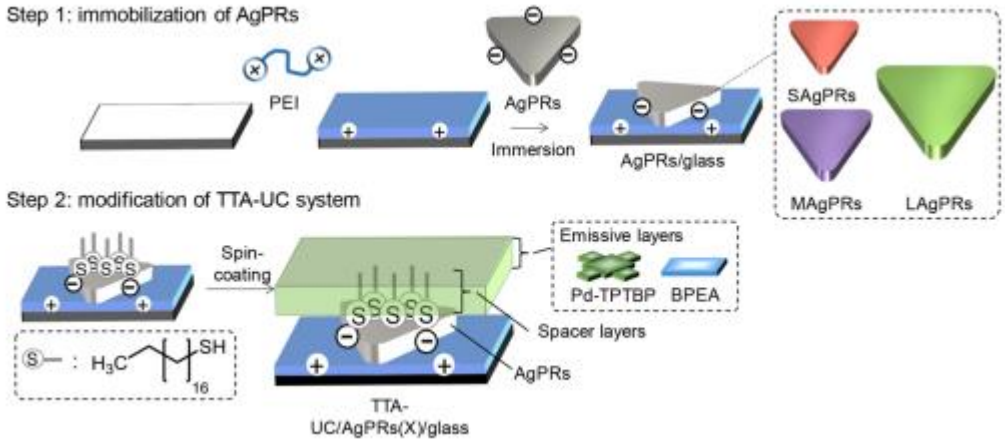

Figure 2-2. Preparation of Hybrids Consisting of the AgPRs and the TTA-UC Systems

We prepared the hybridized systems consisting of AgPRs and TTA-UC thin solid films according to the following procedure. The AgPRs synthesized in this study had a negatively charged surface because they were protected with citric acid. Therefore, the AgPRs were immobilized on the surface of a glass plate (20 mm × 15 mm) via the electrostatic adsorption process by immersing the positively charged polyethylenimine (PEI)-modified glass plate in the colloidal aqueous solution (Step 1 in Figure 2-2). When the distance between a fluorophore and a metal nanoparticle is too close, a large enhancement due to the plasmonic effects would be expected, but the undesirable quenching owing to the presence of metal cannot be ignored. Therefore, to moderately increase the distance, self-assembled monolayers (SAMs) of octadecanethiol (ODT, thickness: approximately 2 nm) were formed on the AgPRs on the glass plate as a quenching suppression layer.[55] Finally, a thin film (estimated thickness of 7.2 ± 0.6 nm by atomic force microscopy (AFM) measurement, Figure 2-3) of ethylene oxide-

epichlorohydrin copolymer (EO-EPI)[20] containing Pd-TPTBP and BPEA was modified on the AgPR-immobilized glass plate by a spin-coating process (Step 2 in Figure 2-2, denoted as TTA-UC/ AgPRs(*X*)/glass, *X*: immersion time (min) of the glass plate in the colloidal solution of AgPRs)). In addition, a reference plate without the AgPRs was prepared by modifying the PEImodified glass plate with the EO-EPI thin films containing the photofunctional molecules (denoted as TTA-UC/glass).

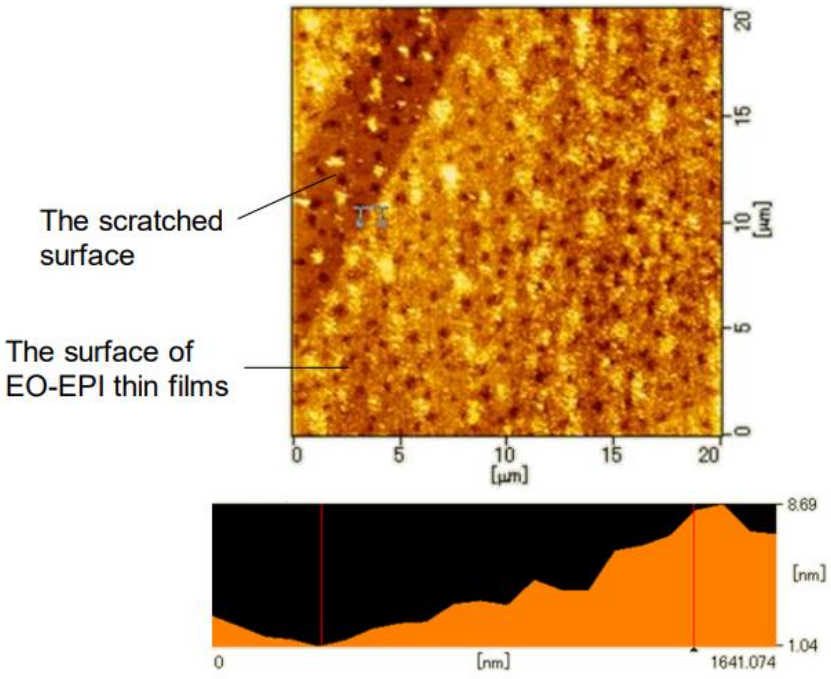

Figure 2-3. AFM image of EO-EPI thin films containing Pd-TPTBP and BPEA.

2-3-2. Effect on the Decay Process of emitter

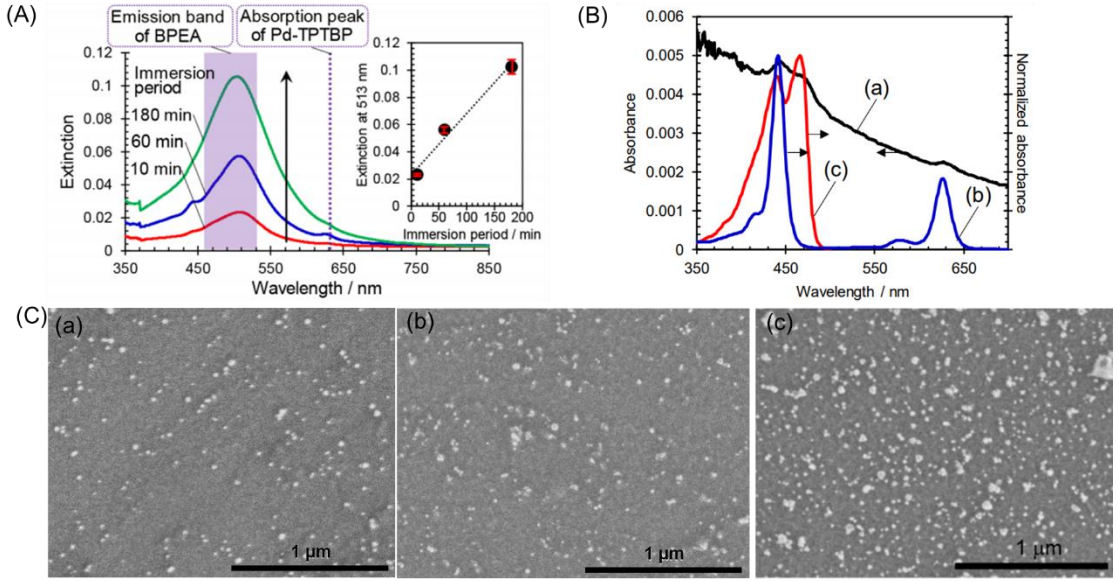

Figure 2-4. Morphological and optical properties of the TTA-UC/SAgPRs(*X*)/glass. (A) Extinction spectra of the TTA-UC/SAgPRs(10, 60, and 180)/glass. Inset shows the plots of extinction intensity at 513 nm against the immersion time in the aqueous solution of SAgPRs. The error bars indicate the standard deviations of three measurements for each point. (B) Absorption spectra of (a) TTA-UC/glass and DMF solutions of (b) Pd-TPTBP and (c) BPEA. (C) SEM image of the SAgPRs-immobilized glass plate for the immersion time of (a) 10min, (b) 60 min, and (c) 180 min.

According to the radiating plasmon model, when the LSP resonance band of metal nanoparticles spectrally overlaps with a fluorescence band of nearby fluorophore, nonradiative energy transfer is induced from the fluorophore to the LSP, which in turn, radiates the emission whose spectral shape is the same as that of the fluorophore.[34,56−58] We first investigated the change in the intensity of TTA-UC emission by inserting the SAgPRs whose LSP resonance band overlapped well with the fluorescence wavelength of BPEA into the TTA-UC system. The extinction spectra of TTA-UC/SAgPRs(10, 60, and 180)/glass are shown in Figure 2-4(A). For all of the substrates, the LSP resonance peak that originated from the in-plane dipole mode of an SAgPR was observed at 513 nm. As the immersion time increased, the extinction intensity of the LSP resonance linearly increased from 0.024 (10 min) to 0.105 (180 min), which corresponds to a linear increase in the coverage of SAgPRs (inset of Figure 2-2(A)). Note that an extinction band originating from the coupling of LSP resonance between the adjacent SAgPRs was not observed, suggesting that the immobilized SAgPRs were well-dispersed on the glass surface without any SAgPR aggregation. In addition, in the extinction spectra shown in Figure 2-2(A), the absorption peaks attributed to the photoexcitation of PdTPTBP and

BPEA were not observed because the absorbances of these absorption peaks were significantly weaker than the extinction intensity of the LSP resonance of the SAgPRs (Figure 2-4(B)). Figure 2-4(B) shows an absorption spectrum of TTA-UC/glass along with those of DMF solutions of Pd-TPTBP and BPEA. A weak absorption peak at 627 nm and a weak absorption band at 400-500 nm, which corresponds to the Q-band of Pd-TPTBP and the overlapped band consisting of the Soret band of Pd-TPTBP and the absorption peaks of BPEA, were observed. These results suggest that the EO-EPI thin films including PdTPTBP and BPEA were modified on the glass plate. The scanning electron microscopy (SEM) image of the SAgPRs-immobilized glass plate prepared with an immersion time of 10 min, 60 min, and 180 min are shown in Figure 2-2(C), which confirmed that the SAgPRs were well-dispersed with a low coverage of 5.5 %, 9.2 %, and 14.9%.

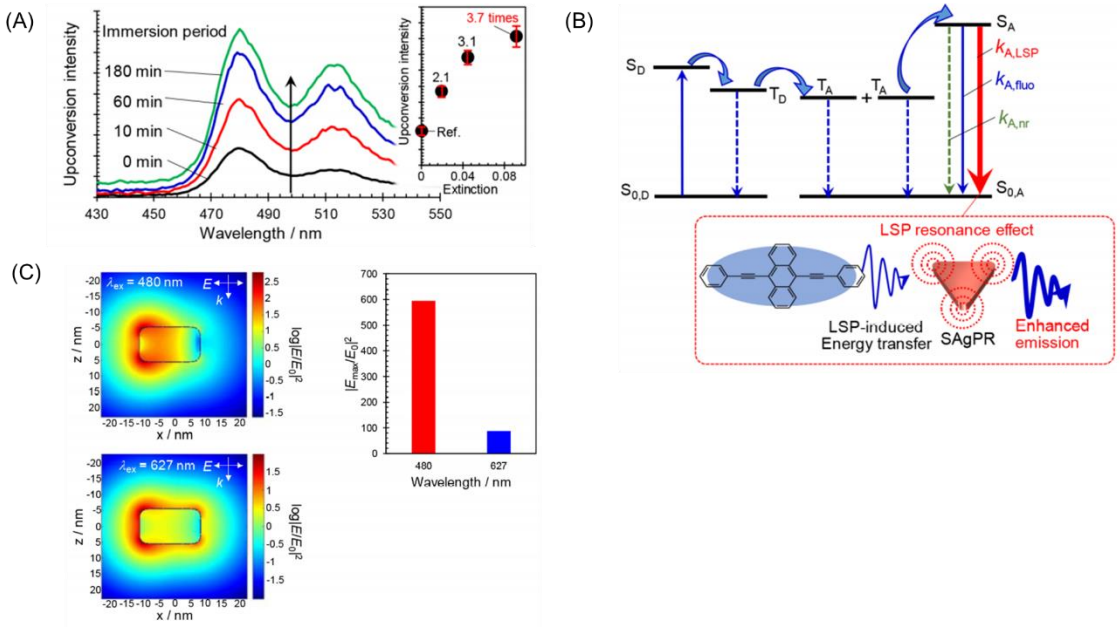

Figure 2-5. (A) Upconverted emission spectra from the TTA-UC/MAgPRs(0, 10, 120, and 180)/glass (λ_{ex}: 627 nm, immersion time of 0 min corresponds to a reference substrate: TTA-UC/glass). Inset shows the dependence of the extinction intensity of LSP resonance band at 627 nm on enhancement factors of the upconverted emission intensity. (B) Enhancement mechanism of the upconverted emission in the TTA-UC/MAgPRs(*X*)/glass. (C) Electromagnetic field intensity of the MAgPRs at 480 and 627 nm calculated using BEM.

The emission spectra from TTA-UC/SAgPRs(*X*)/glass through the TTA-UC process (λ_{ex} = 627 nm) are shown in Figure 2-5(A). The intensity of upconverted emission observed at 460−530 nm from all of the TTA-UC/SAgPRs(*X*)/glass was stronger than that from the

TTA-UC/glass. Furthermore, the emission intensity gradually increased with increase in the extinction intensity and tended to saturate after an immersion time of 180 min as shown in the inset in Figure 2-5(A). The maximum enhancement factor, which is based on the comparison with the TTA-UC/glass, was consequently estimated to be 3.7 times as a reserved value. It is reasonable that an increase in the radiative decay rate from the photoexcited state of the emitter was a dominant mechanism in the enhancement in the TTA-UC emission (Figure 2-5B) because the LSP resonance band of the SAgPRs overlapped well with the fluorescence wavelengths of BPEA (460−530 nm) but not well with the photoexcitation wavelengths of PdTPTBP (Figure 2-4(A)). To further clarify this enhancement mechanism, we calculated the intensity of local electromagnetic fields generated at around the SAgPRs using a boundary element method. As shown in Figure 2-5(C), the calculated maximum field intensity ($|E_{max}/E_0|^2$ = 595) at the fluorescence wavelength of BPEA (480 nm) was stronger than that at 627 nm ($|E_{max}/E_0|^2$ = 87), the excitation wavelength of Pd-TPTBP.

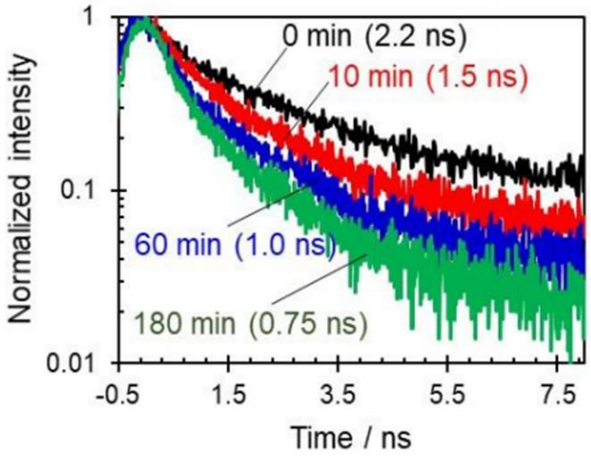

Figure 2-6. Fluorescence lifetime of the directly-excited BPEA in the TTA-UC/SAgPRs(*10, 60, and 180)*/glass and TTA-UC/glass (λ_{ex} = 405 nm).

The radiative rate increase is also supported by the fluorescence lifetimes by the direct photoexcitation of BPEA (λ_{ex} = 405 nm) in the TTA-UC/SAgPRs(10, 60, and 180)/ glass (Figure 2-6). The LSP-modified fluorescence lifetime ($\tau_{LSP,fluo}$) of BPEA is given by eq 1.

$$\tau_{LSP,fluo} = \frac{1}{k_{A,fluo} + k_{A,LSP} + k_{A,nr}} \quad (1)$$

where $k_{A,fluo}$, $k_{A,LSP}$, and $k_{A,nr}$ are unmodified radiative decay rate, LSP-induced radiative

decay rate, and nonradiative decay rate, respectively, of the acceptor (A) molecule (i.e., BPEA, Figure 2-5(B)). Two possibilities may be invoked for the lifetime to be shortened. One is the increase of the LSP-induced radiative decay rate ($k_{A,LSP}$) with the increase of the coverage of SAgPRs. The other possibility is that $k_{A,nr}$ gets larger as the coverage of SAgPRs gets larger due to the quenching effect of the metal. The former mechanism should dominate over the latter, because the fluorescence quantum yield ($\phi_{LSP,fluo}$, eq 2) also increased with the increasing coverage of SAgPRs (Figure 2-4(A) and Figure 2-5(A)).

$$\tau_{LSP,fluo} = \frac{k_{A,fluo} + k_{A,LSP}}{k_{A,fluo} + k_{A,LSP} + k_{A,nr}} \quad (2)$$

One might argue that the more than 3-fold increase in fluorescence intensity cannot be explained by the increase in the fluorescence quantum yield of BPEA, which is already as high as 80−100% in the absence of the LSP resonance effect.[59,60] However, these high values of fluorescence quantum yields are those in solution. We measured the fluorescence quantum yield of BPEA enclosed in the EO-EPI film using an absolute quantum yield spectrometer, which gave a value of approximately 7% with the excitation wavelength range between 400 and 470 nm. Thus, the enhancement of TTA-UC emission observed in this study can be explained by an increase in the decay rate induced by the LSP resonance of SAgPRs whose wavelength range is overlapped well with the fluorescence wavelength of BPEA.

2-3-3. Effect on Photoexcitation Process of sensitizer

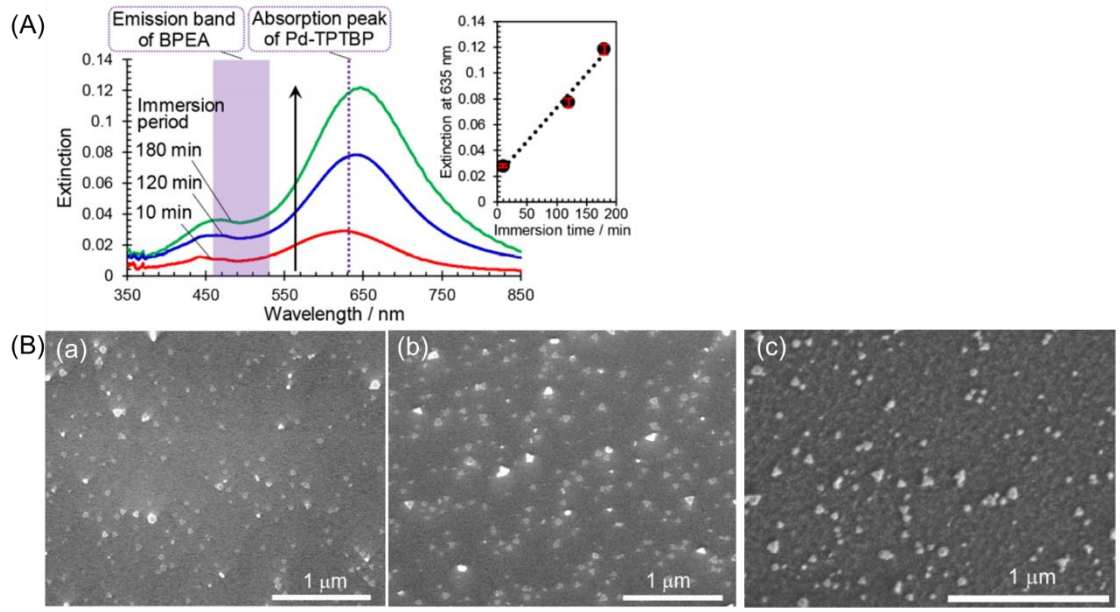

Figure 2-7. Morphological and optical properties of the TTA-UC/MAgPRs(*X*)/glass. (A) Extinction spectra of the TTA-UC/MAgPRs(10, 120, and 180)/glass. Inset shows the plots of extinction intensity at 635 nm upon the immersion time into the aqueous solution of MAgPRs. (B) SEM images of the MAgPRs-immobilized glass plate for the immersion time of (a) 10 min, (b) 60 min, and (c) 180 min.

Plasmonic nanoparticles, which function as a strong light-harvesting nanoantenna, lead to the enhancement in the efficiency of the photoexcitation process of nearby dye molecules.[25–32] Considering the mechanism in the TTA-UC system, enhancing the photoexcitation efficiency of the sensitizer is promising for not only the enhancement of the upconverted emission but also the reduction of the I_{th}, which is a well-known figure-of-merit of TTA-UC (vide infra). We next clarify this enhancement phenomenon by utilizing the MAgPRs as a plasmonic nanoparticle, because the LSP resonance band from the MAgPRs effectively overlaps with the photoexcitation wavelength (Q-band) of Pd-TPTBP. The MAgPRs-immobilized glass plates were prepared according to the process described in Step 1 in Figure 2-2 (TTA-UC/ MAgPRs(*X*)/glass, *X*: 10, 120, and 180 min). The LSP resonance band of the in-plane dipole mode of the MAgPRs was observed around 635 nm, which is longer than that of SAgPRs, and the extinction intensity linearly increased as the immersion time increased (Figure 2-7(A)). Up to the immersion time of 180 min, the coupling mode of LSP resonance by closely deposited MAgPRs was not observed. This was also confirmed from the SEM image (Figure 2-7(B)) that the MAgPRs were well dispersed on the glass plate for the immersion time of 10 min, 60 min, 180 min (coverage: 4.2 %, 9.1 %, and 13.7%).

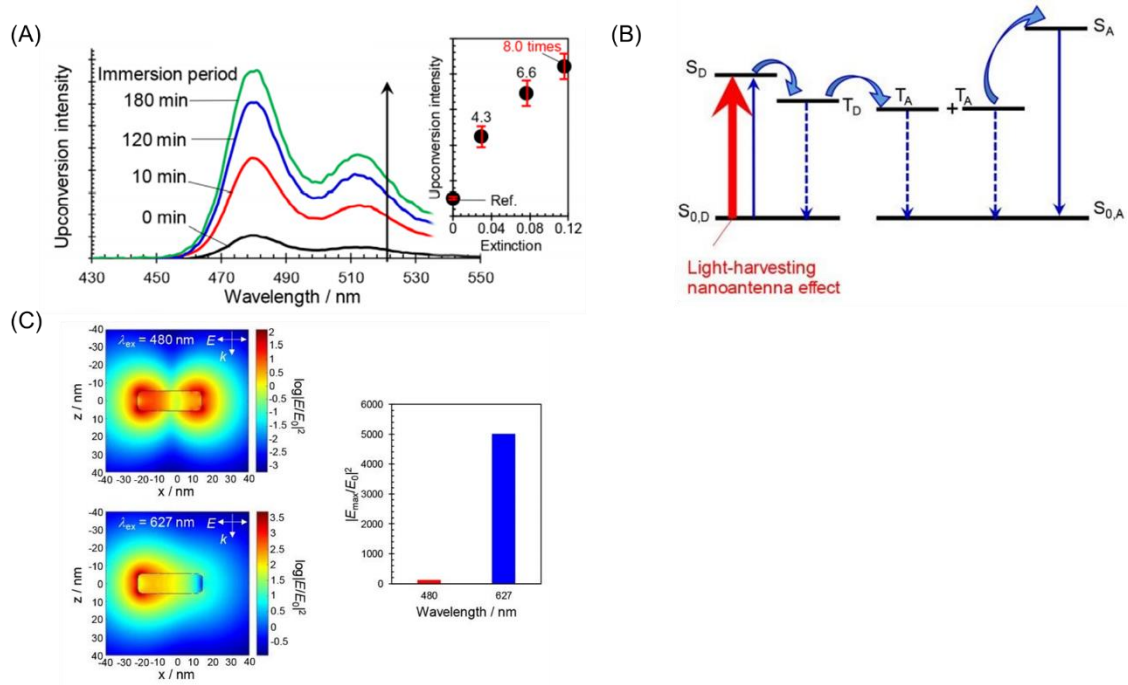

Figure 2-8. (A) Upconverted emission spectra from the TTA-UC/MAgPRs(*0, 10, 120, and 180*)/glass (λ_{ex}: 627 nm, immersion time of 0 min corresponds to a reference substrate: TTA-UC/glass). Inset shows the dependence of the extinction intensity of LSP resonance band at 627 nm on enhancement factors of the upconverted emission intensity. (B) Enhancement mechanism of the upconverted emission in the TTA-UC/MAgPRs(*X*)/glass. (C) Electromagnetic field intensity of the MAgPRs at 480 and 627 nm calculated using BEM.

Figure 2-8(A) shows the TTA-UC emission spectra obtained from the TTA-UC/MAgPRs(*X*)/glass and the TTA-UC/glass (λ_{ex} = 627 nm). The upconverted emission gradually increased with growing the LSP resonance band of the MAgPRs and finally achieved an enhancement factor of 8.0 from the TTAUC/MAgPRs(180)/glass. The contribution of enhancement of photoexcitation efficiency to the upconverted emission enhancement must be large (Figure 2-8(B)) because of the effective overlap between the main LSP resonance band (inplane dipole mode, center wavelength: ca. 635 nm) of the MAgPRs and the Q-band wavelength of Pd-TPTBP, as shown in Figure 2-7(A). Although the in-plane quadrupole mode also overlaps with the 480 nm fluorescence wavelength of BPEA, the extinction of this mode is quite low. We calculated the distribution of local electromagnetic fields generated at the MAgPRs at the respective wavelengths. The maximum local electromagnetic field intensity ($|E_{max}/E_0|^2$ = 5015) at 627 nm photoexcitation wavelength of Pd-TPTBP was significantly stronger than that ($|E_{max}/E_0|^2$ = 123) at the 480 nm fluorescence wavelength of BPEA (Figure 2-8(C)). These results show that the large enhancement of TTA-UC was mainly attributed to the plasmonic

nanoantenna-induced enhancement of photoexcitation of Pd-TPTBP.

2-3-4. Effect of LSP Resonance on Low Upconversion Excitation Intensity

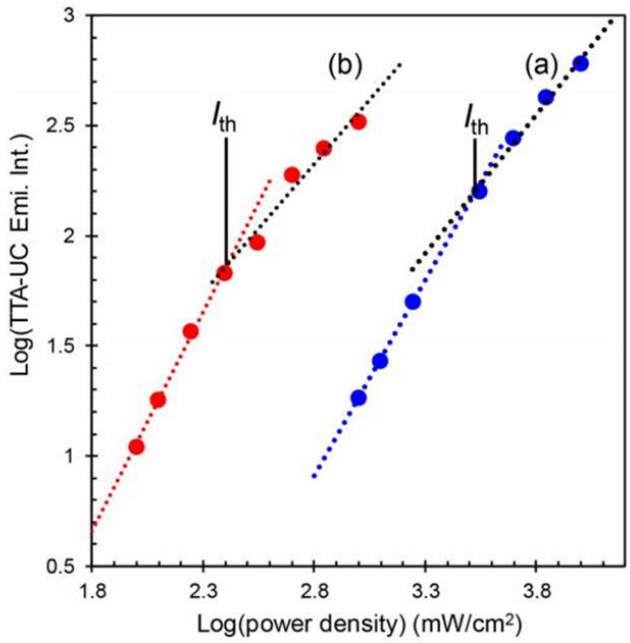

Figure 2-9. TTA-UC emission intensities observed for the (a) TTAUC/glass and (b) TTA-UC/MAgPRs(180)/glass as a function of the power density of 642 nm excitation. The dashed lines are the fitting results with slopes of (a) 1.27 and 1.78 and (b) 1.17 and 2.00, and Ith was determined as (a) 3500 and (b) 240 mW/cm^2 from the crossing point of these two lines.

The incident power dependence of TTA-UC emission intensity exhibits a dual behavior: a quadratic dependence at low excitation powers and a linear dependence at high excitation powers. While the linear property indicates that the triplet excited state of emitter relaxed preferentially through the TTA process, the quadratic behavior indicates that spontaneous relaxation of triplet excited state emitter dominates. The incident power beyond which the TTA was the dominant mechanism (I_{th}), is a critical figure of merit determining the performance of TTA-UC systems.[61,62] The enhancement of the photoexcitation efficiency of the sensitizer through the light-harvesting nanoantenna effect of LSP resonance is expected to lead to a beneficial decrease of I_{th}. To verify this hypothesis, the I_{th} of the TTA-UC/ MAgPRs(180)/glass using a 642 nm CW laser as an excitation source was measured (Figure 2-9). Consequently, the I_{th} of TTA-UC/MAgPRs(180)/glass (240 mW/cm^2) significantly decreased by 93% as compared with that of TTA-UC/glass (3500 mW/cm^2). These results strongly suggest that the enhancement in the photoexcitation efficiency of a sensitizer by the LSP-based light

harvesting nanoantenna is beneficial for the development of practical solid-based TTA-UC systems.

2-3-5. Effect on Decay Process of Sensitizer

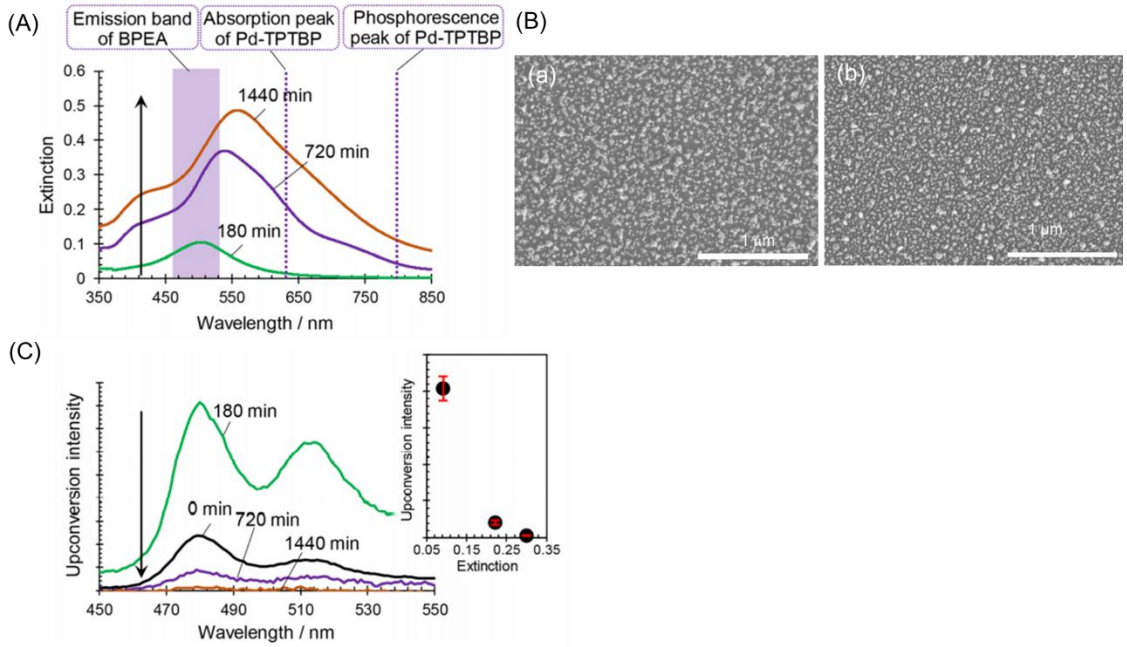

Figure 2-10. Morphological and optical properties of the TTA-UC/ SAgPRs/glass. (A) Extinction spectra of the TTA-UC/SAgPRs(180, 720, and 1440)/glass. (B) SEM image of the SAgPRs-immobilized glass plate for the immersion time of 1440 min. (C) Upconverted emission spectra from the TTA-UC/SAgPRs(180, 720, and 1440)/ glass (λex: 627 nm, immersion time of 0 min corresponds to a reference substrate: TTA-UC/glass). Inset shows the dependence of the extinction intensity of LSP resonance band at 627 nm on enhancement factors of the upconverted emission intensity.

Another important result obtained from the upconverted emission behavior by inserting the SAgPRs and the MAgPRs into a TTA-UC system is that, despite the linear growth of the LSP resonance band with an increasing immersion time of the colloidal solution of S(M)AgPRs, the increase in the emission intensity gradually slowed down and the intensity tended to saturate at an immersion time of 180 min (Figures 2-5(A) and 2-8(A)). To further investigate the phenomenon, we evaluated the change in the upconverted emission intensity by further prolonging the immersion time in the colloidal solution of SAgPRs. Figure 2-10(A) shows the extinction spectra of the TTAUC/SAgPRs(180, 720, and 1440)/glass. The LSP resonance bands of both TTA-UC/SAgPRs(720 and 1440)/glass broadened and the extinction maximum wavelengths redshifted as compared with that of the TTA-UC/SAgPRs(*180*)/ glass (maximum wavelength of each immersion time: 180 min, 505 nm; 720 min, 542 nm; and 1440 min, 560 nm). These spectral changes in the LSP resonance band are derived from the coupling of LSP resonance based on the dipole−dipole interaction owing to an increase in the coverage of SAgPRs as supported

by the SEM images with estimated coverages to 34.5 % and 43.5% for the immersion time of 720 min and 1440 min (Figure 2-10(B). Note that the intensity of upconverted emissions were significantly lower than that of the TTA-UC/ SAgPRs(180)/glass, as shown in Figure 2-10(C), even though the extinction intensities of LSP resonance at both the emission wavelength of BPEA and the photoexcitation wavelength of Pd-TPTBP increased as compared with the TTA-UC/ SAgPRs(180)/glass. These results suggest that the effects of LSP resonance on the emission behavior of a TTA-UC system include beneficial enhancement and harmful quenching. We focused on the spectral overlap between the LSP resonance bands of TTA-UC/SAgPRs(720 and 1440)/glass, which were red-shifted by the LSP coupling, as shown in Figure 2-10A, and the phosphorescence wavelength (ca. 800 nm) of Pd-TPTBP. In the presence of plasmonic metal nanoparticles, energy transfer from the sensitizer to the plasmonic metal nanoparticles can be induced, even at a separation distance greater than 10 nm between them through LSP induced mechanisms including fluorescence resonance energy transfer, nanometal surface energy transfer, and plasmon-enhanced fluorescence energy transfer.[63−66] Since the average thickness of TTA-UC thin films was measured as 7.2 nm, there is a high possibility that the TTET and the energy transfer to metal nanoparticles would compete in the deactivation process of the triplet excited sensitizer in the films. Consequently, by overlapping the LSP band with the phosphorescence wavelength of the sensitizer, the appearance of a new pathway of energy transfer to the LSP of metal nanoparticles, $k_{D,LSP}$, should effectively suppress the TTET efficiency, thereby resulting in a decrease in the upconverted emission intensity, as shown in Figure 2-11(A) and eqs 3 and 4. [67,68]

$$\Phi_{0,TTET} = \frac{k_{D,TTET}}{k_{D,phos} + k_{D,nr} + k_{D,TTET}} \tag{3}$$

$$\Phi_{LSP,TTET} = \frac{k_{D,TTET}}{k_{D,phos} + k_{D,nr} + k_{D,TTET} + k_{D,LSP}} \tag{4}$$

where $\phi_{0,\mathrm{TTET}}$ and $\phi_{LSP,TTET}$ indicate the TTET efficiency to the emitter in the absence and presence of plasmonic metal nanoparticles, respectively. The rate constants, $k_{D,TTET}$, $k_{D,phos}$, $k_{D,nr}$, and $k_{D,LSP}$, respectively, denote rate constants of TTET decay, phosphorescence radiative decay, nonradiative decay, and energy transfer to the metal nanoparticles from the triplet excited sensitizer (donor, D).

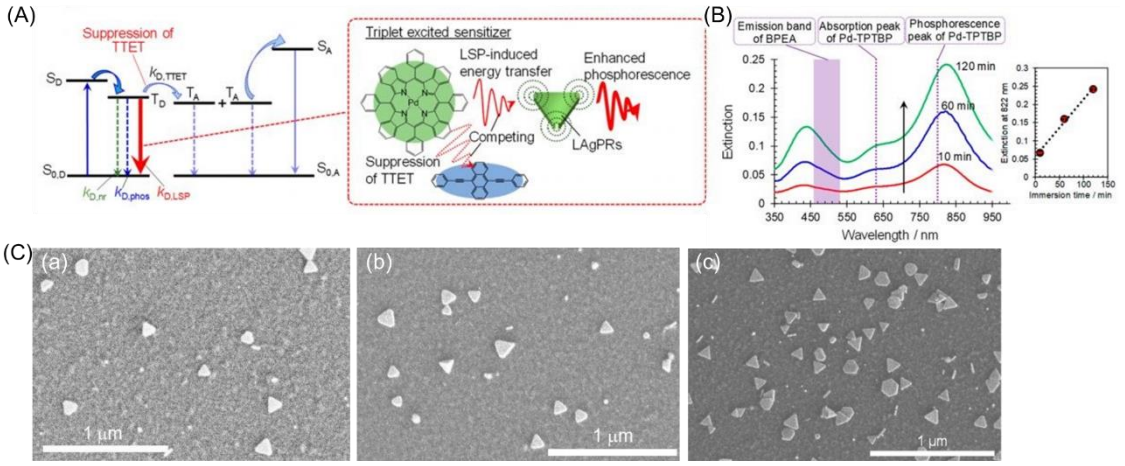

Figure 2-11. Morphological and optical properties of the TTA-UC/LAgPRs/glass. (A) Suggested quenching mechanism of upconverted emission by the presence of plasmonic metal nanoparticles. (B) Extinction spectra of the TTA-UC/LAgPRs(10, 60, and 120)/glass. Inset shows the plots of extinction intensity at 794 nm upon the immersion time into the aqueous solution of LAgPRs. (C) SEM images of the LAgPRs-immobilized glass plate for the immersion times of 10 min, 60 min, and 120 min.

To verify this hypothesis, we developed hybrids consisting of TTA-UC thin films and AgPRs with a larger aspect ratio (LAgPRs) that exhibit a main LSP resonance band at wavelengths of Pd-TPTBP phosphorescence (denoted as TTA-UC/LAgPRs(*X*)/glass, *X*: 10, 60, and 120 min). From the extinction spectra of TTA-UC/LAgPRs(*X*)/glass shown in Figure 2-11(B), it was confirmed that a strong extinction peak of inplane dipole resonance at 830 nm with a weak shoulder around 630 nm grew by increasing the immersion time into the colloidal solution of LAgPRs. The well-dispersed LAgPRs on a glass plate were observed from the SEM images of TTA-UC/LAgPRs(10, 60, 120)/glass (coverage: 8.2 %, 14.2 %, and 23.7%, Figure 2-11(C)).

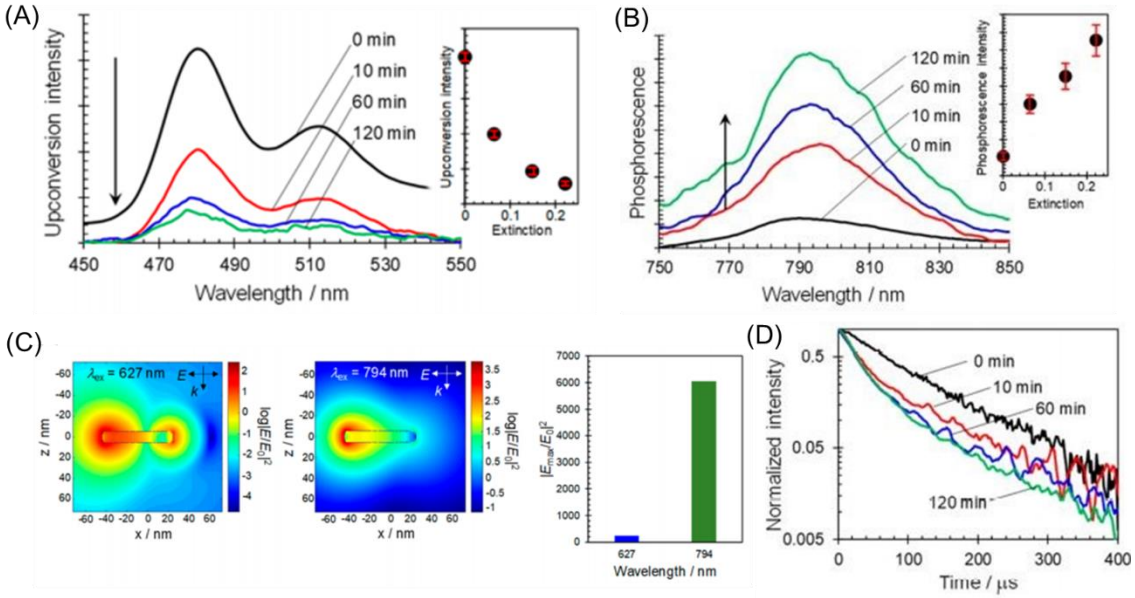

Figure 2-12. (A) Upconverted emission spectra from the TTA-UC/LAgPRs(0, 10, 60, and 120)/glass (λex: 627 nm, immersion time of 0 min corresponds to a reference substrate: TTA-UC/glass). Inset shows the dependence of the extinction intensity of LSP resonance band at 794 nm on enhancement factors of the upconverted emission intensity. (B) Phosphorescence spectra from the TTA-UC/ LAgPRs(0, 10, 60, and 120)/glass (λex: 627 nm). Inset shows the dependence of the extinction intensity of LSP resonance band at 794 nm on phosphorescence intensity. (C) Electromagnetic field intensity of the LAgPRs at 627 and 794 nm calculated using BEM. (D) Phospherescence lifetime of the excited Pd-TPTBP in the TTA-UC/LAgPRs(0, 10, 60, and 120)/glass (λex: 633 nm).

Note that the upconverted emission intensity gradually decreased as the LSP resonance band of LAgPRs grew, and the intensity of the TTA-UC/LAgPRs(120)/glass decreased by 85% compared with that of the TTA-UC/glass (Figure 2-12(A)). If the decrease in upconverted emission is induced by the efficient energy transfer from the triplet excited state of the sensitizer to the LSP of LAgPRs (kD,LSP), a decrease in the phosphorescence lifetime as well as an increase in the phosphorescence intensity (generation of plasmon-coupled phosphorescence)[58,69,70] are induced by the addition of a new radiative decay pathway (eqs 5 and 6 and Figure 2-11(A)).

$$\Phi_{0,Phos} = \frac{1}{k_{D,phos} + k_{D,nr} + k_{D,TTET}} \quad (5)$$

$$\Phi_{LSP,Phos} = \frac{1}{k_{D,phos} + k_{D,nr} + k_{D,TTET} + k_{D,LSP}} \quad (6)$$

The phosphorescence spectra of TTA-UC/LAgPRs(*X*)/glass (λ_{ex} = 627 nm) are shown in Figure 2-12(B). The phosphorescence intensities around 794 nm from all of the TTA-UC/ LAgPRs(10, 60, and 120)/glass were higher than that from the TTA-UC/glass, and the intensity gradually increased as the immersion time in the LAgPRs solution increased. From the calculation results of electromagnetic fields of LAgPRs, the maximum field intensity at 794 nm, corresponding to the phosphorescence wavelength of Pd-TPTBP, was significantly stronger than that at 627 nm, corresponding to the photoexcitation wavelength of Pd-TPTBP (Figure 2-12(C)). In addition, all of the average phosphorescence lifetimes of TTAUC/LAgPRs(X)/glass (λ_{ex} = 633 nm) were significantly shorter than that of TTA-UC/glass (see Figure 2-12(D): TTA-UC/glass, 100 μs; TTA-UC/LAgPRs(10)/glass, 60 μs; TTAUC/LAgPRs(60)/glass, 55 μs; and TTA-UC/LAgPRs(120)/ glass, 55 μs). These results strongly suggest that the energy transfer from the triplet-excited state of the sensitizer to the LAgPRs through the LSP resonance excitation largely contributed to the suppression of the generation of upconverted emission (Figure 2-11(A)).

2-3-6. Summary of the Beneficial and Detrimental Effects of LSP Resonance

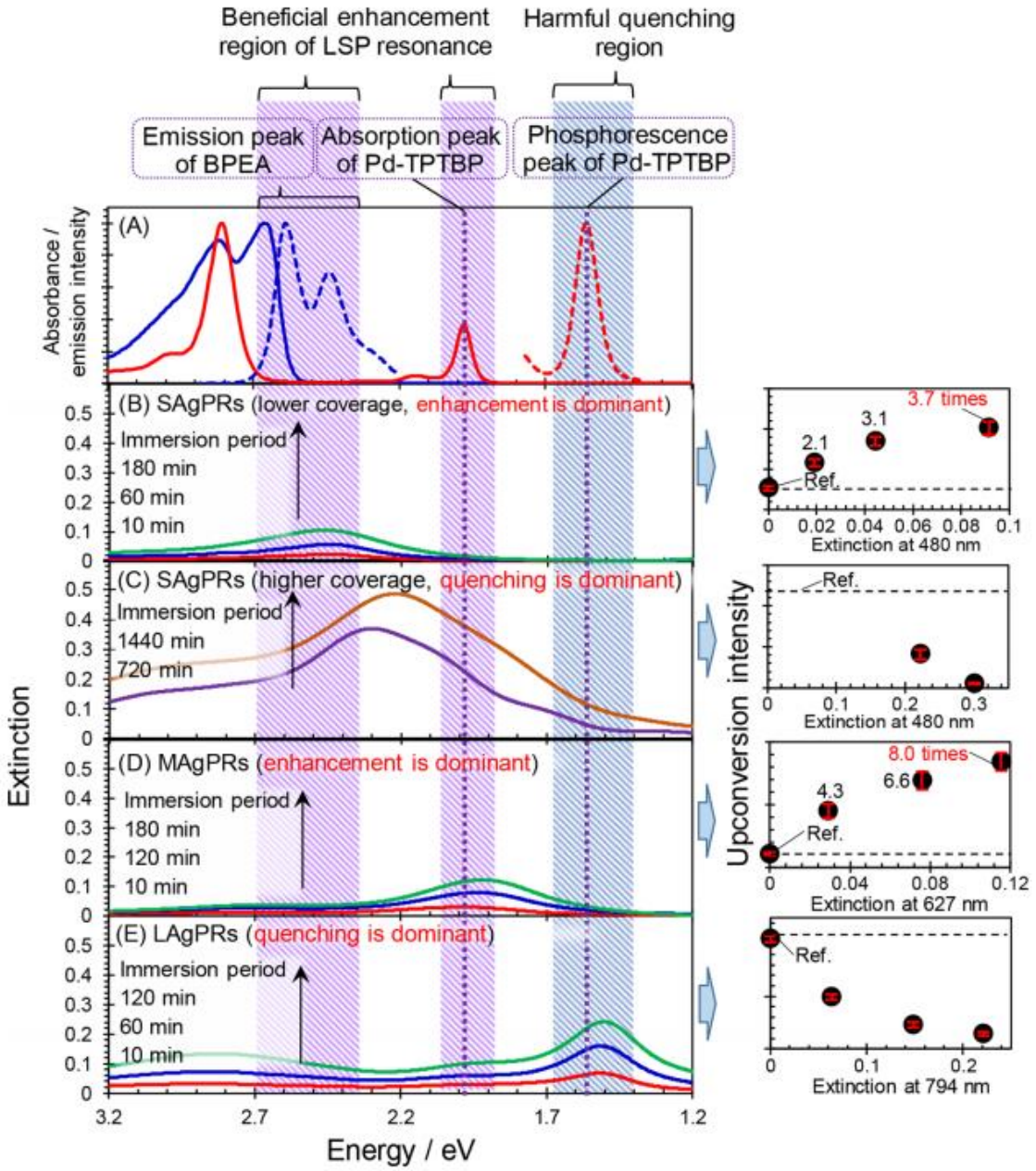

Figure 2-13. Summary of the relations between the spectral overlap of various sizes of AgPRs, TTA-UC systems, and the upconverted emission intensities.

For the fluorescence enhancement phenomenon of single downconverted fluorophores, it is recognized that the effective overlap between the LSP resonance band and both wavelengths of photoexcitation and fluorescence of fluorophore is important.[71–73] Therefore, the wider the line width of the LSP resonance band, the more effective the spectral overlap becomes. Significant fluorescence enhancement was achieved by

utilizing metal nanostructures that exhibit broad LSP resonance bands including large-size Au nanostars,[71] Au nanorods,[72] and Au bowtie nanoantennas.[73] On the contrary, we demonstrated in this study that a more precise tuning of the generation wavelength of LSP resonance band is required for the efficient enhancement of TTA-UC emission. Figure 2-13 summarizes the relations between the spectral overlap of various sizes of AgPRs, TTA-UC systems, and the upconverted emission intensities. In the hybrids of TTA-UC systems and SAgPRs exhibiting a main LSP resonance band at 513 nm, the upconverted emission enhanced up to 3.7× (Figure 2-13(B)) through the increase in the radiative decay rate by the effective spectral overlap between the LSP resonance band and the fluorescence wavelengths of BPEA (460−530 nm). Also, the upconverted emission enhanced up to 8.0× by the effective spectral overlap between the LSP resonance band of MAgPRs with a center wavelength of 635 nm and the photoexcitation wavelength (627 nm) of sensitizer, Pd-TPTBP (Figure 2-13(D)). This is explained by the strong light-harvesting nanoantenna effect of MAgPRs. On the other hand, the upconverted emission rather decreased as a result of generating the coupling modes between the LSP resonance of SAgPRs at the wavelengths where the phosphorescence of Pd-TPTBP occurs (ca. 800 nm, Figure 2-13(C)). A similar phenomenon was also observed in the hybrids of the TTA-UC systems and the LAgPRs having a LSP resonance band (830 nm) at the region of Pd-TPTBP phosphorescence, as shown in Figure 2-13(E). The effective overlap with the Pd-TPTBP phosphorescence band leads to the generation of a new pathway of energy transfer from the triplet excited state of Pd-TPTBP to the LSP and, consequently, the TTET is effectively suppressed. The anisotropic silver nanoparticles that generate a relatively sharp LSP resonance band, of which the generating wavelength can be tuned, are considered to be suitable for the efficient enhancement of TTA-UC emission. In addition, for the effective fluorescence enhancement of single fluorophores, the utilization of hot spots generated at an interstitial region between metal nanoparticle dimers is useful because of the generation of extremely strong local electromagnetic fields.[74,75] However, these nanostructures may not be suitable for the enhancement of TTA-UC emission because the hot spots are accompanied by a LSP resonance band drastically broadened over a wide wavelength region.

2-4. Conclusion

In this study, we have experimentally demonstrated that, depending on the resonance wavelength, the LSP resonance of anisotropic silver nanoparticles can induce both the enhancement and the quenching of TTA-UC emission. Precise control of the LSP resonance wavelength is required: the resonance band should be spectrally overlapped with the photoexcitation of the sensitizer and the fluorescence of the emitter and should not be overlapped with the phosphorescence of the sensitizer. We are currently developing metal nanostructures that fulfill the requirements as well as generate strong local electromagnetic fields for the significant enhancement of TTA-UC emission. Furthermore, we experimentally demonstrated that the photoexcitation enhancement contributes significantly to the reduction of threshold light excitation intensity. Ideally, the threshold light excitation intensity should be reduced below the intensity of solar irradiance, which is a great challenge in solid matrices. We conclude from this study that the plasmonic light-harvesting nanoantenna effect, combined with high-mobility excitons or a matrix having a lower glass transition temperature, is very promising for the achievement of TTA-UC-based high performance optical devices.

2-5. References

(1) Fujishima, A.; Rao, T. N.; Tryk, D. A. Titanium dioxide photocatalysis. *J. Photochem. Photobiol. C* **2000**, *1*, 1-21.

(2) Fujishima, A.; Honda, K. Electrochemical Photolysis of Water at a Semiconductor Electrode. *Nature* **1972**, *238*, 37−38.

(3) Cui, C.; Tou, M.; Li, M.; Luo, Z.; Xiao, L.; Bai, S.; Li, Z. Heterogeneous Semiconductor Shells Sequentially Coated on Upconversion Nanoplates for NIR-Light Enhanced Photocatalysis. *Inorg. Chem.* **2017**, *56*, 2328−2336.

(4) Yang, G.; Yang, D.; Yang, P.; Lv, R.; Li, C.; Zhong, C.; He, F.; Gai, S.; Lin, J. A Single 808 nm Near-Infrared Light-Mediated Multiple Imaging and Photodynamic Therapy Based on Titania Coupled Upconversion Nanoparticles. *Chem. Mater.* **2015**, *27*, 7957− 7968.

(5) Liu, Z.; Wang, J.; Li, Y.; Hu, X.; Yin, J.; Peng, Y.; Li, Z.; Li, Y.; Li, B.; Yuan, Q. Near-Infrared Light Manipulated Chemoselective Reductions Enabled by an Upconversional Supersandwich Nanostructure. *ACS Appl. Mater. Interfaces* **2015**, *7*, 19416−19423.

(6) Jang, Y. J.; Kim, E.; Ahn, S.; Chung, K.; Kim, J.; Kim, H.; Wang, H.; Lee, J.; Kim, D.-W.; Kim, D. H. Upconversion-Triggered Charge Separation in Polymer Semiconductors. *J. Phys. Chem. Lett.* **2017**, *8*, 364−369.

(7) Roh, J.; Yu, H.; Jang, J. Hexagonal β-NaYF4Yb3+Er3+ NanoprismIncorporated Upconverting Layer in Perovskite Solar Cells for NearInfrared Sunlight Harvesting. *ACS Appl. Mater. Interfaces* **2016**, *8*, 19847−19852.

(8) Monguzzi, A.; Tubino, R.; Hoseinkhani, S.; Campione, M.; Meinardi, F. Low power, non-coherent sensitized photon upconversion: modelling and perspectives. *Phys. Chem. Chem. Phys.* **2012**, *14*, 4322−4332.

(9) Gray, V.; Dzebo, D.; Abrahamsson, M.; Albinsson, B.; MothPoulsen, K. Triplet−triplet annihilation photon-upconversion: towards solar energy applications. *Phys. Chem. Chem. Phys.* **2014**, *16*, 10345−10352.

(10) Baluschev, S.; Miteva, T.; Yakutkin, V.; Nelles, G.; Yasuda, A.; Wegner, G. Up-Conversion Fluorescence: Noncoherent Excitation by Sunlight. *Phys. Rev. Lett.* **2006**, *97*, 143903/1−143903/3.

(11) Duan, P.; Yanai, N.; Kimizuka, N. Photon Upconverting Liquids: Matrix-Free Molecular Upconversion Systems Functioning in Air. *J. Am. Chem. Soc.* **2013**, *135*, 19056−19059.

(12) Cao, X.; Hu, B.; Zhang, P. High Upconversion Efficiency from Hetero Triplet-Triplet Annihilation in Multiacceptor Systems. *J. Phys. Chem. Lett.* **2013**, *4*, 2334−2338.

(13) Ye, C.; Wang, J.; Wang, X.; Ding, P.; Liang, Z.; Tao, X. A new medium for triplet-triplet annihilated upconversion and photocatalytic application. *Phys. Chem. Chem. Phys.* **2016**, *18*, 3430−3437.

(14) Duan, P.; Yanai, N.; Kurashige, Y.; Kimizuka, N. AggregationInduced Photon Upconversion

through Control of the Triplet Energy Landscapes of the Solution and Solid States. *Angew. Chem. Int. Ed.* **2015**, *54*, 7544−7549.
(15) Vadrucci, R.; Weder, C.; Simon, Y. C. Low-power photon upconversion in organic glasses. *J. Mater. Chem. C* **2014**, *2*, 2837− 2841.
(16) Duan, P.; Yanai, N.; Nagatomi, H.; Kimizuka, N. Photon Upconversion in Supramolecular Gel Matrixes: Spontaneous Accumulation of Light-Harvesting Donor-Acceptor Arrays in Nanofibers and Acquired Air Stability. *J. Am. Chem. Soc.* **2015**, *137*, 1887−1894.
(17) Monguzzi, A.; Mauri, M.; Bianchi, A.; Dibbanti, M. K.; Simonutti, R.; Meinardi, F. Solid-State Sensitized Upconversion in Polyacrylate Elastomers. *J. Phys. Chem. C* **2016**, *120*, 2609−2614.
(18) Monguzzi, A.; Bianchi, F.; Bianchi, A.; Mauri, M.; Simonutti, R.; Ruffo, R.; Tubino, R.; Meinardi, F. High efficiency up-converting single phase elastomers for photon managing applications. *Adv. Energy Mater.* **2013**, *3*, 680−686.
(19) Kim, J.-H.; Deng, F.; Castellano, F. N.; Kim, J.-H. High Efficiency Low-Power Upconverting Soft Materials. *Chem. Mater.* **2012**, *24*, 2250−2252.
(20) Singh-Rachford, T. N.; Lott, J.; Weder, C.; Castellano, F. N. Influence of Temperature on Low-Power Upconversion in Rubbery Polymer Blends. *J. Am. Chem. Soc.* **2009**, *131*, 12007−12014.
(21) Islangulov, R. R.; Lott, J.; Weder, C.; Castellano, F. N. Noncoherent Low-Power Upconversion in Solid Polymer Films. *J. Am. Chem. Soc.* **2007**, *129*, 12652−12653.
(22) Kelly, K. L.; Coronado, E.; Zhao, L. L.; Schatz, G. C. The Optical Properties of Metal Nanoparticles: The Influence of Size, Shape, and Dielectric Environment. *J. Phys. Chem. B* **2003**, *107*, 668− 677.
(23) Kreibig, U.; Vollmer, M. Optical Properties of Metal Clusters. *Springer Series in Materials Science 25; Springer: Berlin*, **1995**.
(24) Zhao, J.; Pinchuk, A. O.; McMahon, J. M.; Li, S. Z.; Ausman, L. K.; Atkinson, A. L.; Schatz, G. C. Methods for describing the electromagnetic properties of silver and gold nanoparticles. *Acc. Chem. Res.* **2008**, *41*, 1710−1720.
(25) Sugawa, K.; Akiyama, T.; Kawazumi, H.; Yamada, S. PlasmonEnhanced Photocurrent Generation from Self-Assembled Monolayers of Phthalocyanine by Using Gold Nanoparticle Films. *Langmuir* **2009**, *25*, 3887−3893.
(26) Ikeda, K.; Takahashi, K.; Masuda, T.; Uosaki, K. Plasmonic Enhancement of Photoinduced Uphill Electron Transfer in a Molecular Monolayer System. *Angew. Chem., Int. Ed.* **2011**, *50*, 1280−1284.
(27) Kawawaki, T.; Takahashi, Y.; Tatsuma, T. Enhancement of Dye-Sensitized Photocurrents by Gold Nanoparticles: Effects of Plasmon Coupling. *J. Phys. Chem. C* **2013**, *117*, 5901−5907.

(28) Kanaizuka, K.; Yagyu, S.; Ishizaki, M.; Kon, H.; Togashi, T. Largely Enhanced Photocurrent via Gap-Mode Plasmon Resonance by a Nanocomposite Layer of Silver Nanoparticles and Porphyrin Derivatives Fabricated on an Electrode. *Appl. Phys. Lett.* **2012**, *101*, 063103.
(29) Matsumoto, R.; Yonemura, H.; Yamada, S. Photoelectrochemical Responses from Zinc Porphyrin-Silver Nanoparticle Composite Films Fabricated on ITO Electrodes. *J. Phys. Chem. C* **2013**, *117*, 2486−2493.
(30) Sugawa, K.; Takeshima, N.; Uchida, K.; Tahara, H.; Jin, S.; Tsunenari, N.; Akiyama, T.; Kusaka, Y.; Fukuda, N.; Ushijima, H.; Tsuchido, Y.; Hashimoto, T.; Hayashita, T.; Otsuki, J. Photocurrent Enhancement of Porphyrin Molecules over a Wide-Wavelength Region Based on Combined Use of Silver Nanoprisms with Different Aspect Ratios. *J. Mater. Chem. C* **2015**, *3*, 11439−11448.
(31) Sugawa, K.; Uchida, K.; Takeshima, N.; Jin, S.; Tsunenari, N.; Takeda, H.; Kida, Y.; Akiyama, T.; Otsuki, J.; Takase, K.; Yamada, S. Extraordinary Enhancement of Porphyrin Photocurrent Utilizing Plasmonic Silver Arrays. *Nanoscale* **2016**, *8*, 15467−15472.
(32) Sugawa, K.; Yamaguchi, D.; Tsunenari, N.; Uchida, K.; Tahara, H.; Takeda, H.; Tokuda, K.; Jin, S.; Kusaka, Y.; Fukuda, N.; Ushijima, H.; Akiyama, T.; Watanuki, Y.; Nishimiya, N.; Otsuki, J.; Yamada, S. Efficient Photocurrent Enhancement from Porphyrin Molecules on Plasmonic Copper Arrays: Beneficial Utilization of Copper Nanoanntenae on Plasmonic Photoelectric Conversion Systems. *ACS Appl. Mater. Interfaces* **2017**, *9*, 750−762.
(33) Lakowicz, J. R. Radiative Decay Engineering: Biophysical and Biomedical Applications. *Anal. Biochem.* **2001**, *298*, 1−24.
(34) Aslan, K.; Gryczynski, I.; Malicka, J.; Matveeva, E.; Lakowicz, J. R.; Geddes, C. D. Metal-Enhanced Fluorescence: an Emerging Tool in Biotechnology. *Curr. Opin. Biotechnol.* **2005**, *16*, 55−62.
(35) Deng, W.; Goldys, E. M. Plasmonic Approach to Enhanced Fluorescence for Applications in Biotechnology and the Life Sciences. *Langmuir* **2012**, *28*, 10152−10163.
(36) Xie, F.; Baker, M. S.; Goldys, E. M. Enhanced Fluorescence Detection on Homogeneous Gold Colloid Self-Assembled Monolayer Substrates. *Chem. Mater.* **2008**, *20*, 1788−1797.
(37) Lakowicz, J. R.; Ray, K.; Chowdhury, M.; Szmacinski, H.; Fu, Y.; Zhang, J.; Nowaczyk, K. Plasmon-Controlled Fluorescence: a New Paradigm in Fluorescence Spectroscopy. *Analyst* **2008**, *133*, 1308− 1346.
(38) Sugawa, K.; Tamura, T.; Tahara, H.; Yamaguchi, D.; Akiyama, T.; Otsuki, J.; Kusaka, Y.; Fukuda, N.; Ushijima, H. Metal-Enhanced Fluorescence Platforms Based on Plasmonic Ordered Copper Arrays: Wavelength Dependence of Quenching and Enhancement Effects. *ACS Nano* **2013**, *7*, 9997−10010.
(39) Ming, T.; Zhao, L.; Yang, Z.; Chen, H.; Sun, L.; Wang, J.; Yan, C. Strong Polarization

Dependence of Plasmon-Enhanced Fluorescence on Single Gold Nanorods. *Nano Lett.* **2009**, *9*, 3896−3903.
(40) Ming, T.; Zhao, L.; Chen, H.; Woo, K. C.; Wang, J.; Lin, H.-Q. Experimental Evidence of Plasmophores: Plasmon-Directed Polarized Emission from Gold Nanorod-Fluorophore Hybrid Nanostructures. *Nano Lett.* **2011**, *11*, 2296−2303.
(41) Ming, T.; Chen, H.; Jiang, R.; Li, Q.; Wang, J. Plasmon Controlled Fluorescence: Beyond the Intensity Enhancement. *J. Phys. Chem. Lett.* **2012**, *3*, 191−202.
(42) Poorkazem, K.; Hesketh, A. V.; Kelly, T. L. Plasmon-Enhanced Triplet−Triplet Annihilation Using Silver Nanoplates. *J. Phys. Chem. C* **2014**, *118*, 6398−6404.
(43) Hyoung-Il, K.; Weon, S.; Kang, H.; Hagstrom, A. L.; Kwon, O. S.; Lee, Y.-S.; Choi, W.; Kim, J.-H. Plasmon-Enhanced Sub-Bandgap Photocatalysis via Triplet−Triplet Annihilation Upconversion for Volatile Organic Compound Degradation. *Environ. Sci. Technol.* **2016**, *50*, 11184−11192.
(44) Park, J. K.; Lee, G. Y.; Jung, K.; Ko, D.-H.; Han, K.; Ko, H. Enhanced triplet−triplet annihilation in bicomponent organic systems by using a gap plasmon resonator. *Nanoscale* **2015**, *7*, 12828−12832.
(45) Westbrook, E. G.; Zhang, P. Plasmon-enhanced triplet-triplet annihilation upconversion of post-modified polymeric acceptors. *Dalton Trans.* **2018**, *47*, 8638−8645.
(46) Cao, X.; Hu, B.; Ding, R.; Zhang, P. Plasmon-enhanced homogeneous and heterogeneous triplet-triplet annihilation by gold nanoparticles. *Phys. Chem. Chem. Phys.* **2015**, *17*, 14479−14483.
(47) Schulze, T. F.; Schmidt, T. W. Photochemical upconversion: present status and prospects for its application to solar energy conversion. *Energy Environ. Sci.* **2015**, *8*, 103−125.
(48) Kwon, O. S.; Song, H. S.; Conde, J.; Kim, H.; Artzi, N.; Kim, J.- H. Dual-Color Emissive Upconversion Nanocapsules for Differential Cancer Bioimaging In Vivo. *ACS Nano* **2016**, *10*, 1512−1521.
(49) Monguzzi, A.; Tubino, R.; Meinardi, F. Multicomponent Polymeric Film for Red to Green Low Power Sensitized Upconversion. *J. Phys. Chem. A* **2009**, *113*, 1171−1174.
(50) Jin, R.; Cao, Y. C.; Hao, E.; Metraux, G. S.; Schatz, G. C.; Mirkin, C. A. Controlling anisotropic nanoparticle growth through plasmon excitation. *Nature* **2003**, *425*, 487−490.
(51) Jin, R.; Cao, Y.; Mirkin, C. A.; Kelly, K. L.; Schatz, G. C.; Zheng, J. G. Photoinduced conversion of silver nanospheres to nanoprisms. *Science* **2001**, *294*, 1901−1903.
(52) Xue, C.; Mirkin, C. A. pH-switchable silver nanoprism growth pathways. *Angew. Chem., Int. Ed.* **2007**, *46*, 2036−2038.
(53) Callegari, A.; Tonti, D.; Chergui, M. Photochemically Grown Silver Nanoparticles with Wavelength-Controlled Size and Shape. *Nano Lett.* **2003**, *3*, 1565−1568.

(54) Stamplecoskie, K. G.; Scaiano, J. C. Light Emitting Diode Irradiation Can Control the Morphology and Optical Properties of Silver Nanoparticles. *J. Am. Chem. Soc.* **2010**, *132*, 1825−1827.
(55) Jalal Uddin, M.; Khalid Hossain, M.; Hossain, M. I.; Qarony, W.; Tayyaba, S.; Mia, M. N. H.; Pervez, M. F.; Hossen, S. Modeling of self-assembled monolayers (SAMs) of Octadecanethiol and Hexadecanethiol on gold (Au) and silver (Ag). *Results Phys.* **2017**, *7*, 2289−2295.
(56) Aslan, K.; Leonenko, Z.; Lakowicz, J. R.; Geddes, C. D. Annealed silver-island films for applications in metal-enhanced fluorescence: interpretation in terms of radiating plasmons. *J. Fluoresc.* **2005**, *15*, 643−654.
(57) Lakowicz, J. R. Radiative decay engineering 5: metal-enhanced fluorescence and plasmon emission. *Anal. Biochem.* **2005**, *337*, 171− 194.
(58) Previte, M. J.R.; Aslan, K.; Zhang, Y.; Geddes, C. D. MetalEnhanced Surface Plasmon-Coupled Phosphorescence. *J. Phys. Chem. C* **2007**, *111*, 6051−6059.
(59) Heller, C. A.; Henry, R. A.; McLaughlin, B. A.; Bliss, D. E. Fluorescence spectra and quantum yields. Quinine, uranine, 9,10- diphenylanthracene, and 9,10-bis(phenylethynyl)anthracenes. *J. Chem. Eng. Data* **1974**, *19*, 214−219.
(60) Demeter, A. First Steps in Photophysics. I. Fluorescence Yield and Radiative Rate Coefficient of 9,10-Bis(phenylethynyl)anthracene in Paraffins. *J. Phys. Chem. A* **2014**, *118*, 9985−9993.
(61) Monguzzi, A.; Mezyk, J.; Scotognella, F.; Tubino, R.; Meinardi, F. Upconversion-induced fluorescence in multicomponent systems: steady-state excitation power threshold. Phys. *Rev. B: Condens. Matter Mater. Phys.* **2008**, *78*, 195112/1−195112/5.
(62) Raisys, S.; Kazlauskas, K.; Jursėnas, S.; Simon, Y. C. The Role of ̇Triplet Exciton Diffusion in Light-Upconverting Polymer Glasses. *ACS Appl. Mater. Interfaces* **2016**, *8*, 15732−15740.
(63) Akhavan, S.; Akgul, M. Z.; Hernandez-Martinez, P. L.; Demir, H. V. Plasmon-Enhanced Energy Transfer in Photosensitive Nanocrystal Device. *ACS Nano* **2017**, *11*, 5430−5439.
(64) Yun, C. S.; Javier, A.; Jennings, T.; Fisher, M.; Hira, S.; Peterson, S.; Hopkins, B.; Reich, N. O.; Strouse, G. F. Nanometal surface energy transfer in optical rulers, breaking the FRET barrier. *J. Am. Chem. Soc.* **2005**, *127*, 3115−3119.
(65) Chaudhuri, D.; Li, D.; Sigmund, E.; Wettach, H.; Hoeger, S.; Lupton, J. M. Plasmonic surface enhancement of dual fluorescence and phosphorescence emission from organic semiconductors: effect of exchange gap and spin-orbit coupling. *Chem. Commun.* **2012**, *48*, 6675−6677.
(66) Zhao, L.; Ming, T.; Shao, L.; Chen, H.; Wang, J. Plasmon Controlled Forster Resonance Energy Transfer. *J. Phys. Chem. C* **2012**, *116*, 8287−8296.
(67) Wu, D. M.; Garcia-Etxarri, A.; Salleo, A.; Dionne, J. A. Plasmon-Enhanced Upconversion. *J. Phys. Chem. Lett.* **2014**, *5*, 4020− 4031.

(68) Kena-Cohen, S.; Wiener, A.; Sivan, Y.; Stavrinou, P. N.; Bradley, D. D.C.; Horsfield, A.; Maier, S. A. Plasmonic Sinks for the Selective Removal of Long-Lived States. *ACS Nano* **2011**, *5*, 9958− 9965.
(69) Seo, C.; Lee, J.; Kim, M. S.; Lee, Y.; Jung, J.; Shin, H.-W.; Ahn, T. K.; Sun, G.; Kim, J.; Kim, J. Plasmon-enhanced phosphorescence of hybrid thin films of metal-free purely organic phosphor and silver nanoparticles. *Chem. Phys. Lett.* **2017**, *676*, 134−139.
(70) Pan, S.; Rothberg, L. J. Enhancement of Platinum Octaethyl Porphyrin Phosphorescence near Nanotextured Silver Surfaces. *J. Am. Chem. Soc.* **2005**, *127*, 6087−6094.
(71) Theodorou, I. G.; Jawad, Z. A.R.; Jiang, Q.; Aboagye, E. O.; Porter, A. E.; Ryan, M. P.; Xie, F. Gold Nanostar Substrates for MetalEnhanced Fluorescence through the First and Second Near-Infrared Windows. *Chem. Mater.* **2017**, *29*, 6916−6926.
(72) Yuan, H.; Khatua, S.; Zijlstra, P.; Yorulmaz, M.; Orrit, M. Thousand-fold Enhancement of Single-Molecule Fluorescence Near a Single Gold Nanorod. *Angew. Chem., Int. Ed.* **2013**, *52*, 1217−1221.
(73) Kinkhabwala, A.; Yu, Z.; Fan, S.; Avlasevich, Y.; Muellen, K.; Moerner, W. E. Large single-molecule fluorescence enhancements produced by a bowtie nanoantenna. *Nat. Photonics* **2009**, *3*, 654−657.
(74) Bek, A.; Jansen, R.; Ringler, M.; Mayilo, S.; Klar, T. A.; Feldmann, J. Fluorescence Enhancement in Hot Spots of AFMDesigned Gold Nanoparticle Sandwiches. *Nano Lett.* **2008**, *8*, 485− 490.
(75) Huang, F.; Baumberg, J. J. Actively Tuned Plasmons on Elastomerically Driven Au Nanoparticle Dimers. *Nano Lett.* **2010**, *10*, 1787−1792.
(76) Waxenegger, J.; Trügler, A.; Hohenester, U. Plasmonics Simulations with the MNPBEM Toolbox: Consideration of Substrates and Layer Structures. Comput. *Phys. Commun.* **2015**, *193*, 138−150.
(77) Rakic, A. D.; Djurisic, A. B.; Elazar, J. M.; Majewski, M. L. Optical properties of metallic films for vertical-cavity optoelectronic devices. *Appl. Opt.* **1998**, *37*, 5271−5283.

Chapter 3

Improvement of Upconverted Emission Efficiency by Optimization of Plasmon-Interacting Sensitizers

3-0. Abstract

In order to improve the quantum yield of TTA-UC, the use of a strong electric field from LSP resonance has attracted attention. In previous study, we found that the optical interplay between the strong local electric fields from the LSP resonance and the photofunctional molecules used in the TTA-UC systems leads to multiple effects including not only beneficial enhancement effects but also harmful quenching effect: the former corresponds to the photoexcitation enhancement of sensitizer and the acceleration of radiative decay rate from the singlet excited emitter and the latter is the suppression of TTET by accelerating the radiative decay rate from the triplet excited sensitizer. In this study, we focus on the optimal selection of sensitizer for extracting the enhancement effects. Surprisingly, the quenching effect was significantly suppressed by changing the metal centre of phosphorescent porphyrin sensitizer, which governs the spin-orbital coupling intensity, from Pd to Pt. Namely, a radiative decay rate from the phosphorescence from Pt porphyrin of which the spin-orbital coupling constant is larger than the Pd porphyrin was difficult to be accelerated by the LSP resonance, resulting in the improvement of TTET suppression. The results obtained in this study provide the resolution of nature for the interaction of LSP resonance with the spin-flip transition-allowed metal complexes as well as the guideline for the significant plasmonic enhancement of TTA-UC systems.

3-1. Introduction

The development of solar energy-based optoelectronic devices including photocatalysts and solar cells are one of the promising strategies for realizing a sustainable society. However, the efficient utilization of solar light by these devices has rarely been achieved because the driving wavelengths are limited by the band gap energy of the photoactive materials for securing the high redox potentials and the high photovoltages.[1,2] Recently, a photon upconversion techniques of which two photons with a low energy are converted into one photon with a high energy have been proposed as a useful method to overcome the bandgap limit because the photoactive materials having a wide bandgap may get a chance to be efficiently photoexcited by the low energy photons.[3-7] In recent years, the upconversion system based on a triplet-triplet annihilation (TTA) phenomenon utilizing two photofunctional molecules, a sensitizer and an emitter, has a significant attention because it can be driven even by the irradiation with low-intensity incoherent light such as sunlight.[8-10] The upconverted emission using TTA can be achieved as follows: (ⅰ) a light absorption producing an excited singlet state of the sensitizer, (ⅱ) an intersystem crossing (ISC) from the singlet excited state to the triplet excited state of the sensitizer, (ⅲ) a triplet-triplet energy transfer (TTET) from the triplet excited sensitizer to emitter, producing the excited triplet state of the emitter, (ⅳ) a TTA process between two emitters with triplet excited state, producing one excited singlet state of the emitter, and finally, (ⅴ) the radiation of emission of which the energy is larger than the absorbed energy in (i) from the excited singlet state of the emitter. The TTET and TTA efficiencies strongly depend on the collision probability between the triplet excited sensitizer and emitter and two triplet excited emitters, respectively because these processes are based on Dexter energy transfer, which is induced only when the molecules are well-approach each other. Several recent studies have achieved high emission quantum yields of TTA-UC over 30% in a liquid phase in which the molecular diffusion rate is sufficiently high.[11-13] On the other hand, for applying of the TTA-UC systems to the solar devices, the development of TTA-UC systems with a high quantum yield in a solid phase is required for the reduction of environmental loading, acquisition of environmental tolerance, and weight reduction. However, in the solid phase system, both TTET and TTA efficiencies are suffered from being decreased owing to the limitation of the molecular diffusion rate. To solve this problem, in addition to the utilization of high exciton mobility instead of the molecular diffusion[14-16] as well as the use of matrix polymer with a low glass transition temperature for improving the molecular diffusion rate,[17-21] recently, the improvement of the upconverted emission from solid-state-based TTA-UC systems has been successful by inserting metal nanoparticles, which can generate localized surface plasmon (LSP)

resonance, into the systems (i.e. plasmonic TTA-UC systems).[22-26] Although the whole improvement mechanism(s) has been rarely discussed until now, we recently found that the optical interplay between the strong local electric fields from the LSP resonance and the photofunctional molecules used in the TTA-UC systems leads to multiple effects including not only beneficial enhancement effects but also harmful quenching effect: the former corresponds to the photoexcitation enhancement of sensitizer and the acceleration of radiative decay rate from the singlet excited emitter (i.e., Purcell effect) and the latter is the suppression of TTET by accelerating the radiative decay rate from the triplet excited sensitizer.[27] If the harmful effect is avoided, a plasmonic TTA-UC system with a further improved performance will be achieved. We succeeded in decreasing the TTET suppression by avoiding the interaction between the LSP resonance and the triplet excited sensitizer by a precise tuning technique of LSP resonance wavelength, which can make no allowance for generating the resonance band at the phosphorescence wavelength of sensitizer. However, the complete avoiding may still be challenging because the conventional LSP resonance including a radiative damping (i.e., a bright mode) usually has a largely-broadened extinction band.[28,29] In this study, we focus on the optimal selection of sensitizer to benefit from only the enhancement effects in the plasmonic TTA-UC systems. Surprisingly, the harmful quenching effect was significantly suppressed by changing the metal centre of phosphorescent porphyrin sensitizer, which governs the spin-orbital coupling intensity, from Pd to Pt. The origin was suggested to be attributed to the unique and systematic change in the optical interaction between the LSP resonance and the phosphorescent metal complexes with the change in the intrinsic spin-orbital coupling constant. Namely, a radiative decay rate from the phosphorescence from Pt octaethylporphyrin of which the spin-orbital coupling constant is larger than that of Pd octaethylporphyrin was difficult to be accelerated by the LSP resonance, resulting in the improvement of TTET suppression. The results obtained in this study provide the resolution of nature for the interaction of LSP resonance with the spin-flip transition-allowed metal complexes as well as the guideline for the significant plasmonic enhancement of TTA-UC systems.

3-2. Experimental section

Materials

Milli-Q-grade water (resistivity: 18.2 MΩ cm) was used to prepare all aqueous solutions. Toluene was purchased from Kishida Chemical (Japan). Sodium tetrahydroborate (NaBH4), silver nitrate ($AgNO_3$), PEI (MW: ~10000), and N,Ndimethylformamide (DMF, 99.5%) from Fujifilm Wako Pure Chemical (Japan). Trisodium citrate dihydrate, sodium hydroxide (NaOH), and hydrogen peroxide solution (H_2O_2, 30%) were purchased from Kanto Chemical (Japan). PSS (MW: ~70,000), PdOEP, PtOEP, $Ru(bpy)_3$, and $Ir(BT)_2(acac)$ were purchased from Sigma-Aldrich (United States). DPA was purchased from Tokyo Chemical Industry (Japan). Modified polyvinyl alcohol (Exceval) was purchased from Kuraray (Japan). All chemicals were used without further purification.

Measurements

Extinction and absorption spectra were measured by a JASCO V-770 spectrophotometer. Fluorescence and phosphorescence spectra were measured by a JASCO FP-8600. The SEM observations were performed using a HITACHI S4500 microscopes. The TEM observations were performed using a Hitachi HF2000 system at an acceleration voltage of 200 kV. The AFM (tapping mode) measurements were conducted using SPA-400 (Hitachi High-Tech Science). Electromagnetic field enhancement contours of the SAgPR and LAgPR were calculated by boundary element method within the QS approximation (QS-BEM) framework with the MNPBEM17 program on MATLAB.[30] The dielectric function of silver used was obtained from the previous report by Rakic et al.[31] The fabrication and the optical measurements of all of the hybrids were performed within a few days after the synthesis of AgPRs.

Synthesis of AgPRs with Different Aspect Ratios.

The AgPRs with 2.7 and 4.1 of aspect ratio were synthesized by a modified photochemical growth methods described previously (From our previous report, the thickness of AgPRs was 10 nm).[32,33-37] Firstly, a colloidal aqueous solution of silver nanospheres was prepared by our reported procedure.[32] An aqueous solution containing $NaBH_4$ (0.2 mM, 1 mL) as a reducer and trisodium citrate (5 mM, 100 mL) as a stabilizer were added to an aqueous solution containing $AgNO_3$ (1 mM, 100 mL) in an ice bath, followed by stirring for 1 h to synthesize silver nanospheres. Next, the pH of the obtained colloidal solution of silver nanospheres was adjusted to 11.2 by addition of an aqueous solution of NaOH (0.2 M). This was followed by irradiation of the colloidal solution for 24 h by light-emitting diodes with center wavelengths of 470 and 525 nm, resulting the formation of SAgPRs (edge length: 27 ± 5 nm) and LAgPRs (edge length: 41 ± 5 nm),

respectively.

Preparation of Hybrids of AgPRs and dye molecule films

The glass substrates (1.5 × 2.0 cm^2) were washed by a mixture solution of H_2O_2 (30 %) and NH_3 (28 %) (1/1 = v/v) at 100 °C for 1 h to clean the glass surfaces, followed by washing with Milli-Q water. Then, the glass substrates were immersed into an aqueous solution of positively charged PEI (4.0 mg/mL) for 1 min, followed by washing with Milli-Q water. The obtained PEI-modified glass substrates were immersed into the aqueous colloidal solution of AgPRs to immobilize the AgPRs onto the glass surfaces by the electrostatic interaction (SAgPRs/glass and LAgPRs/glass) for an arbitrary time. In order to suppress the quenching by electron transfer from photofunctional molecules to AgPRs, polyelectrolyte multilayers consisting of positively charged PEI and negatively charged PSS were inserted between them following an electrostatic layer-by-layer process. First, the AgPRs/glass were immersed in an aqueous solution of PEI (0.1 wt %) for 1 s, followed by washing with Milli-Q water for 10 s. Next, the resultant PEI-modified AgPRs/glass were immersed into an aqueous solution of PSS (0.2 wt %) for 1 s, followed by washing with Milli-Q water for 10 s. The hybrids of the AgPRs and the TTA-UC systems were prepared by spin-coating (3000 rpm for 20 s) a DMF solution containing EO-EPI (1 wt%), PdOEP (50 μM), PtOEP (50 μM), $Ru(bpy)_3$ (1 mM), $Ir(BT)_2(acac)$ (1 mM), and DPA (2.5 mM). Finally, an aqueous solution of PVA (10 wt%, 50 μL) was cast onto the surface of the hybrid thin films and then dried under vacuum. The hybrids were covered with PVA thin films having a low oxygen permeability to suppress the quenching effect of the oxygen because the triplet excited state of the sensitizer can be quenched by the presence of oxygen.

3-3. Results and Discussion

3-3-1. Preparation of Plasmonic TTA-UC Systems.

In this study, Pd and Pt complexes of which the ligand are the same as an octaethylporphyrin (PdOEP and PtOEP) and 9,10-diphenylanthracene (DPA) were employed as a sensitizer and an emitter, respectively (molecular structures: Figure 1 (A)). These photofunctional molecules have conventionally been used in TTA-UC systems.[38,39] Their absorption and emission spectra of *N,N*-dimethylformamide (DMF) solutions of PdOEP, PtOEP, and DPA are shown in Figure 1 (B), (C), and (D). The absorption spectra of PdOEP and PtOEP solutions are similar; a strong absorption peak attributed to the Soret band at 391 and 380 nm and relatively weak absorption peak attributed to the Q-band at 545 and 534 nm with a shoulder at 511 and 500 nm were observed for PdOEP and PtOEP, respectively. The emission spectrum of PdOEP solution showed a strong phosphorescence emission band at 665 nm concomitant with a very small fluorescence band around 550 nm because the complex has a very high ISC efficiency (Φ_{ISC}: ~1)[40] owing to the presence of Pd(II) metal centre to exhibit a high spin-orbital coupling constant. Meanwhile, PtOEP showed only a phosphorescence emission band at 665 nm without any fluorescence band. This is because that the spin-orbital coupling constant of Pt(II) metal centre is further larger than that of Pd(II). In order to investigate in detail the effect of LSP resonance on each photoinduced process in the TTA-UC, we used triangular silver nanoplates (silver nanoprisms: AgPRs) as an LSP resonator because of their LSP resonance-induced strong local electromagnetic fields and the tunability of LSP resonance wavelengths over a wide visible region by adjusting their aspect ratio (i.e., the ratio of edge length to thickness).[33-35] We synthesized two types of AgPRs by a photoinduced growth method.[36,37] Each AgPRs showed a LSP resonance peak attributed to in-plane dipole mode at 491 nm and 598 nm, respectively. Furthermore, the LSP resonance band attributed to the out-of-plane dipole mode was observed around 410 nm in both SAgPRs and LAgPRs (Figure 1 (D)). The edge lengths of the AgPRs were estimated from transmission electron microscopy (TEM) images to be 27 ± 4 nm (small-size AgPRs (SAgPRs)) and 41 ± 4 nm (large-size AgPRs (LAgPRs)), as shown in Figure 1 (E). We reported previously that the thicknesses of AgPRs, which were estimated approximately 10 nm regardless of the edge length.[41] Therefore, the larger aspect ratio (SAgPRs: 2.7 and LAgPRs: 4.1) led to the longer wavelength of in-plane dipole resonance, agreeing with the previous report.[27]

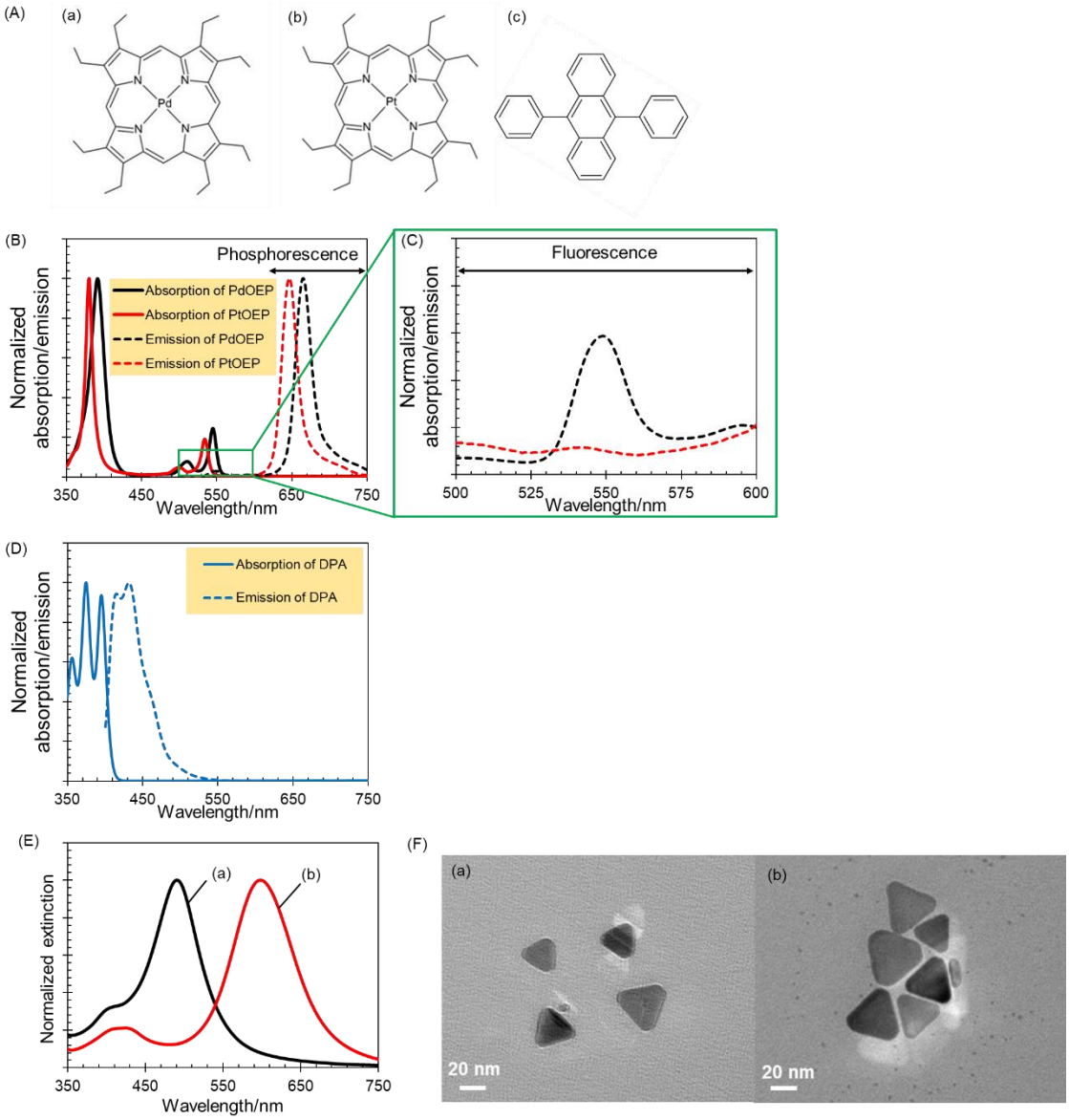

Figure 3-1. Optical properties of the materials used in this study (A) Molecular structures of (a) PdOEP, (b) PtOEP, and (c) DPA. (B) Normalized absorption and emission (λ_{ex} = 390 nm) spectra of DMF solutions of (a) PdOEP (5 μM), (b) PtOEP (5 μM). (C) Magnified fluorescence spectra of PdOEP and PtOEP. (D) Normalized absorption and emission (λ_{ex} = 350 nm) spectra of DMF solutions of DPA (25 μM). (E) Extinction spectra of colloidal aqueous solutions of (a) SAgPRs and (b) LAgPRs. (E) TEM images of (a) SAgPRs and (b) LAgPRs.

We prepared the hybridized systems consisting of AgPRs and TTA-UC thin solid films according to the following procedure (Scheme.3-1). The negatively-charged AgPRs were immobilized on a glass substrate via the electrostatic adsorption process by immersing a positively-charged polyethylenimine (PEI)-modified glass substrate in the colloidal aqueous solution (Step 1 in Scheme. 3-1). In STEP 2 in Scheme 1, first, the a couple of

layers of positively-charged PEI and negatively-charged polystyrenesulfonate (PSS) was inserted between AgPRs and emissive layer based on TTA-UC to suppress the strong electron transfer quenching from the photoexcited molecules to AgPRs.[42] To investigate the thickness of a PEI-PSS bilayer, the AFM measurements were carried out for the PEI-PSS(*Z*)/glass substrate (*Z* = 10 and 15). The probe needle was scanned over the layer surfaces scratched by a sharp tweezer. The thickness of PEI-PSS(10)/glass and of PEI-PSS(15)/glass are estimated to be 25.1 ± 0.1 nm and 41.5 ± 0.2 nm, respectively. Therefore, the thickness of one bilayer was estimated to be ca. 2.7 nm. Second, an emissive layer of ethylene oxide-epichlorohydrin copolymer (EO-EPI) containing PdOEP (or PtOEP) and DPA of which the thickness was estimated to be 26.0 ± 0.3 nm by a AFM measurement (Figure 3-3)[43] was deposited on the AgPRs-immobilized glass plate by a spin-coating process. Finally, a polyvinyl alcohol film with a gas barrier property was modified on the top of the hybridized film by a dip-coating process because it is well known that the triplet excited state of the sensitizer contained in the emissive layer is harmfully quenched by triplet oxygen in the atmosphere (denoted as *X*/AgPRs(*Y*)/glass, *X*: the combinations of TTA-UC elements (PdOEP-DPA or PtOEP-DPA), *Y*: maximum extinction intensity of in-plane dipole resonance band). In addition, a reference substrate consisting of an emissive layer without any AgPRs was prepared by modifying the PEI/PSS-modified glass with the EO-EPI thin films containing the TTA-UC elements (denoted as X/glass). The substrate was protected with the polyvinyl alcohol films according to the same manner as *X*/AgPRs(*Y*)/glass.

Scheme 3-1. Schematic diagram for the preparation of plasmonic TTA-UC thin solid films.

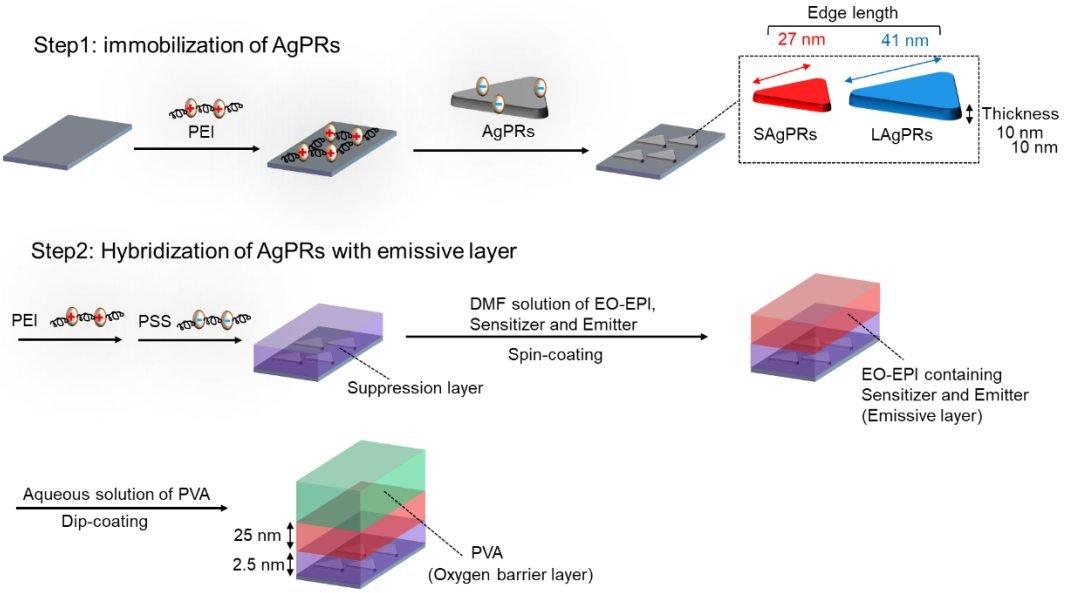

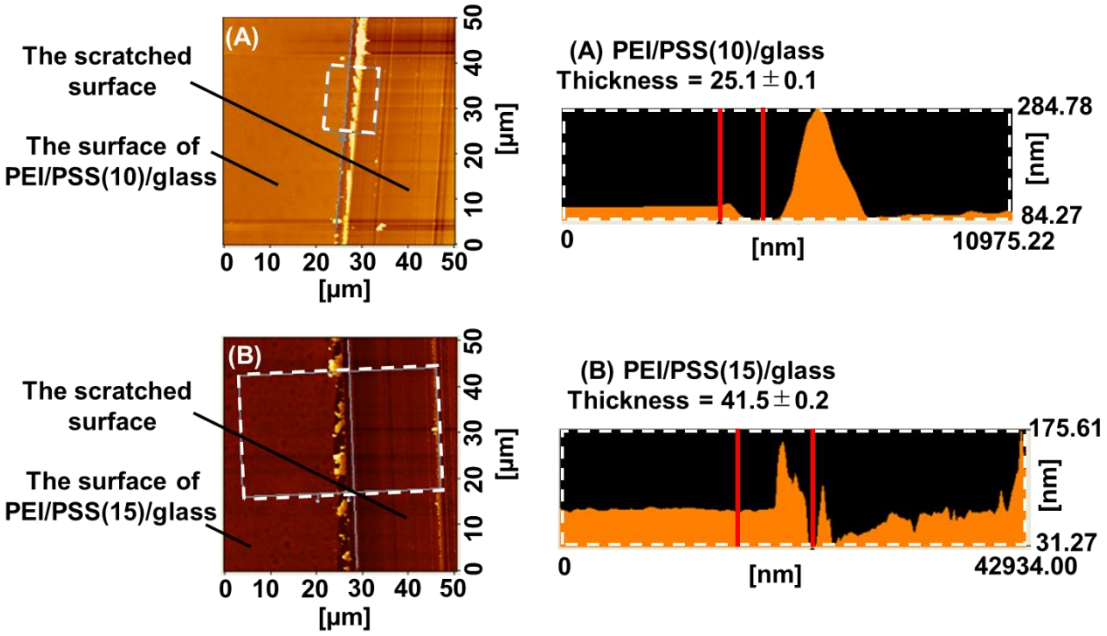

Figure 3-2. AFM images obtained from (A) PEI-PSS(10)/glass and (B) PEI-PSS(15)/glass for the estimation of the thickness of PEI-PSS bilayers.

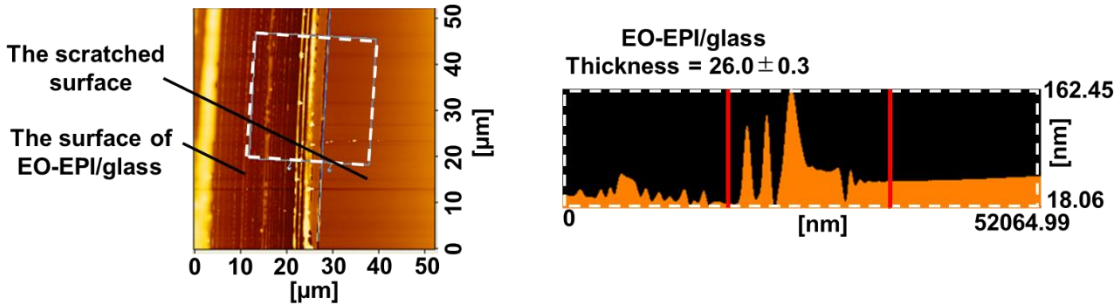

Figure 3-3. AFM images obtained from EO-EPI/glass for the estimation of the thickness of EO-EPI thin films.

Plasmonic nanoparticles, which function as a light-harvesting nanoantenna, lead to the enhancement in the efficiency of the photoexcitation process of nearby photofunctional molecules.[39-41] The enhancement of the photoexcitation efficiency of sensitizer is promising for the enhancement of the upconverted emission in the TTA-UC systems, as demonstrated by our recent study.[27] We first investigated the change in the upconverted emission intensity by inserting the SAgPRs in the TTA-UC system. As shown in the extinction spectra of PdOEP-DPA/SAgPRs(*Y*) (Figure 3-4(A)), the main LSP resonance band was red-shifted to approximately 540 nm, which was compared with that of dispersion state in an aqueous phase (Figure 3-1(E)), owing to the increase in the surrounding refractive index from water (refractive index (*n*): 1.333) to the inhomogeneous environment consisting of glass (*n*: 1.458) and polymers (*n*: 1.493). Consequently, the LSP resonance wavelength overlapped well with the Q-band of PdOEP. The extinction intensity of LSP resonance band was tuned from 0.17 to 0.27 while maintaining the spectral shape by adjusting the immersion time of the PEI-modified glass plate into the colloidal solution of SAgPRs ((b) in Figure 3-4(A)), implying that the increase in the immersion time of led to the increase in the coverage of AgPRs while maintaining the high dispersibility of SAgPRs on a glass plate. The scanning electron microscopy (SEM) images of the SAgPRs on a glass plate strongly support the suggestion; SAgPRs on all plates were well-dispersed without any aggregated AgPRs on a glass plate and the coverage increased with increasing the extinction intensity (Figure 3-4(B)). The absorption peaks attributed to the photoexcitation of PdOEP and DPA were not observed for PdOEP-DPA/SAgPRs(*Y*) because the absorbances of these absorption peaks were significantly weaker than the extinction intensity of the LSP resonance of the SAgPRs (Figure 3-5). The upconverted emission spectra of PdOEP-DPA/SAgPRs(*Y*) through the TTA-UC process (λ_{ex} = 540 nm) are shown in Figure 3-4(C). The upconverted emission observed at 400−500 nm from all of the PdOEP-DPA/SAgPRs(*Y*)/glass was

stronger than that from the PdOEP-DPA/glass. Furthermore, as shown in Figure 3-4(D), the upconverted emission intensity at 431 nm was eventually enhanced with increasing in the extinction intensity of LSP resonance at 540 nm up to 0.27. We concluded that the enhancement mechanism was mainly governed by the photoexcitation enhancement of sensitizer (Figure 3-4(E)) due to the following reasons. First, the LSP resonance band spectrally overlapped with the photoexcitaion wavelength, not with the fluorescence band of emitter (400-450 nm). Second, the intensity of local electromagnetic fields generated at around the SAgPRs calculated using a boundary element method (BEM, the geometric model of SAgPRs is described in Figure 3-6) was very strong at 540 nm ($|E_{max}/E_0|^2$ = 3162, Figure 3-4(F)).

On the other hand, for PdOEP-DPA/SAgPRs(0.33 and 0.35) with coverage of SAgPRs of 37.9 and 43.2 %, respectively, obtained by further increasing the immersion time (Figure 3-4(B)), the enhancement factor of upconverted emission was rather decreased despite the increase in the extinction intensity of LSP resonance at the excitation wavelength (540 nm) ((a) in Figure 3-4(A)). These results suggest that the harmful quenching effect of upconverted emission overcomes the beneficial enhancement effect. Both the prominent enhancement at the lower coverage of plasmonic nanoparticles and the noticeable occurrence of quenching at the higher coverage qualitatively coincide to our previous results obtained using a plasmonic TTA-UC system employing palladium(II) tetraphenyltetrabenzoporphyrin (Pd-TPTBP) and 9,10-bis-(phenylethynyl)anthracene as a sensitizer and emitter, respectively. The singular common point between the present and previous systems is that the Pd(II) metal centre was employed for obtaining the high ISC efficiency.

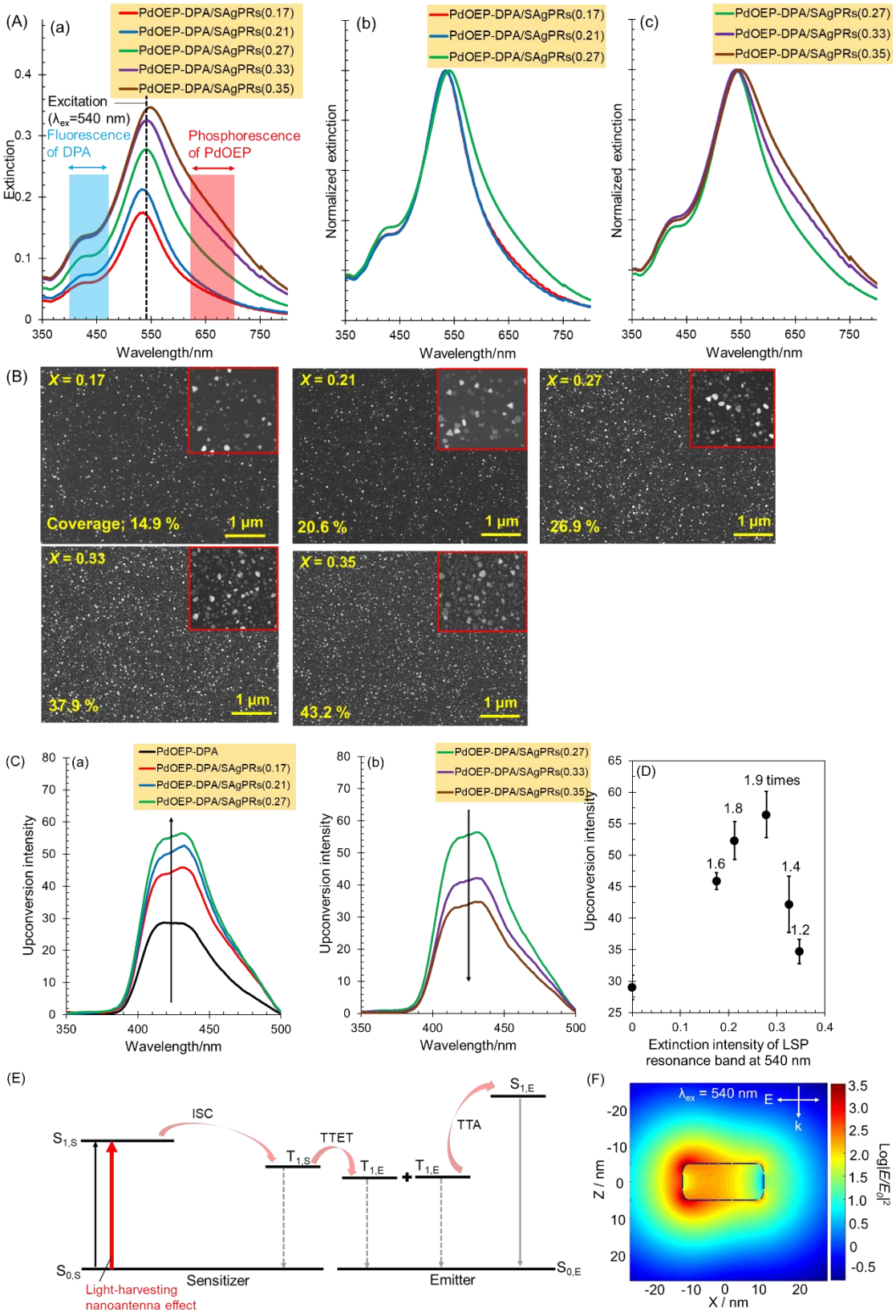

Figure 3-4. Upconverted emission properties of PdOEP-DPA/SAgPRs(*Y*)/glass and the enhancement mechanism. (A) Extinction spectra of (a) PdOEP-DPA/SAgPRs(0.17, 0.21, 0.27, 0.33, and 0.35) and

normalized extinction spectra of (b) PdOEP-DPA/SAgPRs(0.17, 0.21, and 0.27) and (c) PdOEP-DPA/SAgPRs(0.27, 0.33 and 0.35). (B) SEM images of SAgPRs(0.17, 0.21, 0.27, 0.33, and 0.35). (C) Upconverted emission spectra of (a) PdOEP-DPA/SAgPRs(0, 0.17, 0.21, and 0.27) and (b) PdOEP-DPA/SAgPRs(0.27, 0.33 and 0.35) (λ_{ex} = 540 nm). (D) Plots of upconverted emission intensity against the extinction intensity of LSP resonance band at 540 nm. (E) Suggested enhancement mechanism of the upconverted emission of the PdOEP-DPA/SAgPRs(*Y*). (F) Electromagnetic field contours of the SAgPRs at 540 nm calculated by a BEM.

Next, we investigated the change in the upconverted emission intensity by inserting the SAgPRs into the PtOEP sensitizer-based TTA-UC thin solid films (PtOEP-DPA/SAgPRs(*Y*)). As shown in Figure 3-5 (A), the extinction spectra of PtOEP-DPA/SAgPRs(*Y*) were similar as those of PtOEP-DPA/SAgPRs(*Y*). The upconverted emission from PtOEP-DPA/SAgPRs(*Y*) showed a tendency to enhance with increasing the extinction intensity of LSP resonance of SAgPRs (*i.e.*, increasing the coverage of SAgPRs), as the same with the case of PdOEP-DPA/SAgPRs(*Y*). On the other hand, it is noted that the conspicuous quenching effect of upconverted emission, which was induced at the higher SAgPRs coverage for PdOEP-DPA/SAgPRs(*Y*), was not observed Figure 3-5 (B, C). The difference between PdOEP-DPA/SAgPRs(*Y*) and PtOEP-DPA/SAgPRs(*Y*) is only the metal centre of sensitizer.

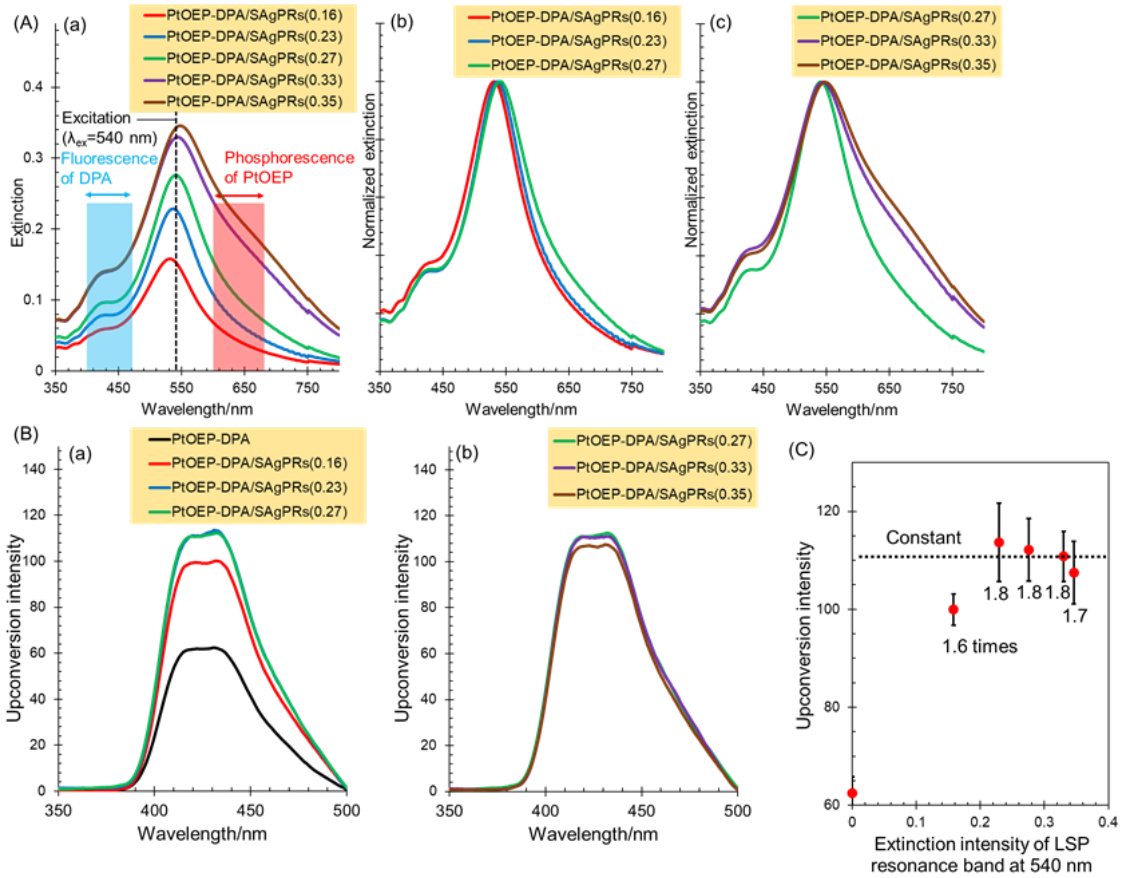

Figure 3-5. Upconverted emission properties of PtOEP-DPA/SAgPRs(*Y*)/glass. (A) Extinction spectra of (a) PtOEP-DPA/SAgPRs(0.17, 0.21, 0.27, 0.33, and 0.35) and normalized extinction spectra of (b) PtOEP-DPA/SAgPRs(0.17, 0.21, and 0.27) and (c) PtOEP-DPA/SAgPRs(0.27, 0.33 and 0.35). (B) Upconverted emission spectra of (a) PtOEP-DPA/SAgPRs(0, 0.16, 0.23, and 0.27) and (b) PdOEP-DPA/SAgPRs(0.27, 0.33 and 0.35) (λ_{ex} = 540 nm). (C) Plots of upconverted emission intensity against the extinction intensity of LSP resonance band at 540 nm.

3-3-2. Mechanism of Quenching Suppression of Upconverted Emission in PtOEP-Based Plasmonic TTA-UC Systems

From the following Equation (1) for the quantum yield of upconverted emission, any one of four processes may lead to the quenching of upconverted emission (i.e., ISC, TTET, TTA, and fluorescence from excited singlet state of emitter).[44,45]

$$\Phi_{UC} \propto \Phi_{ISC} \cdot \Phi_{TTET} \cdot \Phi_{TTA} \cdot \Phi_{Em} \quad (1)$$

where Φ_{UC}, Φ_{ISC}, Φ_{TTET}, Φ_{TTA}, and Φ_{Em} indicate the quantum yields of upconverted emission, intersystem crossing of sensitizer, triplet-triplet energy transfer from the triplet-excited sensitizer to emitter, triplet-triplet annihilation between the triplet-excited emitter, and fluorescence from the singlet-excited state of emitter, respectively. Both the ΦTTA, and Φ_{Em} may be changed by interacting the emitter with the SAgPRs. Indeed, it was experimentally confirmed that the Φ_{Em} suffered to be decreased by 38% by the electron and/or FRET-like energy transfers from the singlet-excited emitter to the SAgPRs (Figure 3-6). However, the change in Φ_{TTA} and Φ_{Em} cannot attributed to the difference in the upconverted emission quenching between PdOEP-DPA/SAgPRs(Y) and PtOEP-DPA/SAgPRs(Y) specifically at the higher coverage of SAgPRs because the interaction between the emitter and SAgPRs should be similar regardless of difference in the employed sensitizer. Therefore, the difference in upconverted emission quenching can be attributed to the difference in the Φ_{ISC} and Φ_{TTET} induced by interacting the sensitizer with

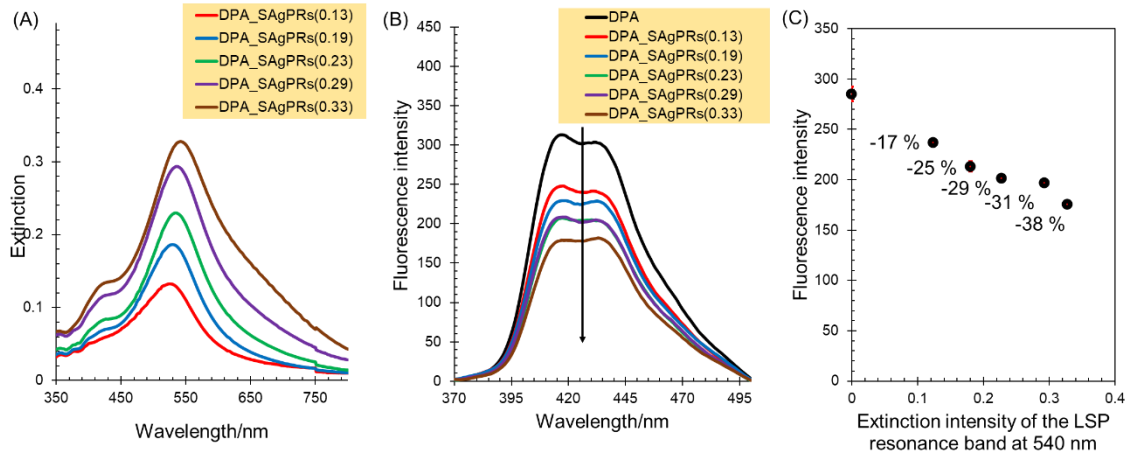

SAgPRs.

Figure 3-6. Emission properties of DPA/SAgPRs(Y)/glass. (A) Extinction spectra of DPA/SAgPRs(0.17, 0.21, 0.27, 0.33, and 0.35) (B) Upconverted emission spectra of DPA/SAgPRs(0.17, 0.21, 0.27, 0.33, and 0.35) (λ_{ex} = 350 nm). (C) Plots of fluorescence intensity against the extinction intensity of LSP resonance band at 540 nm.

Figure 5(A) shows plots of the extinction intensity of LSP resonance at the wavelengths of phosphorescence, fluorescence, and photoexcitation as well as the enhancement factors of upconverted emission for PdOEP-DPA/SAgPRs(*Y*) and PtOEP-DPA/SAgPRs(*Y*) with increasing the coverage of SAgPRs as obtained from Figure 3-7(A) and 3-7(B). While the extinction intensity at the excitation and fluorescence wavelengths rapidly increased at the lower coverage (14.9-26.9%) and then began to saturate above 37.9%, that at the phosphorescence wavelength, which is longer than the former two wavelengths, rapidly increased above the coverage of 20.6%. This is the result of inducing the plasmon coupling between the in-plane dipole modes of adjacent SAgPRs at the longer wavelength (around 650 nm) by the excessive increase in the SAgPR coverage. Thus, the triplet-excited sensitizer can be coupled with the newly-generated coupling mode of LSP.

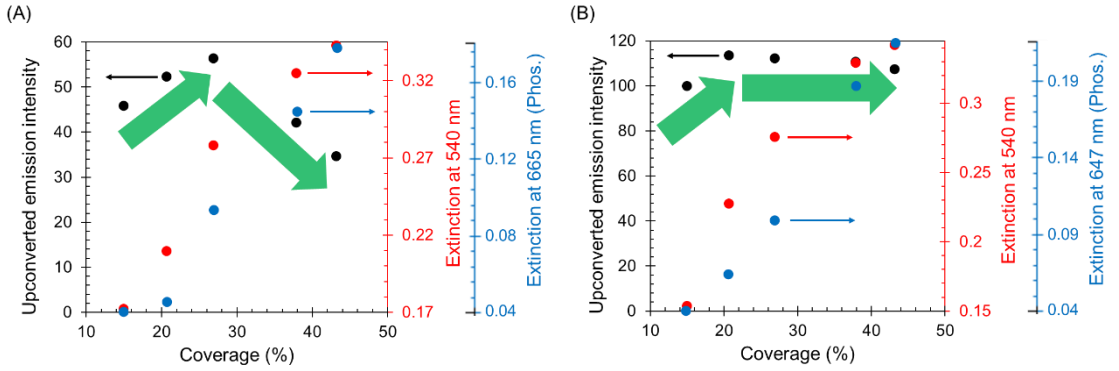

Figure 3-7. Relationship between the upconverted emission intensity and the excitation of LSP resonance. The upconverted emission intensity and the extinction intensity at 540 nm (the excitation wavelength in TTA-UC thin solid films) and 665 nm and 647 nm (the phosphorescence wavelengths of PdOEP and PtOEP, respectively.) for (A) PdOEP-DPA/SAgPRs(*Y*) and (B) PtOEP-DPA/SAgPRs(*Y*)

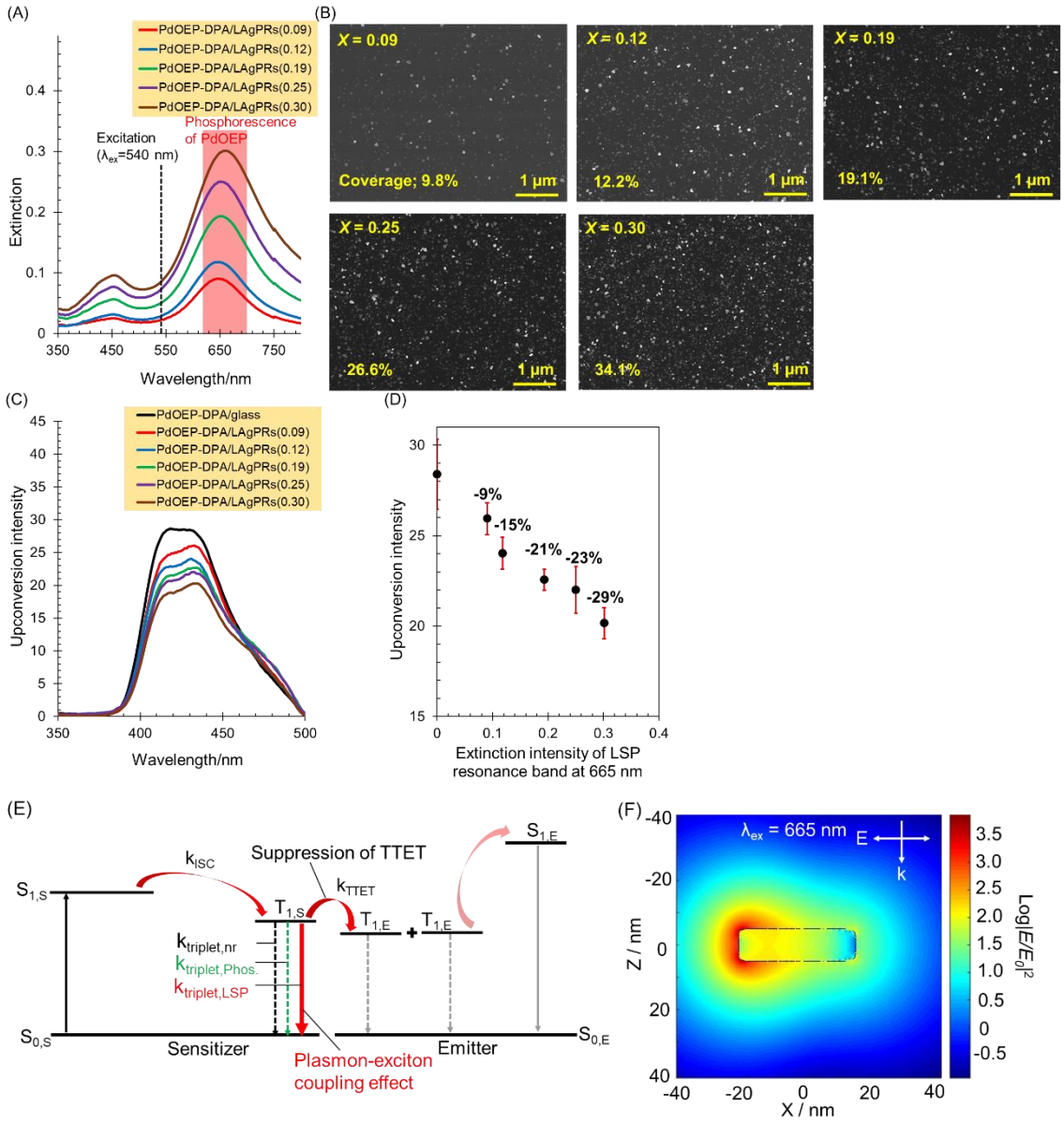

Figure 3-8. Upconverted emission properties of PdOEP-DPA/LAgPRs(*Y*)/glass and the quenching mechanism. (A) Extinction spectra of PdOEP-DPA/LAgPRs(0.09, 0.12, 0.19, 0.25, and 0.30). (B) SEM images of LAgPRs(0.09, 0.12, 0.19, 0.25, and 0.30). (C) Upconverted emission spectra of PdOEP-DPA/LAgPRs(0.09, 0.12, 0.19, 0.25, and 0.30) (λ_{ex} = 540 nm). (D) Plots of upconverted emission intensity against the extinction intensity of LSP resonance band at 665 nm. (E) Suggested quenching mechanism of the upconverted emission of the PdOEP-DPA/LAgPRs(*Y*). (F) Electromagnetic field contours of the LAgPRs at 665 nm calculated by a BEM.

the newly-generated coupling mode of LSP overlaps well with the phosphorescence wavelength of the sensitizer (PdOEP/PtOEP). Therefore, we suspected that the acceleration of the phosphorescence decay rate from the excited triplet state of the sensitizer by Plasmon-exciton coupling effect inhibits the TTET process. When LSP interacts on the phosphorescence decay of sennsitizer, the decrease of TTET efficiency is derived as follows.[46]

$$\Phi_{TTET} = \frac{k_{TTET}}{k_{triplet,nr} + k_{triplet,Phos.} + k_{TTET}} \quad (2)$$

$$\Phi_{TTET,LSP} = \frac{k_{TTET}}{k_{triplet,nr} + k_{triplet,Phos.} + k_{TTET} + k_{triplet,LSP}} \quad (3)$$

Here, $k_{triplet,nr}$, $k_{triplet,Phos.}$, k_{TTET}, and $k_{triplet,LSP}$ are the nonradiative decay rate from the excited triplet state, the phosphorescence decay rate, the TTET rate from the sensitizer to the emitter, and the phosphorescence decay rate accelerated by plasmon-exciton coupling effect. Therefore, the difference in TTET efficiency with and without LSP resonance is dependent on the scale of $k_{triplet,LSP}$ from Equations 2 and 3. We synthesized LAgPRs which generate strong LSP resonance near the phosphorescence wavelength of sensitizer (PdOEP/PtOEP), prepared composite substrate (PdOEP or PtOEP-DPA/LAGPRs (*Y*)/glass) as well as SAgPRs, and carried out the optical characteristic evaluation. Figure 3-8 (A) shows that the LSP resonance of PdOEP-DPA/LAgPRs (*Y*) is strongest around 650 nm and overlaps well with the phosphorescence wavelength (665 nm) of PdOEP, while the overlap with the excitation wavelength (540 nm) is small. Therefore, plasmons are expected to dominate the phosphorescence emission process. From SEM images, the coverage densities of LAgPRs (0.09, 0.12, 0.19, 0.25, 0.30)/glass were estimated to be 9.8%, 12.2%, 19.1%, 26.6%, and 34.1%, respectively (Figure 3-8 (B)). In LAgPRs (0.25, 0.30)/glass, the broadening of the extinction spectra was observed by the generation of the optical absorption which was attributed to the LSP coupling mode. The upconverted emission decreased with increasing the extinction intensity of PdOEP-DPA/LAgPRs (*Y*), and decrease of up to 29% was observed compared with the system without LAgPRs (Figure 3-8 (C, D)). We concluded that the quenching mechanism was mainly governed by suppression of TTET process by the acceleration of phosphorescence decay rate of sensitizer (Figure 3-8 (E)) due to the following reasons. First, the LSP resonance band spectrally overlapped with the phosphorescence wavelength (665 nm), hardly with the excitation band of sensitizer (540

nm). Second, the intensity of local electromagnetic fields generated at around the LAgPRs calculated using a BEM, was very strong at 665 nm ($|E_{max}/E_0|^2$ = 4365, Figure 3-8 (F)).

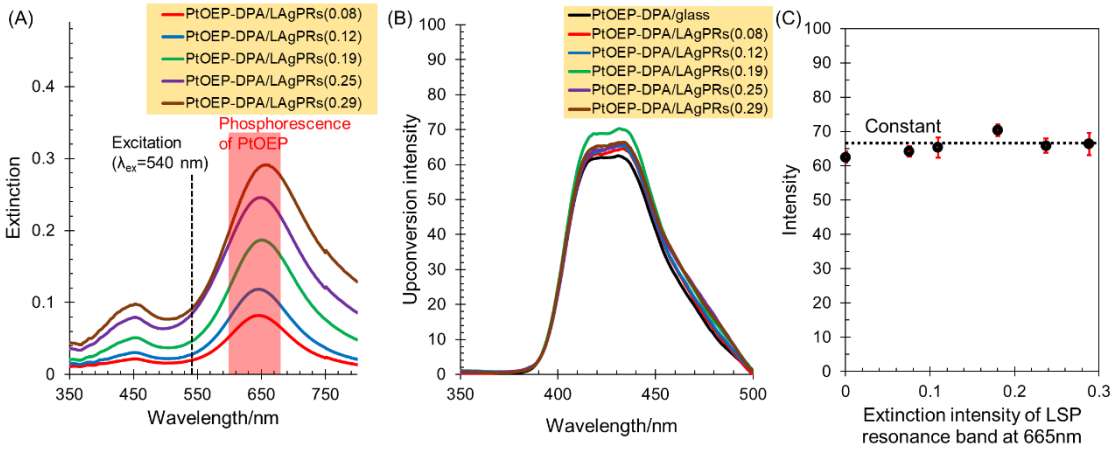

Figure 3-9. Emission properties of PtOEP-DPA/LAgPRs(*Y*)/glass. (A) Extinction spectra of PtOEP-DPA/LAgPRs(0.09, 0.12, 0.19, 0.25, and 0.30) (B) Upconverted emission spectra of PtOEP-DPA/LAgPRs(0.08, 0.12, 0.19, 0.25, and 0.29) (λ_{ex} = 540 nm). (C) Plots of fluorescence intensity against the extinction intensity of LSP resonance band at 665 nm.

On the other hand, we investigated the change in the upconverted emission intensity by inserting the LAgPRs into the PtOEP sensitizer-based TTA-UC thin solid films (PtOEP-DPA/LAgPRs(*Y*)). As shown in Figure 3-9 (A), the extinction spectra of PtOEP-DPA/LAgPRs(*Y*) were similar as those of PdOEP-DPA/LAgPRs(*Y*). The upconverted emission from PtOEP-DPA/LAgPRs(*Y*) showed a constant tendency with increasing the extinction intensity of LSP resonance of LAgPRs (*i.e.*, increasing the coverage of LAgPRs). On the other hand, it is noted that the conspicuous quenching effect of upconverted emission, which was induced at the LAgPRs for PdOEP-DPA/LAgPRs(*Y*), was not observed Figure 3-9 (B, C). The difference between PdOEP-DPA/LAgPRs(*Y*) and PtOEP-DPA/LAgPRs(*Y*) is only the metal centre of sensitizer, and this result was similar to the SAgPRs system (PdOEP-DPA/SAgPRs(*Y*) and PtOEP-DPA/SAgPRs(*Y*)).

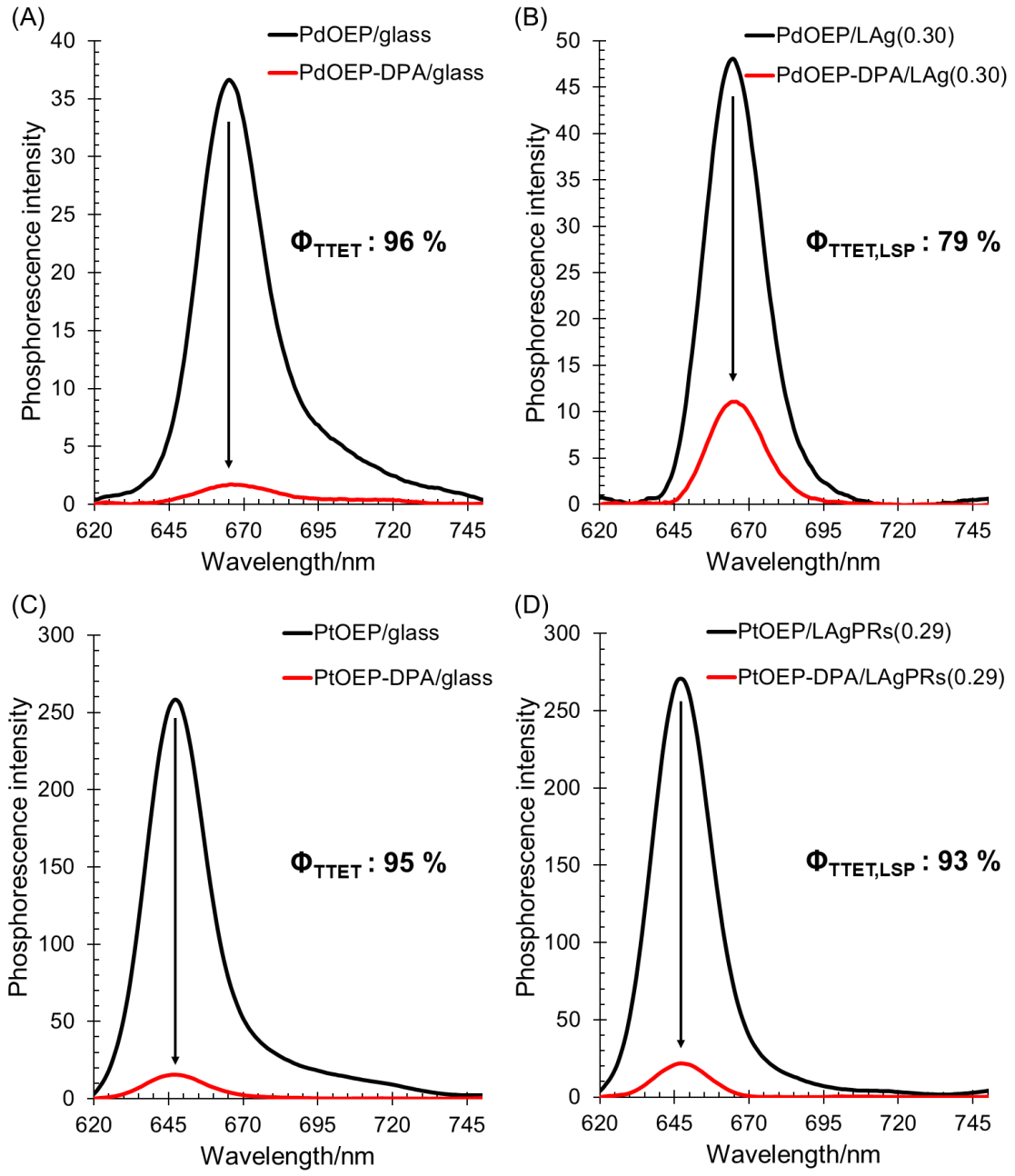

Figure 3-10. Evaluation of the TTET efficiency (Φ_{TTET}) in (A) PdOEP-DPA on glass, (B) PdOEP-DPA on LAgPRs, (C) PtOEP-DPA on glass, and (D) PtOEP-DPA on LAgPRs. TTET efficiency was obtained by substituting phosphorescence peak intensity (I_0) of sensitizer and phosphorescence peak intensity (I) of sensitizer in the presence of emitter into $(1- (I/I_0))\times100$.

We estimated the TTET efficiencies of PdOEP-DPA and PtOEP-DPA in the presence and absence of LAgPRs, and quantitatively investigated whether the change in TTET efficiency due to the plasmon-exciton coupling effect shown in Equations 2 and 3 actually occurs. From the phosphorescence peak intensity (I_0) of PdOEP in the absence of DPA in the emitting layer and the phosphorescence peak intensity (I) of PdOEP in the presence of DPA and Eq. 4,[47] the TTET efficiency in PdOEP-DPA on a glass substrate was estimated experimentally to be 96% (Figure 3-10 (A)).

$$\Phi_{TTET,Experiment} = \left(1 - \frac{I}{I_0}\right) \tag{4}$$

Notably, PdOEP-DPA on LAgPRs also significantly reduced TTET efficiency, estimated from the measured values of I_0 and I and Equation 4, to 79% (Figure 3-10 (B)). The TTET efficiency of PdOEP-DPA was reduced by 17% by the insertion of LAgPRs. Therefore, it was quantitatively clarified that TTET was inhibited by the acceleration of the phosphorescence decay rate, when LSP resonance interacts on the phosphorescence process of sensitizer. On the other hand, the TTET efficiency of PtOEP-DPA was 95% on glass substrates (Figure 3-10 (C))and 93% on LAgPRs (Figure 3-10 (D)), with little change compared with PdOEP-DPA. Little change in TTET efficiency between PtOEP-DPA/glass and PtOEP-DPA/LAgPRs (*Y*)/glass was correlated with no upconversion quenching observed in Figure 3-5 (C) and Figure 3-9 (C).

We recently suggested that the LSP resonance-induced quenching effect of upconverted emission observed for the TTA-UC system employing Pd-TPTBP as a sensitizer was attributed to the acceleration of phosphorescence radiative decay rate from the triplet-excited sensitizer by the strong local electric fields of LSP resonance. At the present systems, although PdOEP-DPA/SAgPRs(*Y*) of which the upconverted emission was prominently quenched with increasing the extinction intensity of LSP resonance at the phosphorescence wavelength is applied to the suggested mechanism, the upconverted emission behavior of PtOEP-DPA/SAgPRs(*Y*) is not applied.

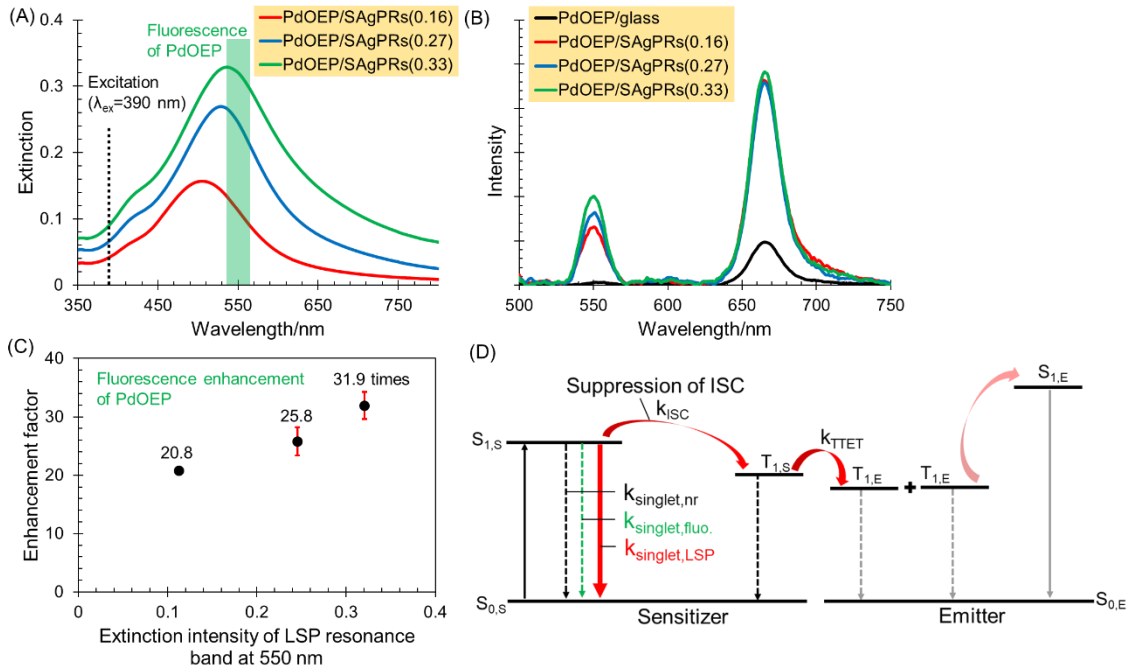

Figure 3-11. (A) Extinction spectra of the PdOEP/SAgPRs(*Y*)/glass. (B) Emission spectra of the PdOEP/glass and PdOEP/SAgPRs(*Y*)/glass (λ_{ex} = 390 nm) (C) Enhancement factors of fluorescence (λ_{em} = 550 nm) along with the extinction intensities at 550 nm in PdOEP/SAgPRs(*Y*)/glass. (D) Quenching mechanism of the upconverted emission by acceleration of fluorescence decay rate in PdOEP/SAgPRs(*Y*)/glass.

Next, we investigated the effect of the decrease of Φ_{ISC} on the extinction of upconverted emission. We set up the following hypothesis. By overlapping the LSP band with the fluorescence wavelength of the sensitizer, the appearance of a new pathway of energy transfer to the LSP of metal nanoparticles, $k_{singlet,LSP}$, should effectively suppress the ISC efficiency, thereby resulting in a decrease in the upconverted emission intensity, as shown in Equation (5) and (6).

$$\Phi_{ISC} = \frac{k_{ISC}}{k_{singlet,nr} + k_{singlet,Fluo.} + k_{ISC}} \tag{5}$$

$$\Phi_{ISC,LSP} = \frac{k_{ISC}}{k_{singlet,nr} + k_{singlet,Fluo.} + k_{ISC} + k_{singlet,LSP}} \tag{6}$$

where $k_{singlet,nr}$ is the non-radiative decay rate from the excited singlet state, $k_{singlet,Fluo.}$ is the radiative decay rate from the excited singlet state, k_{ISC} is the intersystem crossing rate

from excited singlet state to excited triplet state, and $k_{singlet,LSP}$ is the energy transfer to the metal nanoparticles from the triplet excited sensitize. To verify this hypothesis, we developed hybrids consisting of PdOEP/SAgPRs(*Y*)/glass, and focused the change of fluorescence intensity by inserting the SAgPRs. The extinction spectra were shown in Figure 3-11 (A), and well overlaps between the LSP bands of PdOEP/SAgPRs (*Y*)/glass and the fluorescence wavelength of PdOEP. Also, the slight overlaps were confirmed between LSP bands of PdOEP/SAgPRs(*Y*)/glass and excitation wavelength (soret band; λ_{ex} = 390 nm). The fluorescence peak and phosphorescence peak of PdOEP/glass were observed at 550 nm and 665 nm, respectively, and were significantly enhanced by the insertion of SAgPRs (Figure 3-11 (B)). Since the LSP bands of SAgPRs slightly overlap with the excitation wavelength (390 nm) of PdOEP, the fluorescence/phosphorescence enhancement includes the enhancement effect of the excitation efficiency by the light-harvesting nanoantenna effect. If only the enhancement of the excitation efficiency occurs, the enhancement of fluorescence and phosphorescence have the same value. However, the maximum enhancement factor of fluorescence (31.9 times) significantly exceeded the maximum enhancement factor of phosphorescence (4.9 times) (Figure 3-11 (C)). This means that plasmon-exciton coupling with fluorescence occurred more dominantly than with phosphorescence. Therefore, in the PdOEP-DPA/SAgPRs(*Y*) /glass systems, significant fluorescence enhancement of PdOEP occurs, and it is highly possible that this suppresses the ISC efficiency and leads to the quenching of the upconverted emission (Figure 3-11 (D)). We reported in 2018 that the fluorescence of PdOEP, whose ISC efficiency was nearly 1, was dramatically enhanced by its interaction with SAgPRs. In the paper, the fluorescence lifetime (15 ps) of PdOEP was shortened to 5 ps by the insertion of SAgPRs, which was concluded to be due to the plasmon-exciton coupling effect (Equations 6 and 7).[48] From these Equations 5, 6, 7, and 8 the ISC efficiency of nearly 100% of PdOEP can be reduced to as low as 33%, resulting in the upconversion quenching.

$$\tau_{Fluo.} = \frac{1}{k_{singlet,nr} + k_{singlet,Fluo.} + k_{ISC}} \tag{7}$$

$$\tau_{Fluo.,LSP} = \frac{1}{k_{singlet,nr} + k_{singlet,Fluo.} + k_{ISC} + k_{singlet,LSP}} \tag{8}$$

These results suggest that when PdOEP is used as a sensitizer, the Φ_{ISC} and Φ_{TTET} are greatly reduced by increasing the fluorescence emission rate and the phosphorescence

emission rate, respectively. On the other hand, when PtOEP was used as a sensitizer, these phenomena were hardly observed. Since PdOEP and PtOEP have the same ligand as octaethylporphyrin, the difference in the central metal must have led to the difference in this phenomenon.

3-3-3. The Relationship between phosphorescence enhancement and spin-orbital coupling constant

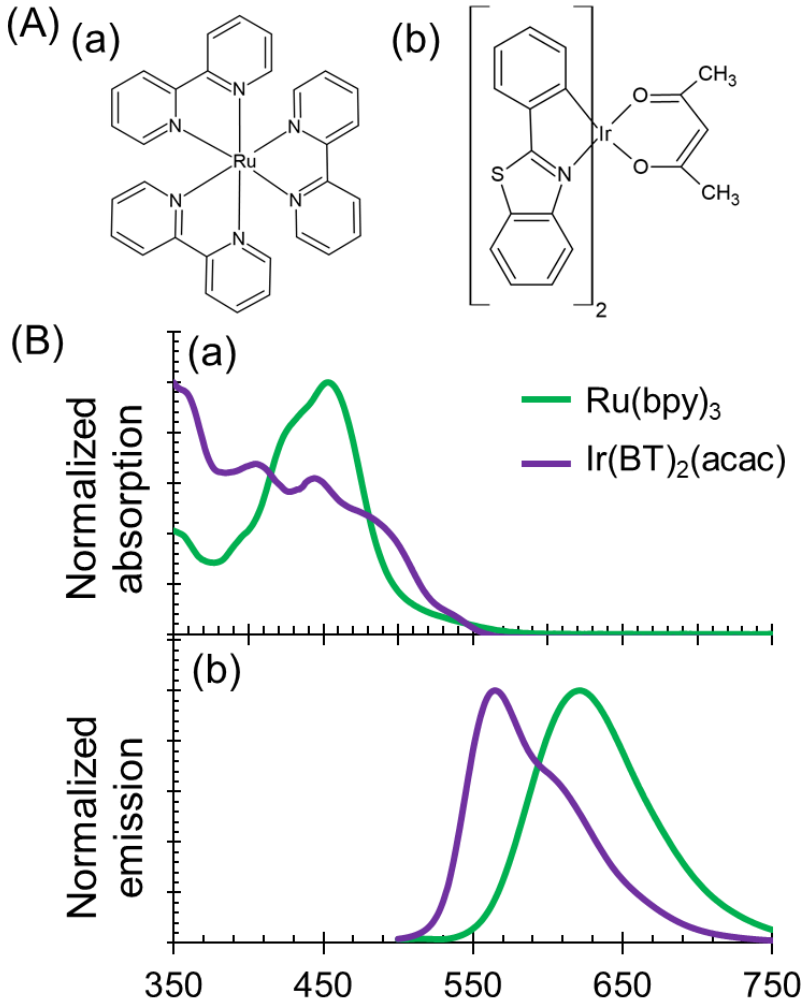

Figure 3-12. (A) Molecular structures of (a) $Ru(bpy)_3$, (b) $Ir(BT)_2(acac)$. (B) Normalized (a) absorption and (b) emission (λ_{ex} = 390 nm) spectra of DMF solutions of $Ru(bpy)_3$ (10 μM) and $Ir(BT)_2(acac)$ (10 μM).

In the previous section, PdOEP induced phosphorescence enhancement and upconversion quenching by LSP resonance, while PtOEP did not induce phosphorescence enhancement and upconversion quenching were not observed. We conjectured that this difference was caused by the difference in the spin-orbital coupling constant of the central

metal (Molecules with larger spin‐orbital coupling constants may be less susceptible to external electric fields.). Then, the complex with ruthenium (Ru) and iridium (Ir) was introduced into the central metal, and the possibility of phosphorescence enhancement was compared.[49,50] The spin‐orbital coupling constants at each atom were reported to be Ru.; 1042 cm^{-1}, Pd; 1460 cm^{-1}, Ir; 3909 cm^{-1}, and Pt; 4253 cm^{-1} cm.[51--53]

The absorption and the emission spectra of a *N,N*-dimethylformamide (DMF) solution (10 μM) of Tris(2,2′-bipyridine)ruthenium(II) hexafluorophosphate ($Ru(bpy)_3$) and Bis(2-benzo[*b*]thiophen-2-ylpyridine)(acetylacetonate)iridium(III) (**(**$Ir(BT)_2(acac)$) (molecular structures are Figure 3-12 (A)) are shown in Figure 3-12 (B). In $Ru(bpy)_3$ solution, absorption attributed to metal to ligand charge transfer (MLCT) was observed at around 450 nm and phosphorescence peak at 622 nm. $Ir(BT)_2(acac)$ solution showed broad absorption spectrum attributed to MLCT was observed at ~ 550 nm, and a phosphorescence peak at 565 nm.

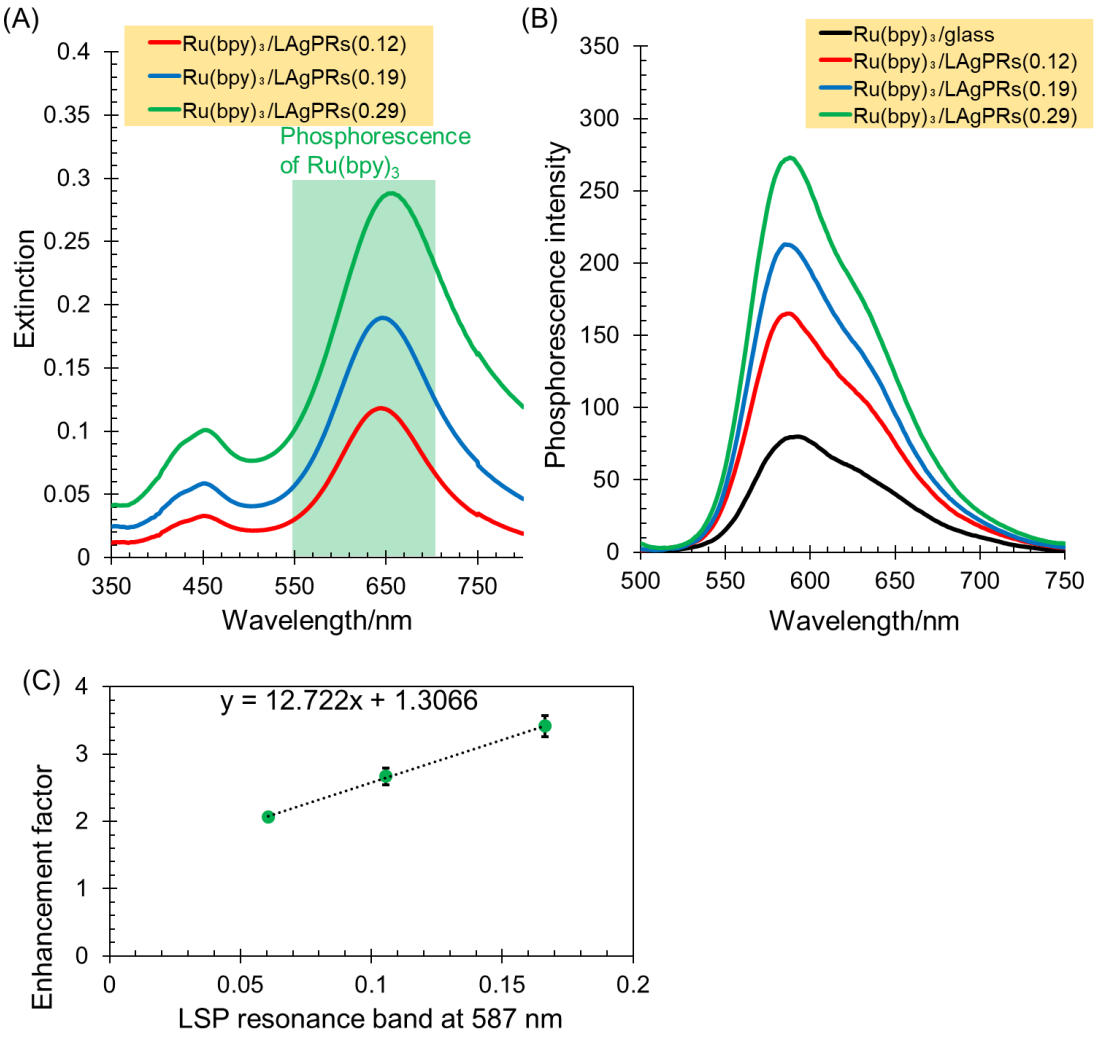

Figure 3-13. Evaluation of phosphorescence property in $Ru(bpy)_3$/glass and $Ru(bpy)_3$/LAgPRs(*Y*)/glass. (A) Extinction spectra and (B) phosphorescence spectra of $Ru(bpy)_3$/LAgPRs(0.12, 0.19, and 0.29). (C) Plots of phosphorescence enhancement factors along with the extinction intensities at 587 nm in LAgPRs(0.12, 0.19, and 0.29).

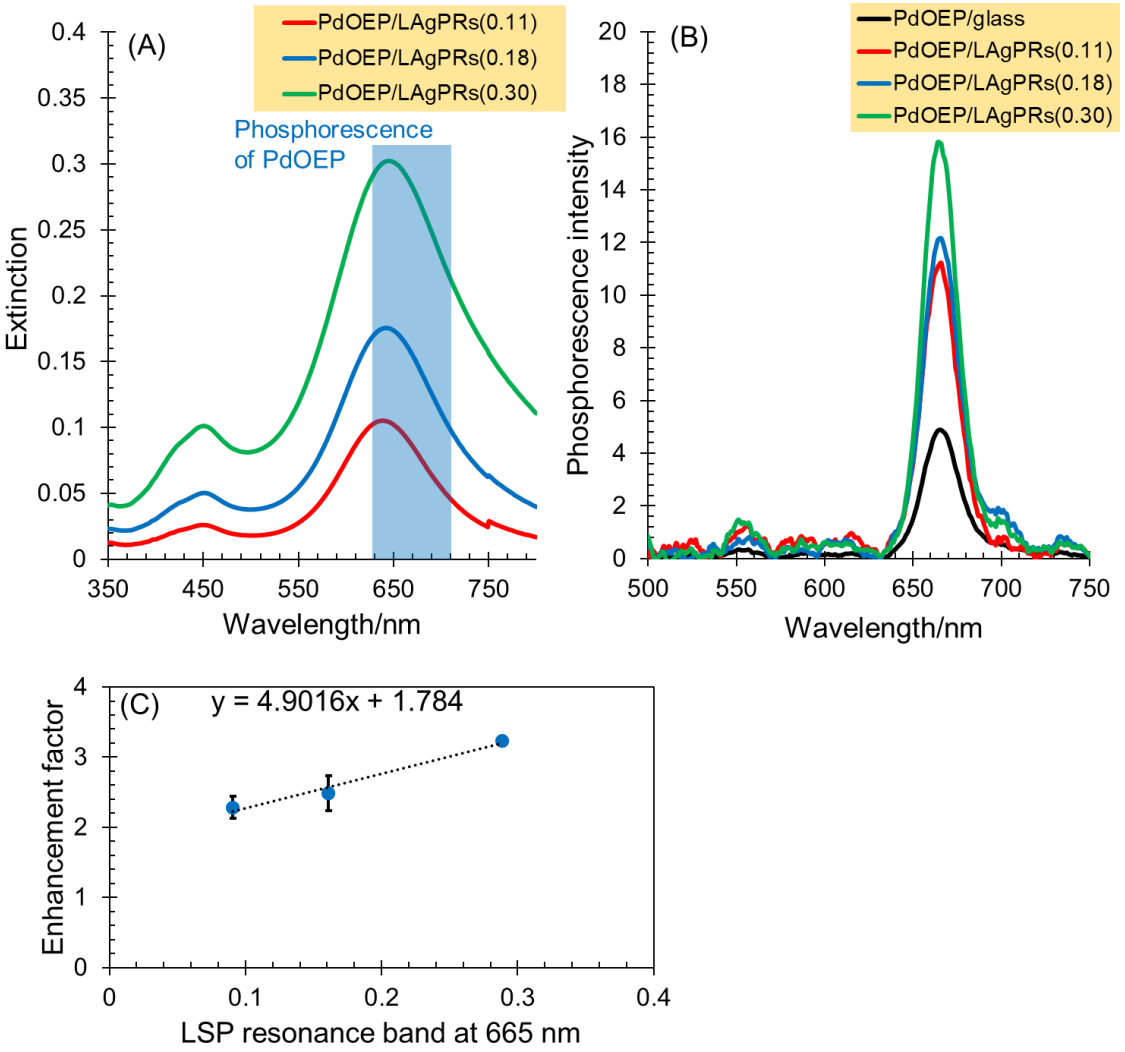

Figure 3-14. Evaluation of phosphorescence property in PdOEP/glass and PdOEP/LAgPRs(*Y*)/glass. (A) Extinction spectra and (B) phosphorescence spectra of PdOEP/LAgPRs(0.11, 0.18, and 0.30). (C) Plots of phosphorescence enhancement factors along with the extinction intensities at 665 nm in LAgPRs(0.11, 0.18, and 0.30).

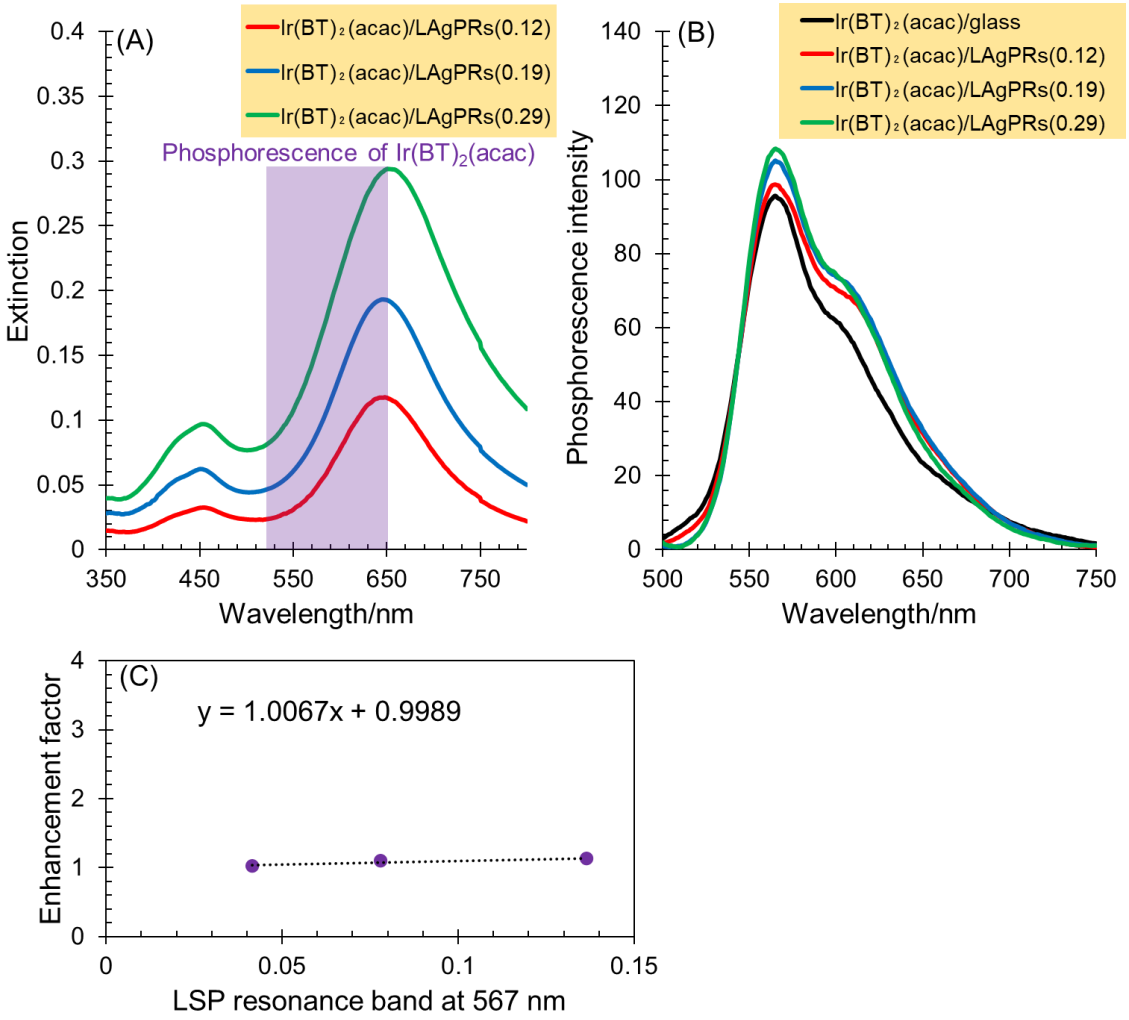

Figure 3-15. Evaluation of phosphorescence property in $Ir(BT)_2(acac)$/glass and $Ir(BT)_2(acac)$/LAgPRs(*Y*)/glass. (A) Extinction spectra and (B) phosphorescence spectra of $Ir(BT)_2(acac)$/LAgPRs(0.12, 0.19, and 0.29). (C) Plots of phosphorescence enhancement factors along with the extinction intensities at 567 nm in LAgPRs(0.12, 0.19, and 0.29).

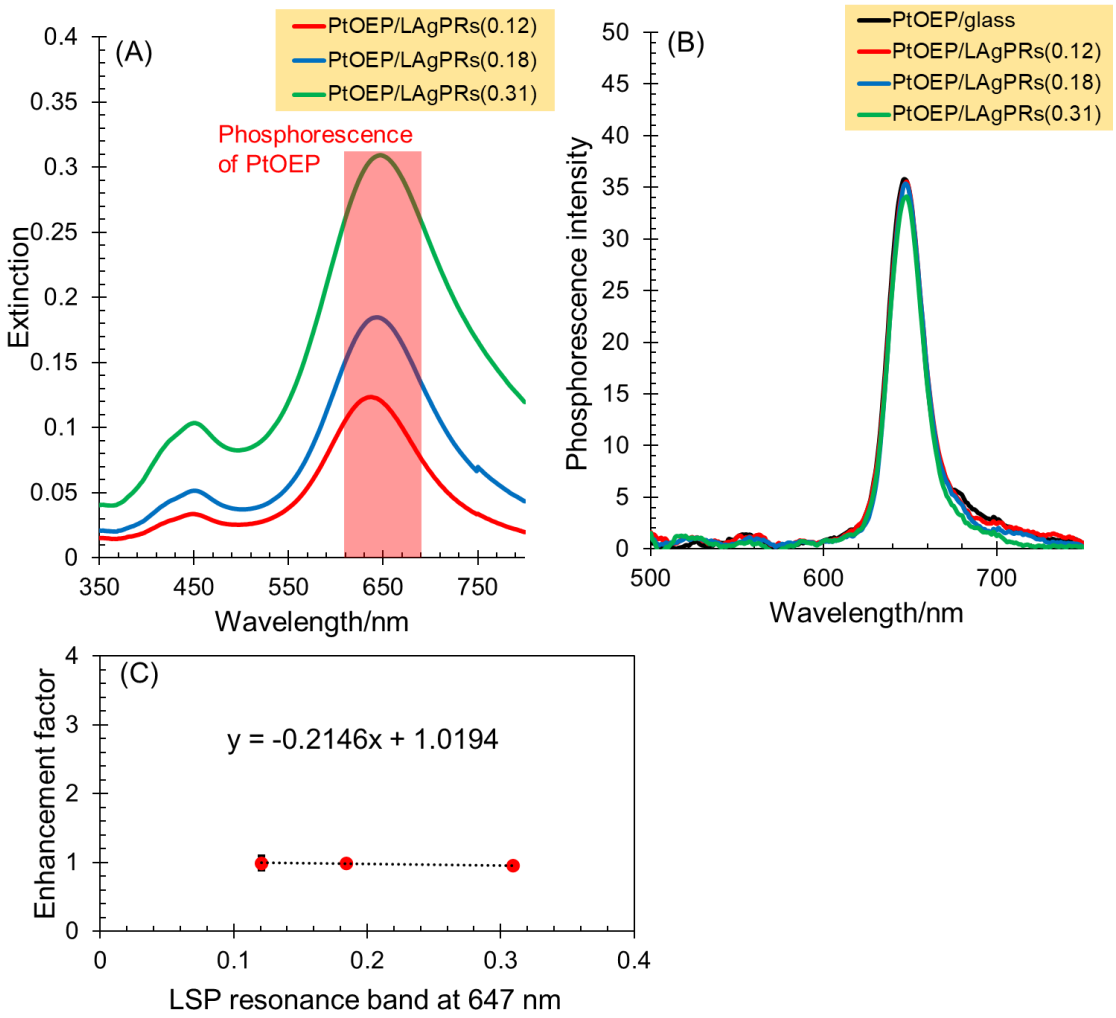

Figure 3-16. Evaluation of phosphorescence property in PtOEP/glass and PtOEP/LAgPRs(*Y*)/glass. (A) Extinction spectra and (B) phosphorescence spectra of PtOEP/LAgPRs(0.12, 0.18, and 0.31). (C) Plots of phosphorescence enhancement factors along with the extinction intensities at 647 nm in LAgPRs(0.12, 0.18, and 0.31).

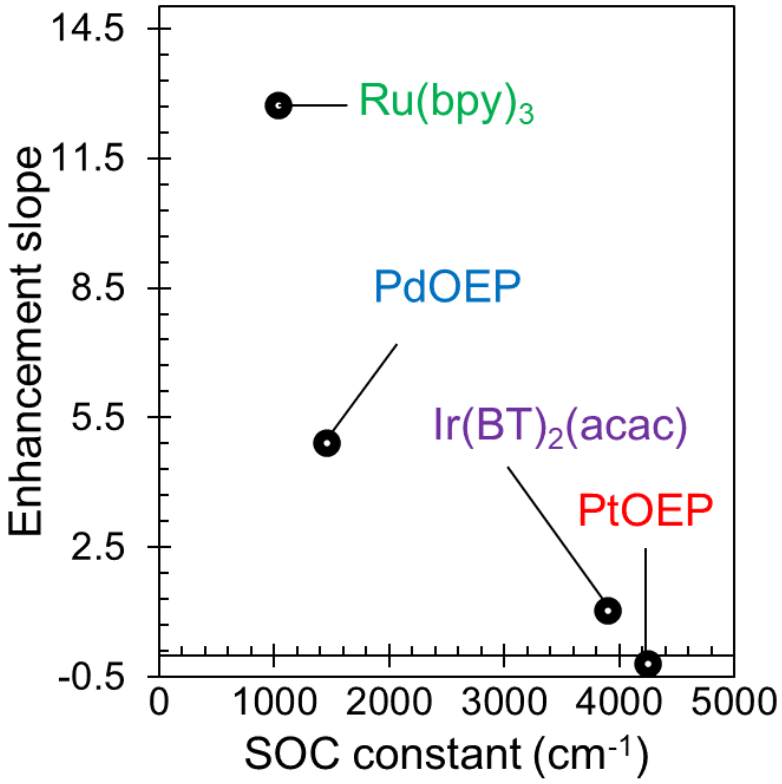

Figure 3-17. Enhancement slope which is slope of the approximate line in Figure 3-13, 3-14,3-15 and 3-16 (C) along with the SOC constant values of the central metal in photofunctional molecules.

The enhancement of the phosphorescence intensity was observed with the increase of the extinction intensity by LSP resonance in $Ru(bpy)_3$/LAgPRs(Y)/glass and PdOEP/LAgPRs(Y)/glass which have small spin-orbital coupling constant (Figure 3-13(C), 3-14(C)), while the phosphorescence intensity hardly changed with the increase of the extinction intensity by LSP resonance in $Ir(BT)_2(acac)$ /LAgPRs(Y)/glass and PtOEP/LAgPRs(Y)/glass which have high spin-orbital coupling constant (Figure 3-15(C), 3-16(C)). Plots of phosphorescence intensity versus extinction intensity were taken for 4 complexes, and the slope was defined as Enhancement slope (indicator of the likelihood of phosphorescence enhancement). Here, when the spin-orbital coupling constant is on the horizontal axis and the enhancement slope is on the vertical axis, it was shown that the enhancement slope reduced exponentially as the spin-orbit coupling constant increases(Figure 3-17). In other words, a complex containing an atom with a large spin-orbital coupling constant was found to be effective as a sensitizer of TTA-UC because of difficult to be accelerated to phosphorescence decay rate.

3-4. Conclusion

We discovered that the quenching effect was significantly suppressed by changing the metal centre of phosphorescent porphyrin sensitizer, which governs the spin-orbital coupling intensity, from Pd to Pt. The origin was suggested to be attributed to the unique and systematic change in the optical interaction between the LSP resonance and the phosphorescent metal complexes with the change in the intrinsic spin-orbital coupling constant. Actually, we investigated whether phosphorescence decay rates of organometallic complexes centered on various metallic elements (Ru(II), Pd(II), Ir(III), Pt(II)) are accelerated by plasmon-exciton coupling. As a result, we found that the phosphorescence enhancement by the plasmon-exciton coupling occurred in the case where the spin-orbital coupling (SOC) constant of the central metal of the complex was comparatively small (Ru(II); 1042 cm^{-1}, Pd(II); 1460 cm^{-1}), and that it hardly occur in the case where SOC constant value was large (Ir(III); 3909 cm^{-1}, Pt(II); 4253 cm^{-1}). The results obtained in this study provide the resolution of nature for the interaction of LSP resonance with the spin-flip transition-allowed metal complexes as well as the guideline for the significant plasmonic enhancement of TTA-UC systems.

3-5. References

(1) Fujishima, A.; Honda, K. Electrochemical Photolysis of Water at a Semiconductor Electrode. *Nature* **1972**, *238*, 37−38.

(2) Fujishima, A.; Rao, T. N.; Tryk, D. A. Titanium dioxide photocatalysis. *J. Photochem. Photobiol., C* **2000**, *1*, 1−21.

(3) Yang, G.; Yang, D.; Yang, P.; Lv, R.; Li, C.; Zhong, C.; He, F.; Gai, S.; Lin, J. A Single 808 nm Near-Infrared Light-Mediated Multiple Imaging and Photodynamic Therapy Based on Titania Coupled Upconversion Nanoparticles. *Chem. Mater.* **2015**, *27*, 7957− 7968.

(4) Liu, Z.; Wang, J.; Li, Y.; Hu, X.; Yin, J.; Peng, Y.; Li, Z.; Li, Y.; Li, B.; Yuan, Q. Near-Infrared Light Manipulated Chemoselective Reductions Enabled by an Upconversional Supersandwich Nanostructure. *ACS Appl. Mater. Interfaces* **2015**, *7*, 19416−19423.

(5) Roh, J.; Yu, H.; Jang, J. Hexagonal β-$NaYF_4Yb^{3+}Er^{3+}$ NanoprismIncorporated Upconverting Layer in Perovskite Solar Cells for NearInfrared Sunlight Harvesting. *ACS Appl. Mater. Interfaces* **2016**, *8*, 19847−19852.

(6) Cui, C.; Tou, M.; Li, M.; Luo, Z.; Xiao, L.; Bai, S.; Li, Z. Heterogeneous Semiconductor Shells Sequentially Coated on Upconversion Nanoplates for NIR-Light Enhanced Photocatalysis. *Inorg. Chem.* **2017**, *56*, 2328−2336.

(7) Jang, Y. J.; Kim, E.; Ahn, S.; Chung, K.; Kim, J.; Kim, H.; Wang, H.; Lee, J.; Kim, D.-W.; Kim, D. H. Upconversion-Triggered Charge Separation in Polymer Semiconductors. *J. Phys. Chem. Lett.* **2017**, *8*, 364−369.

(8) Baluschev, S.; Miteva, T.; Yakutkin, V.; Nelles, G.; Yasuda, A.; Wegner, G. Up-Conversion Fluorescence: Noncoherent Excitation by Sunlight. *Phys. Rev. Lett.* **2006**, *97*, 143903/1−143903/3.

(9) Monguzzi, A.; Tubino, R.; Hoseinkhani, S.; Campione, M.; Meinardi, F. Low power, non-coherent sensitized photon upconversion: modelling and perspectives. *Phys. Chem. Chem. Phys.* **2012**, *14*, 4322−4332.

(10) Gray, V.; Dzebo, D.; Abrahamsson, M.; Albinsson, B.; MothPoulsen, K. Triplet−triplet annihilation photon-upconversion: towards solar energy applications. *Phys. Chem. Chem. Phys.* **2014**, *16*, 10345−10352.

(11) Duan, P.; Yanai, N.; Kimizuka, N. Photon Upconverting Liquids: Matrix-Free Molecular Upconversion Systems Functioning in Air. *J. Am. Chem. Soc.* **2013**, *135*, 19056−19059.

(12) Cao, X.; Hu, B.; Zhang, P. High Upconversion Efficiency from Hetero Triplet-Triplet Annihilation in Multiacceptor Systems. *J. Phys. Chem. Lett.* **2013**, *4*, 2334−2338.

(13) Ye, C.; Wang, J.; Wang, X.; Ding, P.; Liang, Z.; Tao, X. A new medium for triplet-triplet annihilated upconversion and photocatalytic application. *Phys. Chem. Chem. Phys.* **2016**, *18*, 3430−3437.

(14) Vadrucci, R.; Weder, C.; Simon, Y. C. Low-power photon upconversion in organic glasses.

J. Mater. Chem. C **2014**, *2*, 2837− 2841.
(15) Duan, P.; Yanai, N.; Nagatomi, H.; Kimizuka, N. Photon Upconversion in Supramolecular Gel Matrixes: Spontaneous Accumulation of Light-Harvesting Donor-Acceptor Arrays in Nanofibers and Acquired Air Stability. *J. Am. Chem. Soc.* **2015**, *137*, 1887−1894.
(16) Duan, P.; Yanai, N.; Kurashige, Y.; Kimizuka, N. AggregationInduced Photon Upconversion through Control of the Triplet Energy Landscapes of the Solution and Solid States. *Angew. Chem. Int. Ed.* **2015**, *54*, 7544−7549.
(17) Islangulov, R. R.; Lott, J.; Weder, C.; Castellano, F. N. Noncoherent Low-Power Upconversion in Solid Polymer Films. *J. Am. Chem. Soc.* **2007**, *129*, 12652−12653.
(18) Singh-Rachford, T. N.; Lott, J.; Weder, C.; Castellano, F. N. Influence of Temperature on Low-Power Upconversion in Rubbery Polymer Blends. *J. Am. Chem. Soc.* **2009**, *131*, 12007−12014.
(19) Kim, J.-H.; Deng, F.; Castellano, F. N.; Kim, J.-H. High Efficiency Low-Power Upconverting Soft Materials. *Chem. Mater.* **2012**, *24*, 2250−2252.
20) Monguzzi, A.; Bianchi, F.; Bianchi, A.; Mauri, M.; Simonutti, R.; Ruffo, R.; Tubino, R.; Meinardi, F. High efficiency up-converting single phase elastomers for photon managing applications. *Adv. Energy Mater.* **2013**, *3*, 680−686.
(21) Monguzzi, A.; Mauri, M.; Bianchi, A.; Dibbanti, M. K.; Simonutti, R.; Meinardi, F. Solid-State Sensitized Upconversion in Polyacrylate Elastomers. *J. Phys. Chem. C* **2016**, *120*, 2609−2614.
(22) Poorkazem, K.; Hesketh, A. V.; Kelly, T. L. Plasmon-Enhanced Triplet−Triplet Annihilation Using Silver Nanoplates. *J. Phys. Chem. C* **2014**, *118*, 6398−6404.
(23) Park, J. K.; Lee, G. Y.; Jung, K.; Ko, D.-H.; Han, K.; Ko, H. Enhanced triplet−triplet annihilation in bicomponent organic systems by using a gap plasmon resonator. *Nanoscale* **2015**, *7*, 12828−12832.
(24) Cao, X.; Hu, B.; Ding, R.; Zhang, P. Plasmon-enhanced homogeneous and heterogeneous triplet-triplet annihilation by gold nanoparticles. *Phys. Chem. Chem. Phys.* **2015**, *17*, 14479−14483.
(25) Hyoung-Il, K.; Weon, S.; Kang, H.; Hagstrom, A. L.; Kwon, O. S.; Lee, Y.-S.; Choi, W.; Kim, J.-H. Plasmon-Enhanced Sub-Bandgap Photocatalysis via Triplet−Triplet Annihilation Upconversion for Volatile Organic Compound Degradation. *Environ. Sci. Technol.* **2016**, *50*, 11184−11192.
(26) Westbrook, E. G.; Zhang, P. Plasmon-enhanced triplet-triplet annihilation upconversion of post-modified polymeric acceptors. *Dalton Trans.* **2018**, *47*, 8638−8645.
(27) Jin, S.; Sugawa, K.; Takeshima, N.; Tahara, H.; Igari, S.; Yoshinari, S.; Kurihara, Y.; Watanabe, S.; Enoki, M.; Sato, K.; Inoue, W.; Tokuda, K.; Akiyama, T.; Katoh, R.; Takase, K.;

Ozawa, H.; Okazaki, T.; Watanabe, T.; Otsuki, J. Precise Control of Localized Surface Plasmon Wavelengths Is Needed for Effective Enhancement of Triplet-Triplet Annihilation-Based Upconversion Emission. *ACS Photonics,* **2018**, *5*, 5025-5037.

(28) Shunping, Zhang; Kui, Bao; Naomi, J. H.; Hongxing, Xu; Peter, N. Substrate-Induced Fano Resonances of a Plasmonic Nanocube: A Route to Increased-Sensitivity Localized Surface Plasmon Resonance Sensors Revealed. *Nano Lett*. **2011**, *11*, 1657-1663.

(29) Kathryn, M., M.; Jason, H., H. Localized Surface Plasmon Resonance Sensors. *Chem. Rev.* **2011**, *111*, 3828-3857.

(30) Waxenegger, J.; Trügler, A.; Hohenester, U. Plasmonics Simulations with the MNPBEM Toolbox: Consideration of Substrates and Layer Structures. *Comput. Phys. Commun.* **2015**, *193*, 138-150.

(31) Rakic, A. D.; Djurisic, A. B.; Elazar, J. M.; Majewski, M. L. Optical properties of metallic films for vertical-cavity optoelectronic devices. *Appl. Opt.* **1998**, *37*, 5271-5283.

(32) Sugawa, K.; Takeshima, N.; Uchida, K.; Tahara, H.; Jin, S.; Tsunenari, N.; Akiyama, T.; Kusaka, Y.; Fukuda, N.; Ushijima, H.; Tsuchido, Y.; Hashimoto, T.; Hayashita, T.; Otsuki, J. Photocurrent Enhancement of Porphyrin Molecules over a Wide-Wavelength Region Based on Combined Use of Silver Nanoprisms with Different Aspect Ratios. *J. Mater. Chem. C,* **2015**, *3*, 11439.

(33) Jin, R.; Cao, Y. C.; Hao, E.; Metraux, G. S.; Schatz, G. C.; Mirkin, C. A. Controlling anisotropic nanoparticle growth through plasmon excitation. *Nature*, **2003**, *425*, 487-490.

(34) Jin, R.; Cao, Y.; Mirkin, C. A.; Kelly, K. L.; Schatz, G. C.; Zheng, J. G. Photoinduced conversion of silver nanospheres to nanoprisms. *Science* **2001**, *294*, 1901-1903.

(35) Xue, C.; Mirkin, C. A. pH-switchable silver nanoprism growth pathways. *Angew. Chem., Int. Ed.* **2007**, *46*, 2036-2038.

(36) Callegari, A.; Tonti, D.; Chergui, M. Photochemically Grown Silver Nanoparticles with Wavelength-Controlled Size and Shape. *Nano Lett.* **2003**, *3*, 1565-1568.

(37) Stamplecoskie, K. G.; Scaiano, J. C. Light Emitting Diode Irradiation Can Control the Morphology and Optical Properties of Silver Nanoparticles. *J. Am. Chem. Soc.*, **2010**, *132*, 1825-1827.

(38) Qian, L.; Tianshe, Y.; Wei, F.; Fuyou L. Blue-Emissive Upconversion Nanoparticles for Low-Power-Excited Bioimaging in Vivo. *J. Am. Chem. Soc.*, **2012**, *134*, 5390-5397.

(39) Jae-H., K.; Jae-H., K.; Encapsulated Triplet−Triplet Annihilation-Based Upconversion in the Aqueous Phase for Sub-Band-Gap Semiconductor Photocatalysis. *J. Am. Chem. Soc.* **2012**, *134*, 17478-17481.

(40) Knyukshto, V. N.; Shul'ga, A. M.; Sagun, E. I.; Zen'kevich, E. I. Spectral Manifestations of Nonplanarity Effects in Pd Complexes of Porphyrins. *Opt. Spectrosc.* **2002**, *92*, 53-62.

(41) Sugawa, K.; Takeshima, N.; Uchida, K.; Tahara H., Jin S.; Tsunenari, N.; Akiyama, T.; Kusaka, Y.; Fukuda, N.; Ushijima, H.; Tsuchido, Y.; Hashimoto, T.; Hayashita, T.; Otsuki, J. Photocurrent Enhancement of Porphyrin Molecules over a Wide-Wavelength Region Based on Combined Use of Silver Nanoprisms with Different Aspect Ratios. *J. Mater. Chem. C*, **2015**, *3*, 11439-11448.

(42) Hagen, D. A.; Foster, B.; Stevens, B.; Grunlan, J. C. Shift-Time Polyelectrolyte Multilayer Assembly: Fast Film Growth and High Gas Barrier with Fewer Layers by Adjusting Deposition Time. *ACS Macro Lett.* **2014**, *3*, 663-666.

(43) Singh-Rachford, T., N.; Lott, J.; Weder, C.; Castellano, F., N. Influence of Temperature on Low-Power Upconversion in Rubbery Polymer Blends. *J. Am. Chem. Soc.*, **2009**, *131*, 12007-12014.

(44). Monguzzi, A.; Tubino, R.; Hoseinkhani, S.; Campione, M.; Meinardi, F. Low power, non-coherent sensitized photon up-conversion: modelling and perspectives. *Phys. Chem. Chem. Phys*, **2012**, *14*, 4322-4332.

(45). Hoseinkhani, S.; Tubino, R.; Meinardi, F.; Monguzzi, A. Achieving the photon up-conversion thermodynamic yield upper limit by sensitized triplet–triplet annihilation. *Phys. Chem. Chem. Phys*, **2015** *17*, 4020-4024.

(46) Zhao, W.; Wang, S.; Liu, B.; Verzhbitskiy, I.; Li, S.; Giustiniano, F.; Kozawa, D.; Loh, K. P.; Matsuda, K.; Okamoto, K.; Oulton, R. F.; Eda, G.; Exciton-Plasmon Coupling and Electromagnetically Induced Transparency in Monolayer Semiconductors Hybridized with Ag Nanoparticles. *Adv. Mater.*, **2016**, *28*, 2709-2715.

(47) Toshiko, M.; Aizitiaili, A.; Kengo, S.; Yusuke, S.; Ritsuki, N.; Tetsuro, J.; Kenji, K. Triplet–triplet annihilation upconversion through triplet energy transfer at a nanoporous solid–liquid interface. *Phys. Chem. Chem. Phys.*, **2020**, *22*, 17807-17813.

(48) Naoto, T.; Kosuke, S.; Hironobu, T.; Shota, J.; Hiroki, W.; Misa, F.; Kyo, T.; Shuto, I.; Kotomi, K.; Yutaro, H.; Ryuzi, K.; Kouichi, T.; Joe O. Plasmonic Silver Nanoprism-Induced Emissive Mode Control between Fluorescence and Phosphorescence of a Phosphorescent Palladium Porphyrin Derivative. *ACS Nano,* **2019**, *13*, 13244-13256.

(49) Alvin, T., Y.; Charles, V., S.; James, K., M. Ultrafast Electron Localization Dynamics Following Photo-Induced Charge Transfer. *Science*, **2000**, *289*, 11.

(50) Yongquan, W.; Hao, J.; Zesheng, D.; Qiang, Z.; Huazhou, W.; Fuyou, L. Ratiometric Phosphorescence Imaging of Hg(II) in Living Cells Based on a Neutral Iridium(III) Complex. *Inorg. Chem.*, **2000**, *289*, 935-938.

(51) Sourav, K.; S.; Parna, G.; Pradipta, P. Efficiency of photoinduced electron transfer in mono- and di-nuclear iridium complexes: a comparative study. *New J. Chem.*, **2017**, *41*, 6540-6545.

(52) Jan, H.; Rainer, F. Winter; Platinum emitters with dye-based r-aryl ligands. *Coordination Chemistry Reviews* **2019**, *400*, 213048.
(53) F., A., Cotton; *Progress in Inorganic Chemistry,* Vol 6.

Chapter 4

Efficient Photothermal Conversion of Gold Nanoparticles by Upconverted Emission

4-0. Abstract

Low-energy visible light was converted into heat energy through the excitation of the localized surface plasmon resonance of gold nanospheres excited by upconverted emission based on triplettriplet annihilation of organic molecules. This system allows easy tuning of absorption/emission wavelengths, which is difficult with conventional photothermal conversion using rare-earth elements.

4-1. Introduction

In recent years, photothermal conversion phenomenon occurring via the deactivation of the localized surface plasmon resonance (LSPR) of metal nanoparticles are attracting much attention for application to solar steam generation, seawater desalination, waste sterilization, and nanotherapy (photothermal therapy and thermal energy-triggered drug delivery).[1,2] Typically, plasmonic gold nanomaterials are suitable photothermal conversion materials because of their high light extinction cross-section and high photothermal conversion efficiency owing to the LSPR excitation,[3,4] which are 4-5 orders of magnitude greater than those of dye molecules and quantum dots.[5,6] Gold nanospheres with diameters several tens of nanometers can be activated by light from the ultraviolet region to around 600 nm region because of the strong interband transition below ~500 nm and the LSPR strongly excited from 500 to 600 nm. However, irradiation of longer-wavelength light (> 600 nm) does not lead to efficient heat generation owing to the low light harvesting ability.[2,7] For solar-light driven photothermal conversion materials, it is required to efficiently convert a wide wavelength range of solar light into thermal energy. In the nanotherapy, photothermal conversion should be efficiently induced within the wavelength region of 600-1300 nm, which corresponds to the biological transparency window. To address this issue, photon upconversion phenomena are being investigated recently, by which conversion of longer-wavelength light (which photothermal materials cannot absorb) into shorter wavelength light can lead to efficient photothermal conversion.[8-13] Inorganic nanoparticles composed of rare-earth ions such as Yb^{3+}, Er^{3+}, and Nd^{3+} have often been utilized as upconversion nanoparticles (UCNPs).[14-18] Efficient near-infrared light-driven photothermal conversion has been recently achieved using hybrid systems of gold nanospheres and UCNPs.[19] However, the use of UCNPs has some critical problems including a need for rare-earth elements limited in supply, difficulty in tuning absorption/emission wavelengths, and narrowness of the obtained emission/absorption band. Therefore, the development of alternative upconversion systems for photothermal conversion is an important challenge. [20-22] In this study, we focus on the utilization of upconversion systems based on triplet-triplet annihilation (TTA-UC) through photoinduced intermolecular energy transfer between organic dye molecules acting as a sensitizer and an emitter, which eliminates the need for rare-earth elements.[23-27] Also, the absorption/emission wavelengths can be simply tuned by combining appropriate sensitizer and emitter and the obtained emission/absorption bands is broader than that from UCNPs. The TTA-UC mechanism involves the following processes (Figure 4-1): i) light absorption to produce the excited singlet state of the sensitizer; ii) generation of the triplet state of the sensitizer through intersystem crossing

from the excited singlet state; iii) generation of the excited triplet state of the emitter by triplet-triplet energy transfer (TTET) from the sensitizer to the emitter iv) generation of the excited singlet state of the emitter via TTA occurring upon collision between the two emitters in the excited triplet state; and v) emission from the excited singlet state of the emitter.[23-27] Application of the TTA-UC to the photothermal conversion with plasmonic metal nanoparticles to improve the conversion efficiency has never been reported as far as we are aware of. We herein demonstrate that the temperature increase through the photothermal conversion with gold nanospheres can be enhanced significantly by processes involving upconverted emission through TTA-UC under irradiation with long-wavelength visible light (642 nm).

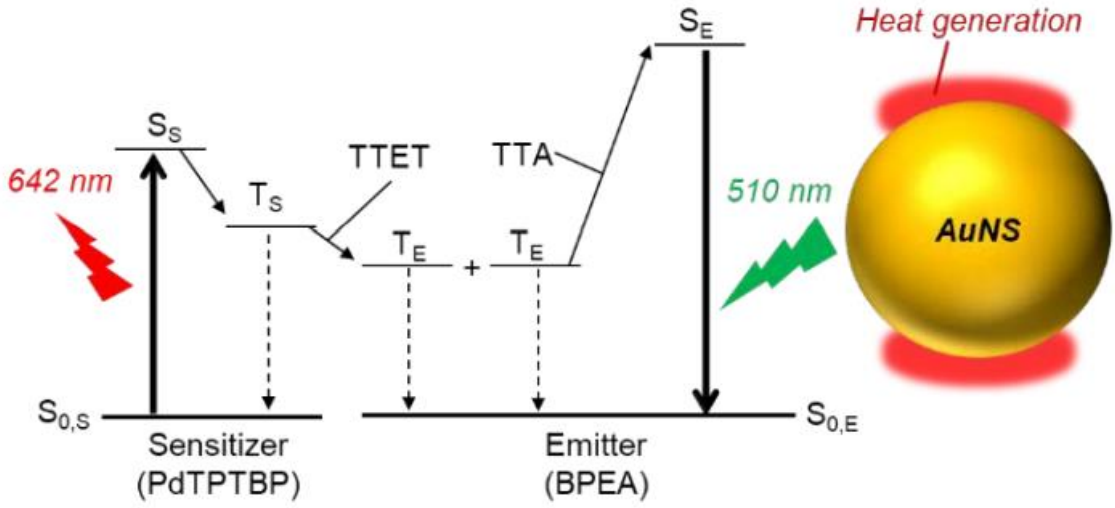

Figure 4-1. Mechanism of photothermal conversion system utilizing TTA-UC.

4-2. Experimental section

Chemicals

Milli-Q-grade water was used to prepare all aqueous solutions. Hydrogen tetrachloroaurate(III) tetrahydrate ($HAuCl_4 \cdot 4H_2O$, NacalaiTesque), trisodium citrate dihydrate (Kanto Chemical), polyvinylpyrrolidone (PVP, Mw: 55000, Sigma Aldrich), palladium(II) tetraphenyltetrabenzoporphyrin (PdTPTBP, Funakoshi), 9,10-bis(phenylethynyl)anthracene (BPEA, Tokyo Chemical Industry), and *N*,*N*-dimethylformamide (DMF, 99.5 %, Wako) were used as received.

Measurements

Extinction and absorption spectra were measured by a JASCO V-630 spectrophotometer. Transmission electron microscopy (TEM) observation were carried out using a Hitachi HF-2000 system at an acceleration voltage of 200 kV. Fluorescence spectra were measured by a JASCO FP-6500 spectrometer. Temperature changes of sample solutions irradiated with a CW laser (642 nm, 100 mW) were measured by an OMEGA HH802U thermometer. Fluorescence lifetimes were measured using a C11367 Quantaurus-Tau (Hamamatsu) apparatus.

Preparation of Colloidal Aqueous Solution of Gold Nanospheres

A colloidal aqueous solution of gold nanospheres was prepared according to a previously reported procedure.[28] Typically, an aqueous solution of $HAuCl_4 \cdot 4H_2O$ (0.01wt%, 100 mL) was refluxed at 100 ºC for 30 min. Next, an aqueous solution of trisodium citrate (1wt%, 1 mL) was injected into the solution and the mixed solution was then refluxed at 100 ºC for 60 min to produce an aqueous solution of citrate-capped gold nanospheres. Next, PVP was coated on the surface of prepared gold nanospheres by stirring for 3 h a mixed solution of the obtained colloidal gold aqueous solution (4 mL) and an aqueous solution of PVP (20 mg/mL, 1 mL). Finally, the resultant colloidal solution was centrifuged for 15 min at 10000 rpm, followed by dispersing the obtained precipitations of gold nanospheres into DMF (5 mL).

4-3. Results and Discussion

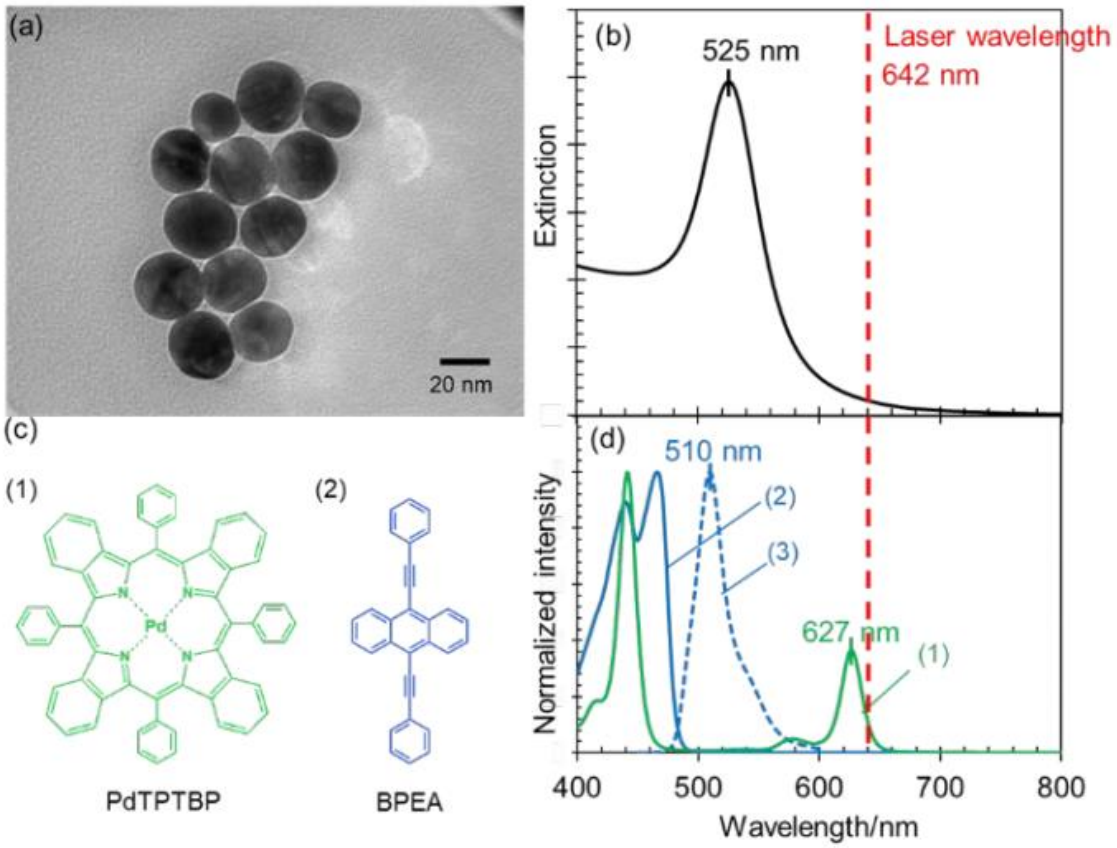

Figure 4-2. (a) TEM image of gold nanospheres protected with PVP. (b) Extinction spectrum of colloidal DMF solution of gold nanospheres protected with PVP. (c) Molecular structures of (1) PdTPTBP and (2) BPEA. (d) Absorption spectra of DMF solutions of (1) PdTPTBP and (2) BPEA and (3) upconverted emission spectrum (λex = 642 nm) of UCsol(12.5 μM).

We employed composite solutions of gold nanospheres and TTAUC systems in dimethylformamide (DMF). A colloidal DMF solution of gold nanospheres with a diameter of 27 ± 2 nm, protected with polyvinylpyrrolidone (PVP), was prepared (Supplementary Information). A transmission electron microscopy (TEM) image of the nanospheres is presented in Figure 4-2(a). The colloidal solution showed an extinction peak at 525 nm, attributed to the LSPR excitation of the dipole mode (Figure 4-2(b)). A TTA-UC system comprising a DMF solution containing palladium meso-tetraphenyltetrabenzoporphyrin (PdTPTBP) as the sensitizer and 9,10-bis(phenylethynyl)anthracene (BPEA) as the emitter in a 1:100 molar ratio was prepared (see Figure 4-2(c) for the molecular structures).[29-31] The component concentrations are shown in Table 4-1 and the samples are denoted as UCsol(X) (X; concentration of sensitizer in μM). The absorption spectra of the dye molecules are shown in Figure 4-

2(d). The absorption peak at 627 nm is attributed to the Q-band of PdTPTBP and the Soret band of PdTPTBP and the absorption bands of BPEA both appear in 400-500 nm region. The upconverted emission from BPEA through TTA-UC is observed in the region of 480-600 nm under excitation at 642 nm. Note that the upconverted emission band overlapped well with the LSPR band of the gold nanospheres.

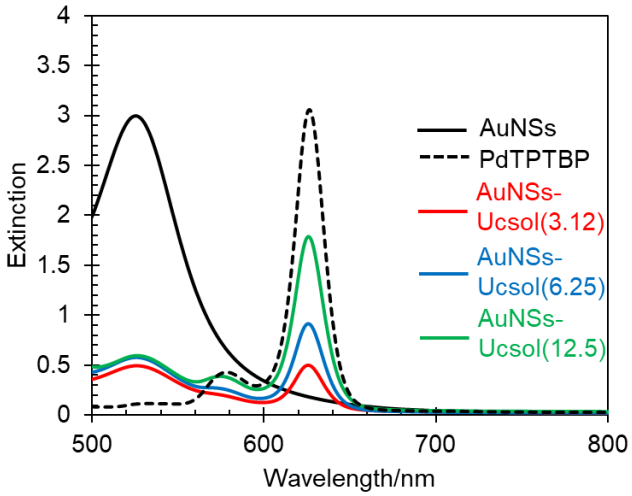

Figure 4-3. Extinction spectra of AuNSs-UCsol(X) (X = 3.12, 6.25, and 12.5), colloidal gold and sensitizer.

Table 4-1. Concentrations of gold nanospheres, sensitizer, and emitter for UCsol(*X*) and AuNSs-UCsol(*X*)

	Gold nanospheres ($\times 10^{11}$ pieces)	Sensitizer/μM	Emitter/μM
Gold nanospheres	2.40	0	0
UCsol(3.12 μM)	0	3.12	312
UCsol(6.25 μM)	0	6.25	625
UCsol(12.5 μM)	0	12.5	1250
AuNSs-UCsol(3.12 μM)	2.40	3.12	312
AuNSs-UCsol(6.25 μM)	2.40	6.25	625
AuNSs-UCsol(12.5 μM)	2.40	12.5	1250

Composite systems were prepared by introducing the gold nanospheres into the TTA-UC systems, which were denoted as AuNSs-UCsol(*X*), for which the absorption spectra are shown in Figure. 4-3. The concentrations of the gold nanospheres and dye molecules in the AuNSs-UCsol(*X*) system are summarized in Table 4-1. The photothermal conversion properties were evaluated by measuring the change in solution temperature using a digital thermocouple thermometer (OMEGA, HH801A) under irradiation with a 642 nm laser (100 mW) until stationary temperature was reached. Dissolved oxygen of all the sample solutions were removed by bubbling with nitrogen gas for 20 min before the measurements.

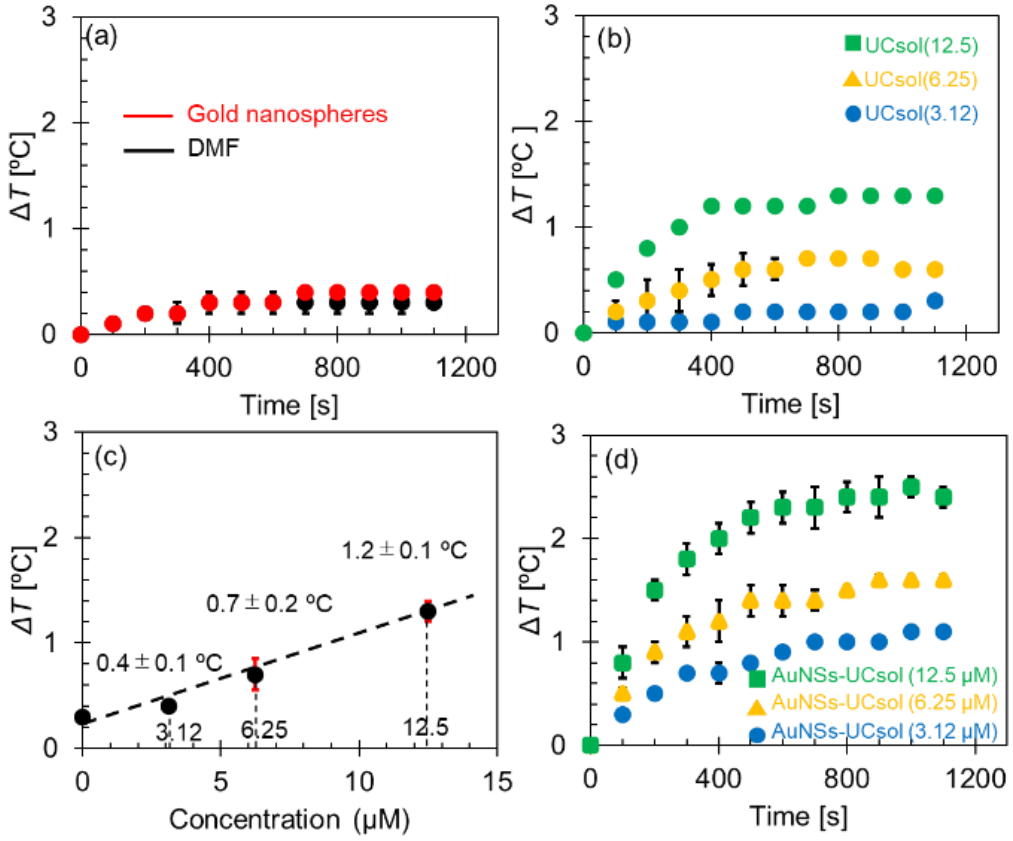

Figure 4-4. Temperature increases of colloidal DMF solutions under irradiation with a 642 nm laser (100 mW) (average ± standard deviation). (a) DMF solution of gold nanospheres and DMF solvent. (b) UCsol(*X*) (*X*: 3.12, 6.25, and 12.5). (c) Temperature increase of UCsol(*X*) against the concentration of sensitizer. (d) AuNSs-UCsol(*X*) (*X*: 3.12, 6.25, and 12.5).

The temperature increase of the DMF solvent (ΔT_{DMF}) and the colloidal gold nanosphere solution (ΔT_{AuNSs}) were measured to be 0.3 ± 0.1 °C and 0.4 ± 0.1 °C, respectively (Figure 4-4(a)). The little margin by the presence of the colloidal gold nanospheres indicates that

the direct excitation at the tail of the LSPR band of gold nanospheres (Figure 4-2(b)) by the 642nm laser is ineffective in photothermal conversion due to a small extinction at this wavelength. The temperature increases for all the UCsol(*X*) samples without gold nanospheres under laser irradiation ($\Delta T_{\mathrm{UCsol}(X)}$) were determined to be 0.4 ± 0.1, 0.7 ± 0.2, and 1.2 ± 0.1 °C, respectively, for UCsol(3.12), UCsol(6.25), and UCsol(12.5) (Figure 4-4(b)). As shown in Figure 4-4(c), $\Delta T_{\mathrm{UCsol}(X)}$ increased linearly with increasing molecular concentrations. Possible processes causing the larger temperature increase in the UCsol(*X*) compared to that of pure DMF include nonradiative decay processes from the singlet excited sensitizer, the triplet excited sensitizer, the triplet excited emitter, and the singlet excited emitter. Among these possibilities, the decay from the singlet excited sensitizer may be excluded because the intersystem crossing to the triplet is very efficient.[32] The decay from the triplet excited sensitizer may also be excluded because the TTET efficiency in the present system is high as judged from the observation that phosphorescence from the sensitizer is mostly quenched in all the UCsol(*X*) systems (Figure 4-6), although the triplet sensitizer significantly contributes to the temperature increase in the absence of emitter, Figure 4-5. The nonradiative process decay from the singlet excited emitter is also excluded because the fluorescence quantum yield of the singlet excited emitter is typically high (85%-100%).[33,34] These considerations lead to a conclusion that the nonradiative decay process from the triplet excited emitter may be the main contributor to the temperature increase. This claim is consistent with the well-known low TTA efficiency between triplet-excited BPEA.[29,31] The temperature increases of AuNSs-UCsol(*X*) ($\Delta T_{\mathrm{AuNSs\text{-}UCsol}(X)}$) were larger than any of the components described above and found to be 1.1 ± 0.1, 1.7 ± 0.1, and 2.5 ± 0.2 °C, respectively (Figure 4-4(d) and Table 4-2). If gold nanospheres and dye molecules (UCsol(*X*)) in AuNSs-UCsol(*X*) contributed independently to the temperature increase, expected temperature increase $\Delta T_{\mathrm{Calc}(X)}$ would be given by Equation 1,

$$\Delta T_{\mathrm{Calc}(X)} = \frac{Ext_{\mathrm{AuNSs}}}{Ext_{\mathrm{AuNSs}}+Ext_{\mathrm{UCsol}(X)}}\Delta T_{\mathrm{AuNSs}} + \frac{Ext_{\mathrm{UCsol}(X)}}{Ext_{\mathrm{AuNSs}}+Ext_{\mathrm{UCsol}(X)}}\Delta T_{\mathrm{UCsol}(X)} \qquad (1)$$

where Ext_{AuNSs} and $Ext_{\mathrm{UCsol}(X)}$ indicate the extinction intensities of gold nanospheres and UCsol(*X*) at 642 nm, respectively. The observed temperature increases for AuNSs-UCsol(*X*) were much higher than the corresponding $\Delta T_{\mathrm{Calc}(X)}$ at all concentrations (Table 4-2).

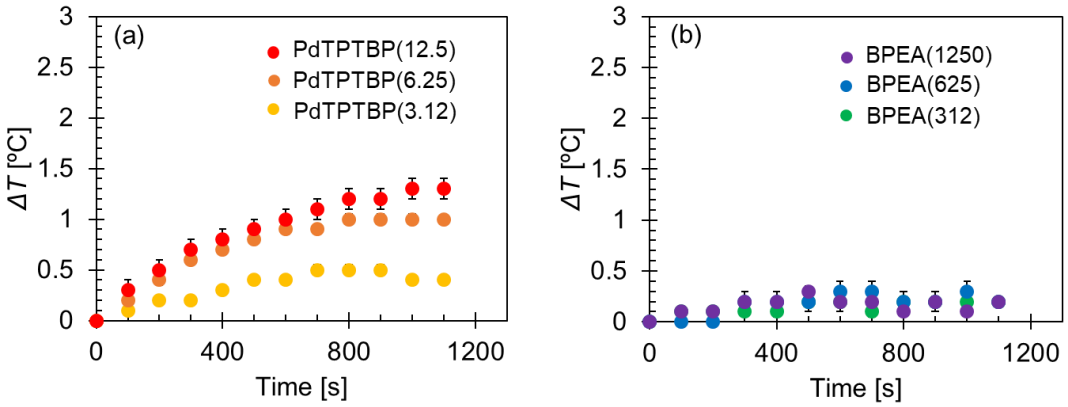

Figure 4-5 Temperature increase profiles (average ± standard dev.) of (a) PdTPTBP(*X*) (*X*: 3.12 μM, 6.25 μM, and 12.5 μM) and (b) BPEA(*X*) (*X*: 312 μM, 625 μM, and 1250 μM). All solutions were measured under irradiation with a 642 nm laser (100 mW).

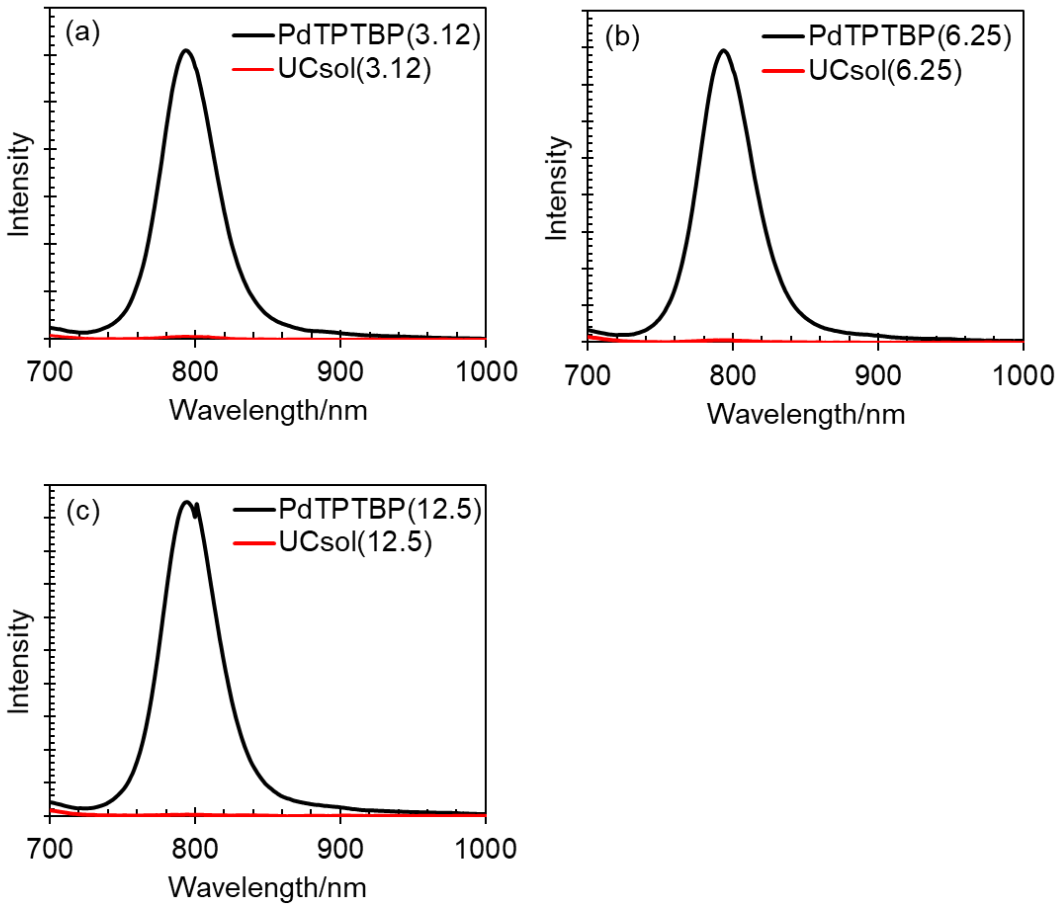

Figure 4-6. Phosphorescence spectra from PdTPTBP in *X* μM PdTPTBP solutions and UCsol(*X*) (*X*; concentration of sensitizer in μM) upon excitation at 642 nm.

Table 4-2. Observed temperature increases ($\Delta T_{AuNSs\text{-}UCsol(X)}$) and calculated temperature increases based on independent components effect ($\Delta T_{Calc(X)}$) for AuNSs-UCsol(X).

	X = 3.12	X = 6.25	X = 12.5
$\Delta T_{AuNSs\text{-}UCsol(X)}$ / °C	1.1 ± 0.1	1.7 ± 0.1	2.5 ± 0.2
$\Delta T_{Calc(X)}$ / °C	0.40	0.66	1.18

No photochemical reactions between the gold nanospheres and dye molecules occurred during laser irradiation, as the extinction spectra of AuNSs-UCsol(X) were unchanged after the laser irradiation (Figure 4-7). Moreover, the change in the diffusion motion of the dye molecules, which can affect the efficiencies of TTET and TTA, due to the presence of gold nanospheres is negligible as the concentration of the nanospheres is too low to affect the solution viscosity in the present system as follows. The solution viscosity of AuNSs-UCsol(X) was estimated by Einstein's viscosity formula (Equation 2),

$$\eta = \eta_0 \, (1 + 2.5 \, VN) \tag{2}$$

where η_0, V, and N are the DMF solution viscosity (9.20 Pa·s), the volume of gold nanospheres (8.24×10^{-18} cm^3) with the radius of 13.5 nm and the number of the gold nanospheres (2.40×10^{11} pieces/cm^3). The VN term is negligibly small, meaning that the effect of gold nanospheres on the viscosity of the solution can be safely ignored. Thus, it is reasonable to assume that the larger temperature increase observed for AuNSs-UCsol(X) than predicted on the basis of independent component effects ($\Delta T_{calc(X)}$) is attributed to pumping LSPR of the gold nanospheres by the organic dyes. The 642nm laser excitation produces the singlet excited state of PdTPTBP, which decays into the triplet state very fast in 97% quantum yield.[32] Subsequently, a quite efficient TTET from the triplet PdTPTBP occurs to produce the triplet BPEA as evidenced by a near complete quenching of phosphorescence of PdTPTBP by BPEA as shown in Figure 4-6. The energy level of the triplet BPEA is too low to pump the LSPR of the gold nanospheres.[35] Therefore, the TTA has to be invoked to generate the singlet excited state of BPEA, of which the energy level matches that of the LSPR of gold nanospheres (compare Figures. 4-4(b) and 4-4(d)). Two mechanisms may be possible for the pumping of the LSPR of gold nanospheres by the singlet excited state of BPEA: (1) resonance energy transfer (RET) and (2) reabsorption of the upconverted emission by the LSPR. In this context, we observed that the upconverted emission intensity from AuNSs-UCsol(X) was attenuated

by 64%-66% as compared to that of UCsol(*X*) (Figure 4-8). In order to clarify the mechanism behind the quenching of upconverted emission, we measured the fluorescence lifetimes of BPEA directly excited at 405 nm in UCsol(*X*) and in AuNSs-UCsol(*X*). As seen from Figure 4-9 and Table 4-3, the lifetimes for AuNSs-UCsol(*X*) were hardly changed from those for UCsol(*X*). It is therefore concluded that the reabsorption of upconverted emission induced by TTA-UC mostly contributed to the pumping of the LSPR of gold nanospheres, which lead to the larger temperature increase observed for AuNSsUCsol(*X*).

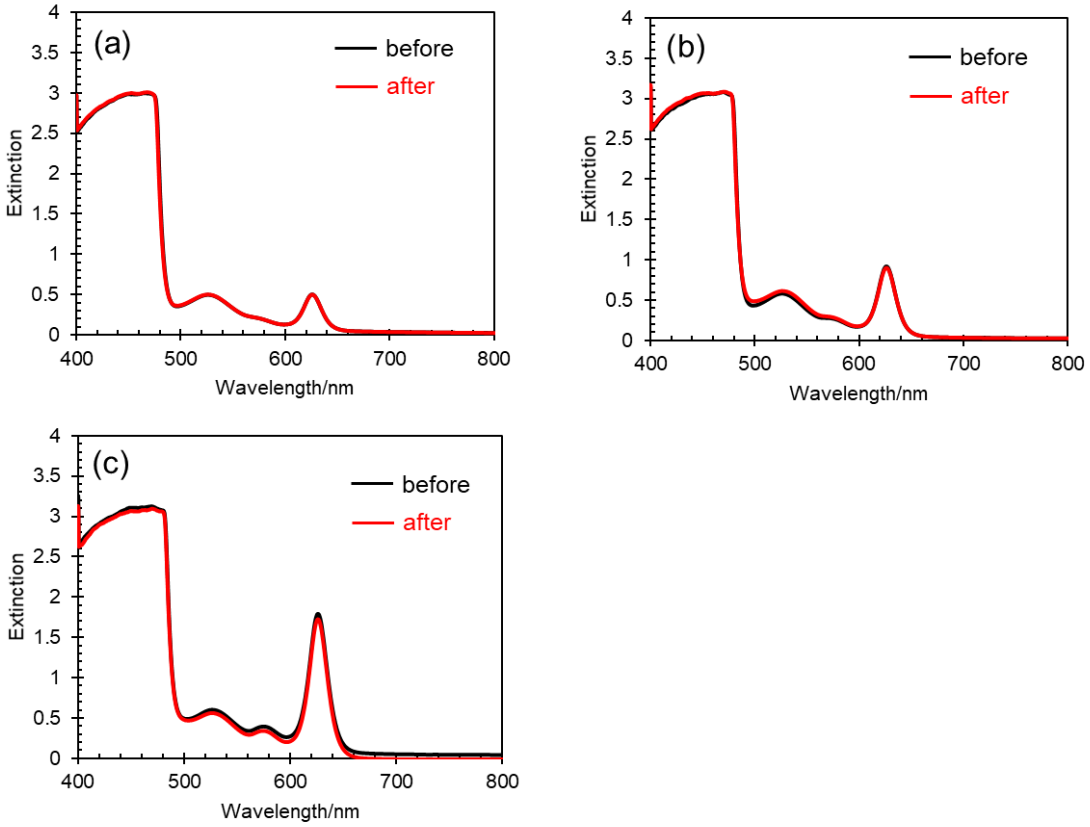

Figure 4-7. Extinction spectra of the AuNSs-UCsol(*X*) (*X* = (a) 3.12, (b) 6.25, and (c) 12.5) before and after the irradiation of 642 nm laser.

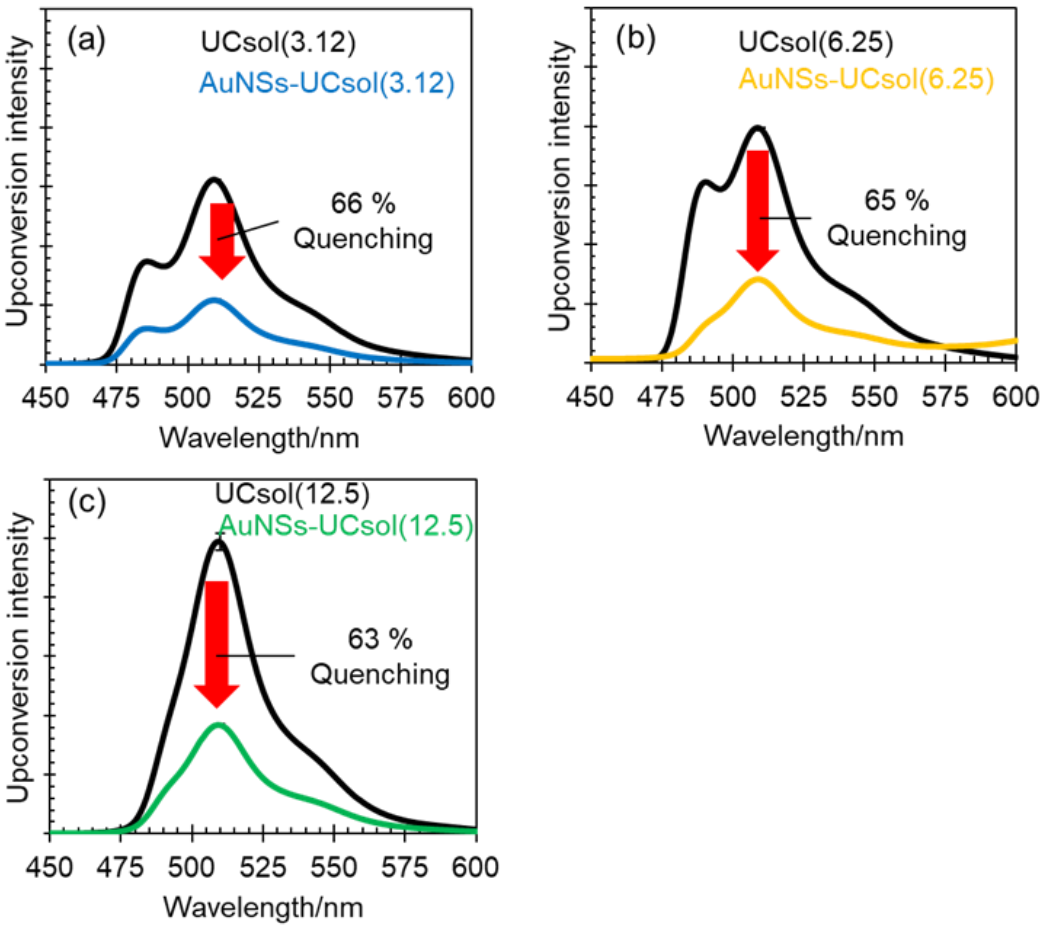

Figure 4-8. Upconverted emission spectra (λ_{ex} = 642 nm) of UCsol(*X*) and AuNSs-UCsol(*X*) with *X* = (a) 3.12, (b) 6.25, and (c) 12.5μM.

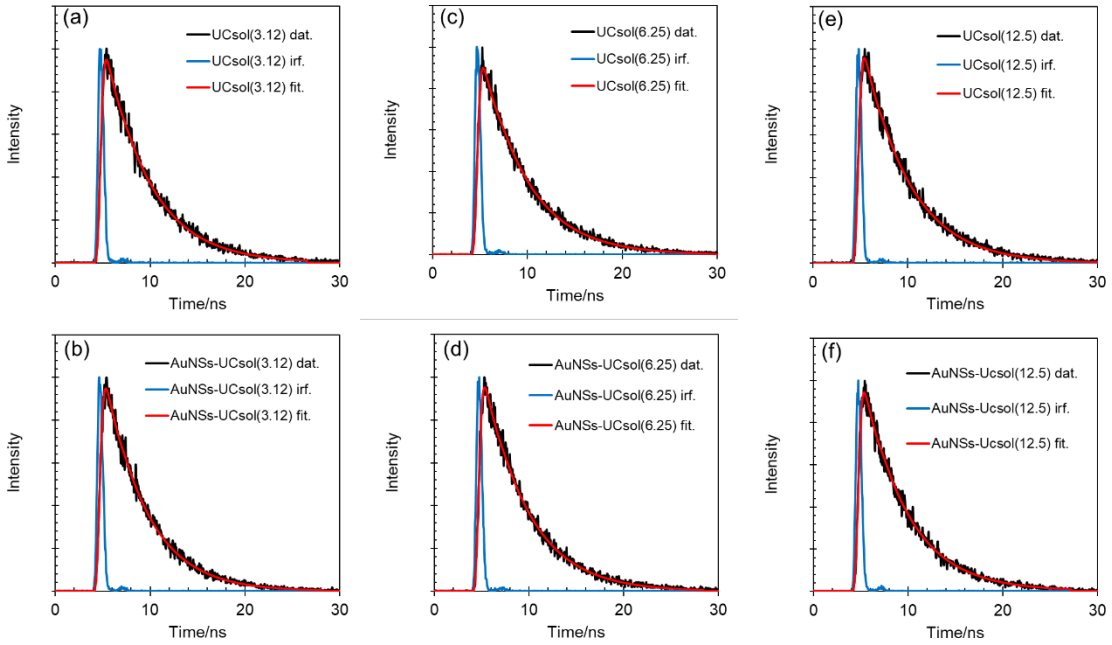

Figure 4-9. Fluorescence lifetime measurements for BPEA excited at 405 nm (black line) and fit (red line): (a) UCsol(3.12), (b) AuNSs-UCsol(3.12), (c) UCsol(6.25), (d) AuNSs-UCsol(6.25), (e) UCsol(12.5), and (f) AuNSs-UCsol(12.5). The fluorescence decay characteristics were recorded with the time correlated single photon counting (TCSPC) method with Quantaurus-Tau fluorescence lifetime measurement system (Hamamatsu Photonics Co.). The fluorescence emission decay was well fitted by a single exponential decay profile.

Table 4-3. Fluorescence lifetimes of BPEA for UCsol(*X*) and AuNSs-UCsol(*X*) and efficiencies of RET and reabsorption.

	UCsol (3.12 μM)	AuNSs-UCsol (3.12 μM)	UCsol (6.25 μM)	AuNSs-UCsol (6.25 μM)	UCsol (12.5 μM)	AuNSs-UCsol (12.5 μM)
Fluorescence lifetime (ns)	4.64	4.39	4.73	4.58	4.90	4.56
RET efficiency (%)	-	5.4	-	3.2	-	6.8
Reabsorption efficiency (%)	-	60.6	-	61.8	-	56.2

4-4. Conclusion

In summary, conversion of 642 nm light into heat energy was achieved through the LSPR excitation of gold nanospheres, which was made possible by the upconverted emission based on TTA-UC. Conversion of even longer-wavelength light into heat may be achieved by developing efficient TTA-UC systems involving sensitizers with larger anti-Stokes shifts. Also, a more effective temperature increase may be obtained by employing an emitter with a higher quantum yield of upconverted emission. These lines of research is under way in our laboratory towards practical upconverted emission-driven photothermal conversion systems.

4-5. References

(1). Loeb, S.; Li, C.; Kim, J.-H. Solar Photothermal Disinfection using Broadband-Light Absorbing Gold Nanoparticles and Carbon Black. *Sci. Technol.* **2018**, *52*, 205-213.

(2). Guo, A.; Fu, Y.; Wang, G.; Wang, X. Diameter effect of gold nanoparticles on photothermal conversion for solar steam generation. *RSC Adv.* **2017**, *7*, 4815-4824.

(3). Qiu, J.; Wei, D., W. Surface Plasmon-Mediated Photothermal Chemistry. *J. Phys. Chem. C*, **2014**, *118*, 20735-20749.

(4). Zhang, H.; Chen, H.-J.; Du, X.; Wen, D. Photothermal conversion characteristics of gold nanoparticle dispersions. *Solar Energy*, **2014**, *100*, 141-147.

(5). Jain, P. K.; Lee, K. S.; El-Sayed, I. H. El-Sayed, M. A. Calculated Absorption and Scattering Properties of Gold Nanoparticles of Different Size, Shape, and Composition: Applications in Biological Imaging and Biomedicine. *J. Phys. Chem. B*, **2006**, *110*, 7238-7248.

(6). Chu, Y.; Schonbrun, E.; Yang, T.; Croziera, K. B. Experimental observation of narrow surface plasmon resonances in gold nanoparticle arrays. *Appl. Phys. Lett.* **2008**, *93*, 181108/1-181108/3.

(7). Jiang, K.; Smith, D. A.; Pinchuk, A. Size-Dependent Photothermal Conversion Efficiencies of Plasmonically Heated Gold Nanoparticles. *J. Phys. Chem. C,* **2013**, *117*, 27073-27080.

(8). Wang, F.; Banerjee, D.; Liu, Y.; Chen, X.; Liu, X. Upconversion nanoparticles in biological labeling, imaging, and therapy. *Analyst*, **2010**, *135*, 1839-1854.

(9). Yi, G. S.; Chow, G. M. Synthesis of Hexagonal‐Phase $NaYF_4$:Yb,Er and $NaYF_4$:Yb,Tm Nanocrystals with Efficient Up‐Conversion Fluorescence. *Adv. Funct. Mater.*, **2006**, *16*, 2324-2329.

(10). Wang, F.; Liu, X. Upconversion Multicolor Fine-Tuning: Visible to Near-Infrared Emission from Lanthanide-Doped $NaYF_4$ Nanoparticles. *J. Am. Chem. Soc.* **2008**, *130*, 5642-5643.

(11). Monguzzi, A.; Tubino, R.; Hoseinkhani, S.; Campione M.; Meinardi, F. Low power, non-coherent sensitized photon up-conversion: modelling and perspectives. *Phys. Chem. Chem. Phys*., 2012, **14**, 4322-4332.

(12). Baluschev, S.; Miteva, T.; Yakutkin, V.; Nelles, G.; Yasuda, A.; Wegner, G. Up-Conversion Fluorescence: Noncoherent Excitation by Sunlight. *Phys. Rev. Lett.,* **2006**, *97*, 143903/1-143903/3.

(13). Singh-Rachford, T. N.; Nayak, A.; Muro-Small, M. L.; Goeb, S.; Therien, M. J.; Castellano, F. N. Supermolecular-Chromophore-Sensitized Near-Infrared-to-Visible Photon Upconversion. *J. Am. Chem. Soc.*, **2010**, *132*, 14203-14211.

(14). Chen, G.; Qiu, H.; Prasad, P. N.; Chen, X. Upconversion Nanoparticles: Design, Nanochemistry, and Applications in Theranostics. *Chem. Rev*. **2014**, *114*, 5161-5214.

(15). Haase M.; Schfer, H. Upconverting Nanoparticles. *Angew. Chem. Int. Ed.* **2011**, *50*, 5808-5829.

(16). Xie, X.; Gao, N.; Deng, R.; Sun, Q.; Xu, Q.-H.; Liu, X. Mechanistic Investigation of Photon Upconversion in Nd^{3+}-Sensitized Core–Shell Nanoparticles. *J. Am. Chem. Soc*. **2013**, *135*, 12608-12611.

(17). Chen, D.; Liu, L.; Huang, P.; Ding, M.; Zhong, J.; Ji, Z. Nd^{3+}-Sensitized Ho^{3+} Single-Band Red Upconversion Luminescence in Core–Shell Nanoarchitecture. *J. Phys. Chem. Lett*. **2015**, *6*, 2833-2840.

(18). Tao, W.; Haifeng, Z.; Zhichao, Y.; Guangjun, Z.; Juan, Z.; Dapeng, H.; Leilei, S.; Peng, G.; Yuzhen, S.; Jifan, H. 808 nm Excited Multicolor Up-Conversion Tuning through Energy Migration in Core-Shell-Shell Nanoarchitecture. *J. Phys. Chem. C* **2018**, *122*, 10113–10124.

(19). Cai, H.; Shen, T.; Kirillov, A., M.; Zhang, Y.; Shan, X., L.; Liu, W.; Tang, Y. Self-Assembled Upconversion Nanoparticle Clusters for NIR-controlled Drug Release and Synergistic Therapy after Conjugation with Gold Nanoparticles. *Inorg. Chem*. **2017**, *56*, 5295-5304.

(20). Wu, X.; Zhang, Y.; Takle, K.; Bilsel, O.; Li, Z.; Lee, H.; Zhang, Z.; Li, D.; Fan, W.; Duan, C.; Chan, E. M.; Lois, C.; Xiang, Y.; Han, G. Dye-Sensitized Core/Active Shell Upconversion Nanoparticles for Optogenetics and Bioimaging Applications. *ACS Nano,* **2016**, *10*, 1060-1066.

(21). Chen, G.; Damasco, J.; Qiu, H.; Shao, W.; Ohulchanskyy, T. Y.; Valiev, R. R.; Wu, X.; Han, G.; Wang, Y.; Yang, C.; Ågren, H.; Prasad, P. N. Energy-Cascaded Upconversion in an Organic Dye-Sensitized Core/Shell Fluoride Nanocrystal. *Nano Lett*., **2015**, *15*, 7400-7407.

(22). Carnall, W. T.; Goodman, G. L.; Rajnak, K.; Rana, R. S. A systematic analysis of the spectra of the lanthanides doped into single crystal LaF_3 *J. Chem. Phys.* **1989**, *90*, 3443-3457.

(23). Singh-Rachford, T. N.; Castellano, F. N. Photon upconversion based on sensitized triplet–triplet annihilation *Coord. Chem. Rev.*, **2010**, *254*, 2560-2573.

(24). Gray, V.; Dzebo, D.; Abrahamsson, M.; Albinsson, B.; Moth-Poulsen, K. Triplet–triplet annihilation photon-upconversion: towards solar energy applications. *Phys. Chem. Chem. Phys.* **2014**, *16*, 10345-10352.

(25). Castellano F. N.; McCusker, C. E. MLCT sensitizers in photochemical upconversion: past, present, and potential future directions. *Dalton Trans.* **2015**, *44*, 17906-17910.

(26). Yanai N.; Kimizuka, N. New Triplet Sensitization Routes for Photon Upconversion: Thermally Activated Delayed Fluorescence Molecules, Inorganic Nanocrystals, and Singlet-to-Triplet Absorption. *Acc. Chem. Res.* **2017**, *50*, 2487-2495.

(27). Gray, V.; Moth-Poulsen, K.; Albinsson, B.; Abrahamsson, M. *Coord. Chem. Rev.* **2018**, *362*, 54-71.

(28). Turkevich, J.; Stevenson, P., C.; Hillier, J. A study of the nucleation and growth processes in the synthesis of colloidal gold. *Discuss. Faraday Soc*. **1951**, *11*, 55-75.

(29). Gray, V.; Dreos, A.; Erhart, P.; Albinsson, B.; Moth-Poulsen, K.; Abrahamsson, M. Loss channels in triplet–triplet annihilation photon upconversion: importance of annihilator singlet and

triplet surface shapes. *Phys. Chem. Chem. Phys*. **2017**, *19*, 10931-10939.
(30). Mongin, C.; Golden, J. H.; Castellano, F. N. Liquid PEG Polymers Containing Antioxidants: A Versatile Platform for Studying Oxygen-Sensitive Photochemical Processes. *ACS Appl. Mater. Interfaces,* **2016**, *8*, 24038-24048.
(31). Baluschev, S.; Yakutkin, V.; Miteva, T.; Wegner, G.; Roberts, T.; Nelles, G.; Yasuda, A.; Chernov, S.; Aleshchenkov, S.; Cheprakov, A. A general approach for non-coherently excited annihilation up-conversion: transforming the solar-spectrum. A. *New J. Phys.*, **2008**, *10*, 013007/1-013007/12.
(32). Rogers, J. E.; Nguyen, K. A.; Hufnagle, D. C.; McLean, D. G.; Su, W.; Gossett, K. M.; Burke, A. R.; Vinogradov, S. A.; Pachter, R.; Fleitz, P. A. Observation and Interpretation of Annulated Porphyrins: Studies on the Photophysical Properties of *meso*-Tetraphenylmetalloporphyrins. *J. Phys. Chem. A,* **2003**, *107*, 11331-11339.
(33). Heller, C. A.; Henry, R. A.; McLaughlin, B. A.; Bliss, D. E. Fluorescence spectra and quantum yields. Quinine, uranine, 9,10-diphenylanthracene, and 9,10-bis(phenylethynyl) anthracenes. *J. Chem. Eng. Data,* **1974**, *19*, 214-219.
(34). Levitus M.; Garcia-Garibay, M. A. Polarized Electronic Spectroscopy and Photophysical Properties of 9,10-Bis(phenylethynyl)anthracene. *J. Phys. Chem. A* **2000**, *104*, 8632-8637.
(35). Quarti, C.; Fazzi, D.; Zoppo, M. D. A computational investigation on singlet and triplet exciton couplings in acene molecular crystals. *Phys. Chem. Chem. Phys*. **2011**, *13*, 18615-18625.

Chapter 5

Conclusion

Conclusion

This thesis investigated the interaction between the LSP resonance and the photophysical processes of TTA-UC through various spectroscopic measurements. The results obtained in this thesis are summarized below.

First, in Chapter 1, I described the fundamental photoelementary process of photon upconversion, the basis of LSP resonance, and the present status of the synthesis technique of AgPRs, which were used in this study, in order to facilitate the understanding of the contents of this thesis. In addition, TTA-UC systems in liquid and solid phase systems that have been studied so far are introduced, to place this work into context.

Second, in Chapter 2, we established a targeted synthesis technique for anisotropic silver nanoparticles that can strongly induce LSP resonance, constructed a composite thin film with photofunctional molecules leading to TTA-UC emission, and performed various spectroscopic measurements to evaluate the photophysical properties of TTA-UC emission. As a result, it was found that the upconverted emission was enhanced when LSP resonance was applied to the excitation and fluorescence processes of TTA-UC, and that the harmful quenching of upconverted emission occurred when LSP resonance was applied to the phosphorescence process.

Third, in Chapter 3, the research was advanced from the viewpoint of preventing the harmful quenching of upconverted emission by the acceleration of the phosphorescence decay rate described in Chapter 2. I used octaethylporphyrin (PdOEP, PtOEP) with palladium or platinum as a central metal as a sensitizing molecule, and prepared composite thin films similar to those used in Chapter 2. Phosphorescence enhancement and upconversion quenching were induced for PdOEP, while neither was induced for PtOEP, by the LSP resonance. We anticipated that this difference was caused by the difference in the spin-orbit coupling constant of the central metal (a metal atom with larger spin‐orbit coupling constants may be less susceptible to external electric fields.). Then, the complex with ruthenium (Ru), palladium (Pd), iridium (Ir), and platinum (Pt) was introduced as the central metal, and the phosphorescence enhancement was compared. As the result, it was clarified from the experiment that the phosphorescence enhancement became difficult to occur as the spin-orbital coupling constant increases (Ru; 1042 cm^{-1}, Pd; 1460 cm^{-1}, Ir; 3909 cm^{-1}, Pt; 4253 cm^{-1}). Therefore, we concluded that the spin-orbit coupling constant plays an important role as one of the selection indexes of sensitizer in the enhancement of TTA-UC emission using plasmons.

Finally, in Chapter 4, conversion of 642 nm light into heat energy was achieved through the LSP resonance excitation of gold nanospheres, which was made possible by the TTA-UC-based emission. Conversion of even longer-wavelength light into heat may be

achieved by developing efficient TTA-UC system involving sensitizers with larger anti-Stokes shifts. Also, a more effective temperature increase may be obtained by employing an emitter with a higher quantum yield of upconverted emission. These lines of research is under way in our laboratory towards practical upconverted emission-driven photothermal conversion systems.

From these results, of quantitative investigation of the interaction of plasmon and photofunctional molecules, a possibility was shown to improve the efficiency of the optical energy conversion system. Therefore, I conclude that the plasmonic light-harvesting nanoantenna effect, combined with high-mobility excitons or a matrix having a lower glass transition temperature, is very promising for the achievement of TTA-UC-based high performance optical devices. Moreover, it was demonstrated that the photothermal conversion drive wavelength of the metal nanoparticle was broadened by the upconverted emission. Therefore, the range of application of the TTA-UC system could be extended. TTA-UC will be close to practical application by the simultaneous progress of basic research (i.e., Improvement of TTA-UC luminous efficiency) and applied research (i.e., Application to a variety of applications).

Publication lists

1. **Shota Jin**, Kosuke Sugawa, Naoto Takeshima, Hironobu Tahara, Shuto Igari, Satoshi Yoshinari, Yuri Kurihara, Shiryu Watanabe, Masami Enoki, Kenta Sato, Wataru Inoue, Kyo Tokuda, Tsuyoshi Akiyama, Ryuzi Katoh, Kouichi Takase, Hiroaki Ozawa, Toshiya Okazaki, Takayuki Watanabe, and Joe Otsuki, (2018), "Precise Control of Localized Surface Plasmon Wavelengths Is Needed for Effective Enhancement of Triplet−Triplet AnnihilationBased Upconversion Emission", *ACS Photonic*, **5**, 5025-5037.

2. **Shota Jin**, Kosuke Sugawa, Naoto Takeshima, Shuto Igari, Wataru Inoue, Jotaro Honda, Satoshi Yoshinari, Shiryu Watanabe, Daisuke Kanai, Kotomi Kanakubo, and Joe Otsuki, (2020), "Upconverted emission-driven photothermal conversion with gold nanospheres based on triplet-triplet annihilation", ***Phys. Chem. Chem. Phys.***, **22**, 18257-18260.

3. Joe Otsuki, Kosuke Sugawa, and **Shota Jin**, (2020), "Plasmonic triangular nanoprism sensors", *Mater. Adv.* in press (https://doi.org/10.1039/D0MA00644K).

4. Naoto Takeshima, Kosuke Sugawa, Hironobu Tahara, **Shota Jin**, Hiroki Wakui, Misa Fukushima, Kyo Tokuda, Shuto Igari, Kotomi Kanakubo, Yutaro Hayakawa, Ryuzi Katoh, Kouichi Takase, Joe Otsuki, (2019), "Plasmonic Silver Nanoprism-Induced Emissive Mode Control between Fluorescence and Phosphorescence of a Phosphorescent Palladium Porphyrin Derivative", *ACS Nano*, ***13***, 13244-13256.

5. Naoto Takeshima, Kosuke Sugawa, Hironobu Tahara, **Shota Jin**, Masaki Noguchi, Yutaro Hayakawa, Yuhei Yamakawa, Joe Otsuki, (2020), "Combined Use of Anisotropic Silver Nanoprisms with Different Aspect Ratios for Multi-Mode Plasmon-Exciton Coupling", *Nanoscale Research Letters, 15,* 1.

6. Naoto Takeshima, Kosuke Sugawa, Masaki Noguchi, Hironobu Tahara, **Shota Jin**, Kouichi Takase, Joe Otsuki, and Kaoru Tamada, (2020) , "Synthesis of Ag Nanoprisms with Precisely-tuned Localized Surface Plasmon Wavelengths by Sequential Irradiation of Light of Two Different Wavelengths", *Chem. Lett.*, 49, 240–243.

謝辞

本論文は著者が，日本大学大学院理工学研究科物質応用化学専攻超分子化学研究室須川グループに，2018 年から 2021 年の 3 年間，在籍した際に得られた研究結果をまとめたものです．本論文は著者一人の力ではなく，多くの人の助けによって完成しました．

指導教員である大月穣先生におかれましては，研究活動および論文執筆の細部にわたり懇切丁寧なご指導を賜り，多くのことを学ばせて頂きました．分野を問わず幅広い知見を有し，その知識の深さには，驚きと尊敬の念に堪えません．3 年間という短い間でしたが，大変お世話になりました．本当にありがとうございました．

須川晃資先生におかれましては，学部 1 年間，修士 2 年間および博士 3 年間の計 6 年間，長きに渡り，研究活動全般に渡り懇切丁寧なご指導を賜りました．私が研究者としての道を歩めるのも，須川先生のご指導の賜物でございます．普段の研究生活から，物事の伝え方，考え方について詳細にご指導頂き，仕事を遂行する上で重要な知識や技術を身につけられたとても実りのある 6 年間となりました．また，研究に対する真摯な姿勢を拝見し，研究者としての在り方を学ばせて頂きました．私にとっての目標であり，尊敬すべき研究者のイメージ像は須川先生でございます．本当にありがとうございました．

加藤隆二先生におかれましては，発光寿命測定，発光量子収率測定に関して大変お世話になりました．加藤先生の技術力と知見，また，加藤先生の研究室の学生の方々のおかげで，論文の質が飛躍的に向上しました．本当にありがとうございました．

田原弘宣先生におかれましては，理論計算に関して大変お世話になりました．田原先生の理論計算により，理論と実験のすり合わせができ，実験結果に自信を持つことができました．本当にありがとうございました．

先輩である武島尚人さんには，先輩としての在り方を学ばせて頂くと共に，研究で行き詰った際には適切なご助言を頂き，何度も助けられてきました．本当にありがとうございました．学部と修士の 3 年間を共に過ごした同期である，金子竜二君，古橋智夫君，恒成夏弥さんには，公私に渡り支えて頂きました．本当にありがとうございました．三人の益々の活躍をお祈り申し上げます．博士 3 年間を共に過ごした後輩である猪狩脩人君，渡邉志龍君には，広い知見と観察力に基づく的確な助言に助けられてきました．本当にありがとうございました．名前を挙げてはいませんが，楽しい時や辛い時を，共に過ごしてくれた全ての学生方のおかげで，本論文の完成に至ることができました．本当にありがとうございました．

これまで公私共に支えてくださった多くの方々に，この場を借りて再度，御礼

申し上げます．本当にありがとうございました．